Università degli Studi di Ferrara

ISTITUTO ITALIANO DI TECNOLOGIA

DOCTORAL COURSE IN

"Translational Neurosciences and Neurotechnologies "

CICLO XXXII

COORDINATOR Prof. Luciano Fadiga

The small GTPase RIT2 rescues LRRK2-dependent autophagy-lysosome pathway impairment to reduce alpha-synuclein accumulation and neurotoxicity

Scientific/Disciplinary Sector (SDS): BIO/11

Candidate

Dott. Obergasteiger Julia

Supervisor

Prof. Morari Michele

Dott. Volta Mattia

Year 2016/2019

Abstract

Parkinson's disease (PD) is the most common neurodegenerative movement disorder and affects about 2-3% of the population over the age of 65. The etiology of PD is still undefined and familial cases provided hints for mechanisms involved in the disease. In particular, alpha-synuclein (aSyn) and leucine-rich repeat kinase 2 (LRRK2) gene alterations lead to autosomal dominant PD with many commonalities to the idiopathic disorder. aSyn containing inclusions, termed Lewy bodies, are one of the neuropathological hallmarks of PD, but the mechanisms involved in formation, maintenance and degradation of these inclusions are still under intense investigation. Several cellular processes are hypothesized to mediate these mechanisms, with a prominent attention directed towards autophagy. Additionally, several PD risk genes have a role in lysosomal biology and autophagy itself. Recombinant neuroblastoma cell lines overexpressing WT and G2019S LRRK2 display defects at different stages of the autophagy-lysosome pathway (ALP), specifically accumulation of autophagosomes and abnormalities in lysosomal morphology and number. Interestingly, G2019S LRRK2 cells display inclusions staining positive for pS129-aSyn. Pharmacological inhibition of LRRK2 kinase activity in G2019S LRRK2 cells reverts ALP defects and most importantly reduces the number of pS129-aSyn inclusions. RIT2, coding for the protein Rin, is a novel PD gene risk factor and has been scarcely investigated. It is a small GTPase mediating neurite outgrowth through p38 and ERK1/2 MAPK signaling pathways. Moreover, Rin is enriched in rodent substantia nigra pars compacta neurons and is reduced in human PD brains. However, the relevance of Rin-dependent signaling pathways and/or its interactions with PD-causing proteins is currently lacking. We observed that RIT2 mRNA levels are reduced in WT and G2019S LRRK2 cells and also RIT2 promoter activity is reduced in these cell lines. Acute overexpression of RIT2 phenocopies the effects of LRRK2 kinase inhibitor treatment, specifically on the number of autphagosomes, morphology and number of lysosomes and their proteolytic function. Moreover, RIT2 overexpression strongly reduces the burden of pS129-aSyn inclusions. Interestingly, acute RIT2 overexpression reduces phosphorylation levels of S1292, but not S935 LRRK2, an aspect distinct from pharmacological LRRK2 kinase inhibition. Furthermore, total LRRK2 levels are not decreased with RIT2 overexpression, unlike after LRRK2 kinase inhibitor treatment. Viral overexpression of RIT2 in an *in vivo* aSyn mouse model ameliorates motor deficits and reduces dopaminergic neuron loss, induced by viral overexpression of aSyn. Viral aSyn overexpression

induces an increase in pS1292 LRRK2 levels, indicating an enhanced activity of endogenous LRRK2. The co-expression of aSyn with RIT2 prevents the increase of LRRK2 kinase activity, indicating that RIT2 is acting on LRRK2. This data suggest that aSyn, LRRK2 and RIT2 might share common cellular mechanisms, in particular autophagy, and ultimately impact the degradation of aSyn. The modulation of RIT2 expression might constitute a new strategy to combat aSyn pathology, applicable to both familial and idiopathic PD and, possibly, other synucleinopathies.

Key words: Parkinson's disease, LRRK2, alpha-synuclein, RIT2, neuroblastoma cells, autophagy, lysosome, kinase inhibitor, protein degradation

Riassunto

La malattia di Parkinson (MdP) é il più comune disturbo neurodegenerativo del movimento, che colpisce circa 2-3% delle persone sopra i 65 anni di età. L´eziologia della malattia non è ancora definita ma casi familiari hanno fornito indizi sui meccanismi coinvolti nella malattia. In particolare, alterazioni genetiche nei geni codificanti alfa-sinucleina (aSyn) e leucine-rich repeat kinase 2 (LRRK2) sono alla base di forme autosomiche dominanti della malattia, le quali ricalcano le caratteristiche salienti della forma sporadica. Le inclusioni intraneuronali, definite corpi di Lewy e costituite prevalentemente da aSyn, sono uno dei segni distintivi della presentazione neuropatologica nella MP. I meccanismi coinvolti nella formazione, mantenimento e degradazione delle inclusioni sono tutt´ora oggetto di studio approfondito. Si ipotizza che diversi processi cellulari siano alla base di tali meccanismi, con una particolare attenzione rivolta all´autofagia. Inoltre, diversi geni associati ad aumento di rischio di MdP rivestono un ruolo nella biologia lisosomale e nell´autofagia stessa.

Linee cellulari ricombinanti di neuroblastoma che sovra esprimono LRRK2 WT o G2019S riportano difetti in diversi stadi della via autofagia-lisosomi, in particolare accumulo di autofagosomi, alterazioni nella morfologia dei lisosomi e nel loro numero. Le cellule LRRK2 G2019S specificamente sono caratterizzate da inclusioni proteiche positive per pS129-aSyn. L´inibizione farmacologica dell´attività chinasica di LRRK2 in queste cellule corregge i deficit nella via autofagia-lisosomi e riduce il numero di inclusioni di pS129-aSyn. RIT2, che codifica per la proteina Rin, è un nuovo fattore di rischio genetico per la MdP che è stato scarsamente studiato finora. Si tratta di una piccola GTPasi che media la crescita neuritica tramite le vie di segnalazione delle MAPK p38 ed ERK1/2. Inoltre, RIT2 è arricchiato nei neuroni della substantia nigra pars compacta nei roditori e la sua espressione è ridotta nel cervello di pazienti di MdP. Tuttavia, non sono disponibili evidenze sperimentali sulle vie di segnalazione dipendenti da Rin e/o sulle eventuali interazioni con proteine legate causalmente alla MdP. Abbiamo appurato che i livelli di mRNA di RIT2 sono ridotti nelle cellule WT e G2019S LRRK2 ed inoltre l´attività del suo promotore è ridotta nelle stesse linee cellulari. La sovra espressione acuta di RIT2 produce una fenocopia del trattamento con l´inibitore chinasico di LRRK2, in riferimento al numero di autofagosomi, alla morfologia e numero di lisosomi e la loro attività proteolitica. In aggiunta, la sovra espressione di RIT2 riduce il carico di inclusioni positive per p S129-aSyn. Questa strategia inoltre riduce la fosforilazione di LRRK2 a carico

della S1292, ma non della S935, e questo aspetto la differenzia dal trattamento farmacologico con inibitore di LRRK2. Inoltre, i livelli di espressione proteina totale di LRRK2 non vengono ridotti dalla sovra espressione di RIT2, a differenza di quanto accade in seguito ad inibizione farmacologica. La sovra espressione di RIT2 tramite vettori virali in un modello in vivo di tossicità di aSyn nel topo porta ad un miglioramento dell´attività motoria e riduce la perdita neuronale dopaminergica, indotta dall´espressione virale di aSyn. Inoltre, aSyn induce un aumento dei livelli di pS1292 LRRK2, indicativi di un´aumentata attività di LRRK2 endogena. La co-espressione con RIT2 previene tale aumento, suggerendo un´azione di RIT2 su LRRK2 stessa. Questi dati indicano che aSyn, RIT2 e LRRK2 sono alla base di meccanismi cellulari comuni, specialmente autofagia, e modulano a valle il catabolismo di aSyn. La modulazione dell´espressione di RIT2 potrebbe quindi costituire una nuova strategia terapeutica indirizzata alla patologia da aSyn, applicabile sia alla MdP familiare che idiopatica e, idealmente, alle altre sinucleinopatie.

Contents

Table of Figures

Abbreviations

AAV	adeno-associated virus
AD	autosomal dominant
ALP	autophagy-lysosome pathway
AR	autosomal recessive
aSyn	alpha-synuclein
ATG	autophagy-related
BCA	BiCinchoninic acid
BSA	bovine serum albumin
CQ	chloroquine
CLEAR	coordinated lysosomal expression and regulation
CMA	chaperone-mediated autophagy
COR	C-terminal of Roc
DA	dopaminergic
DAT	dopamine transporter
ddPCR	digital droplet PCR
DLB	Dementia with Lewy bodies
DMEM	Dulbecco's Modified Eagle Medium
DNA	Deoxyribonucleic acid
dNTPs1	Deoxynucleotide triphosphate
DTT	Dithiothreitol
EDTA	Ethylenediaminetetraacetic acid
ER	endoplasmatic reticulum
ERK	extracellular signal–regulated kinases
FBS	Fetal Bovine Serum
GCase	Glucocerebrosidase
GFP	Green Fluorescent Protein
GDP	Guanosine Diphosphate
GTP	Guanosine Triphosphate
GWAS	genome-wide association study

HBSS	Hank's Balanced Salt Solution
HRP	horseradish peroxidase
ICC	immunocytochemistry
IHC	immunohistochemistry
IF	immunofluorescence
iPSC	induced pluripotent stem cells
KO	knock-out
LB	Lewy body
L-DOPA	levodopa
LRR	leucine-rich repeat
LRRK2	leucine-rich repeat kinase 2
MAO-B	monoamine oxidase B
MAPK	mitogen-activated protein kinase
MPP+	1-methyl-4-phenylpyridinium
MPTP	1-methyl-4-phenyl-1,2,3,6-tetrahydropyridine
MSA	Multiple system atrophy
OCT	Optimal cutting temperature compound
PCR	polymerase chain reaction
PBS	phosphate-buffered saline
PBS-T	phosphate-buffered saline with Tween
PD	Parkinson’s disease
PFA	paraformaldehyde
PF475	PF-06447475
PLA	proximity ligation assay
pS129	phosphorylated Serine 129
pS1292	phosphorylated Serine 1292
pS935	phosphorylated Serine 935
PVDF	polyvinylidene fluoride
qPCR	quantitative PCR
Rin	Ras-like protein expressed in neurons
Rit	Ras-like protein expressed in many tissues

RIT1	Ras Like Without CAAX 1
RIT2	Ras Like Without CAAX 2
RNA	Ribonucleic acid
ROC	Ras of complex
RT	room temperature
SNARE	soluble N-ethylmaleimide-sensitive-factor attachment receptor
SNc	substantia nigra pars compacta
SNP	single-nucleotide polymorphism
TBS	Tris-buffered saline
TBS-T	Tris-buffered saline with Tween
TE	Tris-EDTA
TFEB	Transcription Factor EB
TH	tyrosine hydroxylase
UPR	unfolded protein response
UPS	ubiquitin proteasome system
WT	wildtype

1 Introduction

1.1 Parkinson's disease

Dr. James Parkinson in 1817 first described a disorder characterized by a "shaking palsy" and difficulties in initiating voluntary movements, which was later named after him, Parkinson's disease (PD). PD is the second most common neurodegenerative disorder and the most common neurodegenerative movement disorder affecting 2-3% of people over the age of 65. The prevalence increases exponentially between the ages of 65 and 90 years (Moghal et al. 1994, Corti et al. 2011). In fact, the major risk factor for developing PD is age with a median age at onset of 60 years (Cantuti-Castelvetri et al. 2007, Lees et al. 2009). Aside, a positive family history for PD is the strongest predictor for increased risk of developing the disease (Semchuk et al. 1993). PD was long thought to be caused by environmental factors, which was supported by the identification of N-methyl-4-phenyl-1,2,3,6-tetrahydropyridine (MPTP) in the early 1980's. MPTP is the precursor of MPP^+, which is produced through Monoamine oxidase B (MAO-B) metabolism of MPTP in astrocytes. MPP^+ inhibits mitochondrial complex 1 leading to a parkinsonian neurodegeneration syndrome in rodents, primates and humans (Langston et al. 1983). The discovery that mutations and multiplications in the *SNCA* gene, coding for alpha-synuclein (aSyn) cause familial PD was the first evidence of a genetic contribution to PD (Polymeropoulos et al. 1997, Spillantini et al. 1997). PD is defined as a multifactorial disorder and the vast majority of cases are classified as idiopathic (i.e. of unknown etiology). A handful of genes, named PARK genes, are known to cause familial (i.e. monogenic) PD in ~10% of all patients (Thomas and Beal 2007). These genes are intensively studied also for their contribution to idiopathic PD, since the clinical presentation of some familial cases is indistinguishable from idiopathic PD, although they display substantial differences in disease features. A good example is the pleomorphic pathology observed in PD patients carrying mutations in the *LRRK2* gene, in the presence of a clinical picture that fully overlaps idiopathic PD. Some patients show typical Lewy body (LB) pathology, while others do not (Zimprich et al. 2004). In fact, LBs are the pathological hallmark of PD and of a group of neurological disorders called synucleinopathies (Goedert et al. 2013), and are found both in idiopathic and familial PD patients. The intracellular inclusions are located in surviving neurons and contain mainly filamentous aSyn. The

pathophysiological significance and mechanisms underlying the formation and clearance of these inclusions are not clearly defined yet (Burke et al. 2008, Goedert et al. 2013, Dickson 2018), and neither is the importance of LBs to the pathogenesis of PD or their exact role in the neurodegenerative process (Lang and Lozano 1998). Clinically, PD presents with characteristic motor symptoms including resting tremor, rigidity, bradykinesia and postural instability (Lang and Lozano 1998, Corti et al. 2011).

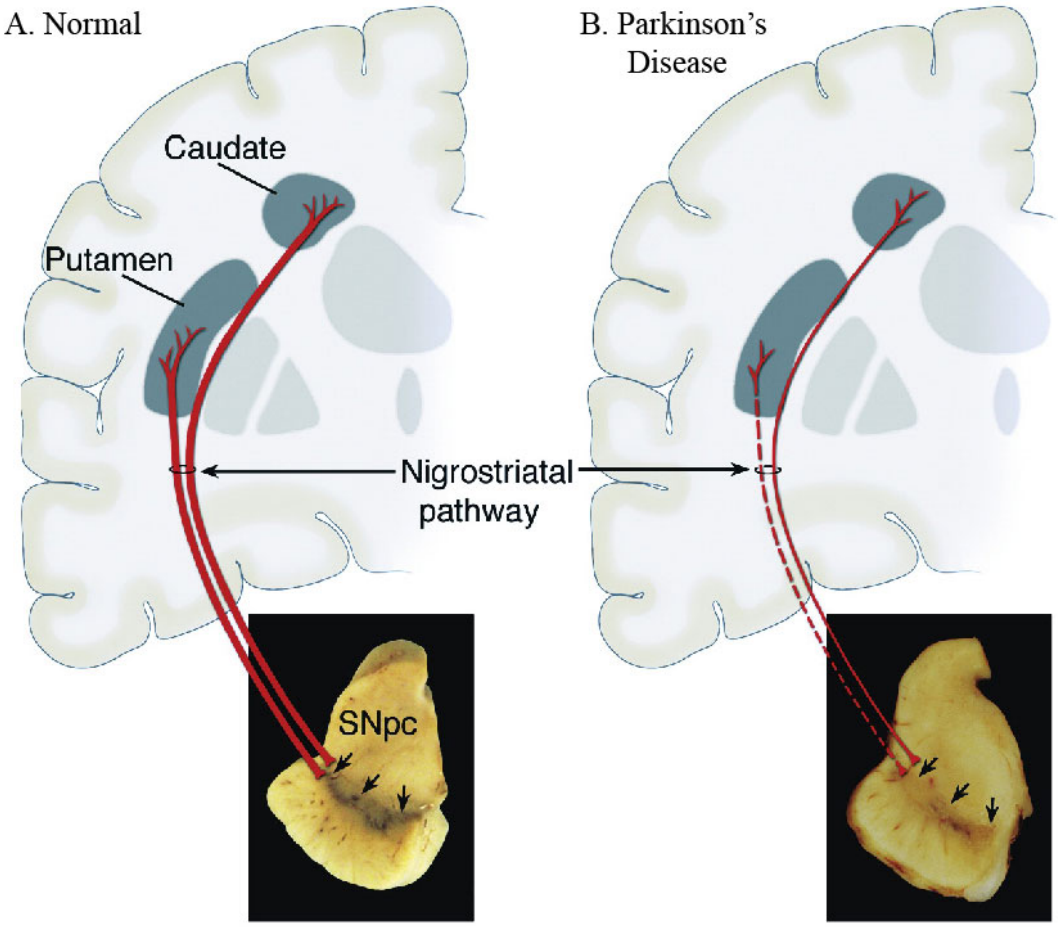

C.

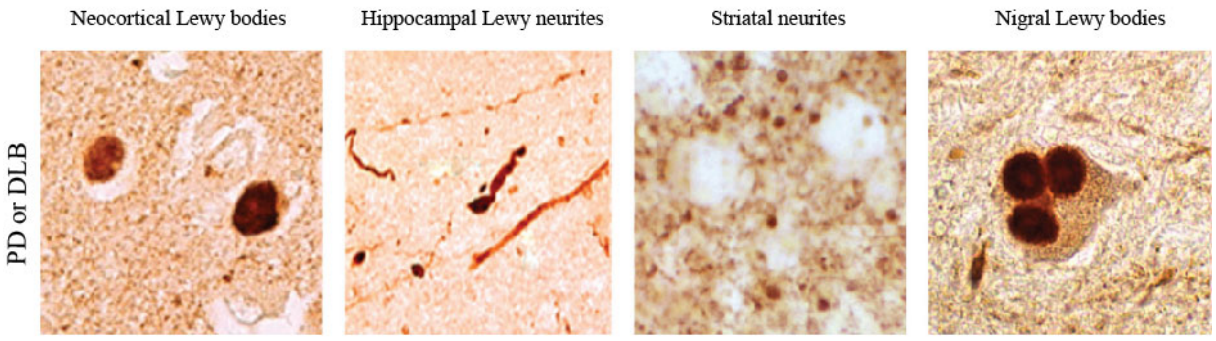

Figure 1: Nigrostriatal pathway and aSyn pathology in patients. A. Schematic representation of the nigrostriatal pathway. It is composed of dopaminergic neurons whose cell bodies are located in the SNc, which project to the basal ganglia and synapse with neurons in the striatum (i.e., putamen and caudate nucleus). B. Schematic representation of the diseased nigrostriatal pathway. Degeneration leads to a marked loss of DA neurons that project to the putamen and the caudate. A and B modified from (Dauer and Przedborski 2003). C. Human Lewy body disease presents with accumulations of insoluble α-synuclein in cell bodies (Lewy bodies) and neuronal processes (dot-like Lewy neurites). Immunostaining for full-length α-synuclein to mark Lewy bodies and Lewy neurites in the cortex, hippocampus, striatum, and substantia nigra. C modified from (Volta et al. 2015).

In addition, patients are affected by non-motor symptoms such as autonomic, psychiatric, sensory and sleep disturbances, cognitive impairments and dementia that often arise even before motor symptoms (Stern et al. 2012, Kalia and Lang 2016). The term *parkinsonism* is used to describe the clinical phenotype of patients, consisting of one or more motor symptoms, but does not implicate a progression. Contrary, in PD the motor and non-motor symptoms typically worsen along the course of the disease (Lin and Farrer 2014). Motor deficits are associated with the loss of DA neurons in the substantia nigra pars compacta (SNc) (Poewe et al. 2017, Tysnes and Storstein 2017), which is the second pathological hallmark of the disorder. Neurodegeneration typically affects the SNc, but other regions are affected by neuronal loss, particularly those brain areas that also display LB pathology (Halliday et al. 1990, Kremer and Bots 1993, Damier et al. 1999, Dijkstra et al. 2014). The SNc counts around 450.000 neurons in a healthy, adult person and the PD-associated neuronal loss leads to DA depletion most prominently in the dorsal and intermediate subdivisions of the putamen (Kish et al. 1988). As mentioned above, LBs represent one of the main pathological hallmarks of PD (Spillantini et al. 1997, Lees et al. 2009). Although they are mainly composed of aggregated aSyn, other proteins like Tau, ubiquitin or amyloid-β (Aβ) are sometimes found at the neuropathological examination, leading to classification of PD as a proteinopathy. In healthy brains, these proteins are mostly present in a monomeric, soluble form, while in PD brains a conformational change occurs triggering the formation of small oligomers, which eventually evolve into higher order structures. An analysis of the LB accumulation in PD patients by Braak and colleagues showed that neuropathology affects brain areas in a characteristic pattern, from the lower brainstem to the higher cortical areas along with disease progression, in a predictable fashion following an ascending trajectory which correlates with clinical symptoms (Braak et al. 2003). This autoptic evidence still constitutes the major foundation for the spreading hypothesis of aSyn pathology. However, the initial observations by Braak and colleagues have been contested, fuelling more hypotheses on the etiology of proteinopathy in PD (Brundin and Melki 2017, Surmeier et al. 2017, Surmeier et al. 2017) .

Table 1: PARK genes and their effect on disease inheritance, progression, response to L-DOPA treatment and LB pathology. AR = Autosomal Recessive; AD = Autosomal Dominant. Modified from (Benson and Huntley 2019)

Gene	Inheritance	Typical age of onset (years)	Progression	Response to L-DOPA	Lewy pathology	References
PARKIN/ PARK2	AR	24–40	Slow	Yes	Rare	(Kitada et al. 1998, Khan et al. 2003)
PINK1/ PARK6	AR	18–56	Slow	Yes	Yes (*n* = 1)	(Hatano et al. 2004{Valente, 2004 #122, Steinlechner et al. 2007, Samaranch et al. 2010)}
DJ-1/ PARK7	AR	24–40	Slow	Yes	Yes (*n* = 1)	(Bonifati et al. 2003, Taipa et al. 2016)
ATP13A2/ PARK9	AR	10–18	Rapid	Yes	Yes	(Ramirez et al. 2006)
FBXO7/ PARK15	AR	35–50	Slow	Yes (non pyramidal)	unknown	(Di Fonzo et al. 2009)
VPS13C/ PARK23	AR	25–46	Rapid	Yes	Yes (*n* = 1)	(Lesage et al. 2016)
SNCA/ PARK1 and PARK4	AD	35–65	Variable	Yes	Yes	(Polymeropoulos et al. 1997, Chartier-Harlin et al. 2004, Ibanez et al. 2004)
		30's	Rapid	Yes	Yes	(Singleton et al. 2003)
LRRK2/ PARK8	AD	50–65	Slow	Yes	Not always	(Paisan-Ruiz et al. 2004, Zimprich et al. 2004)
VPS35/ PARK17	AD	50–52	Slow	Yes	No (*n* = 1)	(Vilarino-Guell et al. 2011, Zimprich et al. 2011)
DNAJC/ auxillin/ *PARK19*	AR	10–42	Rapid	Mixed	unknown	(Edvardson et al. 2012)
SJ1/ synaptojanin/ *PARK20*	AR	20–30	Rapid	Yes but develop dyskinesia	unknown	(Krebs et al. 2013)

Major discoveries were also made using genome-wide association studies (GWAS), which nominated a vast number of risk loci (Pankratz et al. 2012, Nalls et al. 2014, Chang et al. 2017, Nalls et al. 2019). Of these, several contain genes that are known to cause monogenic PD (Kalinderi et al. 2016). In the most recent GWAS report, 90 loci were associated with an increased risk of developing PD, and 38 of them were newly identified. However, the biological mechanisms by which these loci influence disease risk are mostly unknown. Furthermore, the specific genetic determinants responsible for the increased risk within the associated loci, and their interactions, must be clarified to fully comprehend their impact on the development of PD.

1.1.1 Therapy

The gold standard for PD diagnosis remains the anamnestic evaluation, sometime assisted by brain imaging (DATScan), performed by a movement disorder neurology specialist, which, however, leads to a percentage of patients not being diagnosed, especially in the early stages of the disease. Indeed, the only way to confirm a diagnosis is the post-mortem brain examination to evidence LB pathology and SNc neuron loss. Interestingly, about 25% of patients are initially misdiagnosed (Lang and Lozano 1998) and the classification re-adjusted at autopsy. Therapies capable of slowing down the progression of PD are currently not available and the mainstay of symptomatic treatment remains the pharmacological replacement of DA using its precursor levodopa (L-DOPA) (Birkmayer and Hornykiewicz 1961). Over 90% of patients show a good response to levodopa treatment in the first stages of the disease (Lang and Lozano 1998). The chronic administration of levodopa can lead to severe side-effects at later stages, also caused by the need to increment doses to maintain efficacy. Another strategy is to use direct dopamine receptor agonists, which can be used in monotherapy at the early stages or in combination with L-DOPA in later phases (Rao et al. 2006). In well-selected and a minor number of patients, deep brain stimulation (DBS) is an alternative treatment option, where electrodes are implanted in specific brain areas most commonly the subthalamic nucleus (Okun et al. 2007). DBS is often effective in ameliorating symptoms, when pharmacological medication is failing (Deuschl et al. 2013). In recent years, stem cells (human embryonic stem cells – hESCs and induced pluripotent stem cells – iPSCs) revealed a new approach in disease understanding and therapy development. iPSCs can be differentiated into genetically identical neurons and drug screening assays can provide a more direct human relevance; for this reason, iPSCs are a powerful tool in drug

screening and development. These cells are also important in eventual cell replacement therapies in PD, when differentiated into DA neurons and transplanted into patients. However, grafting of cells derived from stem cells has still to overcome safety concerns (Henchcliffe and Parmar 2018).

1.2 Familial genes implicated in PD

1.2.1 Alpha-synuclein

aSyn is encoded by the *SNCA* gene and the aggregated protein is the major component of LBs. It was first identified in 1996 by linkage mapping and is the first gene linked to familial PD (Polymeropoulos et al. 1997). *SNCA* mutations (A30P, E46K, H50Q, G51D and A53T) and multiplications are causative of about 1-2% of familial PD cases (Polymeropoulos et al. 1997, Kruger et al. 1998, Singleton et al. 2003, Zarranz et al. 2004, Nishioka et al. 2009, Trinh and Farrer 2013). Moreover, an association between single-nucleotide polymorphisms (SNPs) in the *SNCA* gene and idiopathic PD has been found (Nalls et al. 2014, Chang et al. 2017, Nalls et al. 2019). The A53T mutation was one of the first ones to be identified, in a single Italian family and later in three Greek families (Polymeropoulos et al. 1997). The A30P mutation was first identified in a German family (Krüger et al. 1998). Patients carrying the A53T mutation have an earlier age of onset compared to A30P mutation carriers, who also present with a milder phenotype (Krüger et al. 1998). Patients carrying *SNCA* mutations mostly develop early-onset PD and initially respond well to L-DOPA treatment (Polymeropoulos et al. 1996). Disease onset in patients with *SNCA* gene multiplications is inversely correlated to the number of multiplications: *SNCA* duplication leads to a later age-of-onset with respect to *SNCA* triplication. Furthermore, *SNCA* triplication carriers present with a more severe disease progression, whereas patients with a gene duplication show a disease progression more similar to idiopathic patients, indicating that disease severity is correlated with aSyn protein levels (Fuchs et al. 2007). Overexpression of aSyn is known to have cytotoxic effects in cell lines, but it does not invariably cause the formation of inclusions (Hasegawa et al. 2004).

The aSyn protein consists of 140 amino acids and is expressed ubiquitously in the brain (Wersinger et al. 2004), is enriched in synaptic terminals, and seems to play important roles in learning, synaptic vesicle trafficking, neurotransmitter release and endo/exocytosis of synaptic

vesicles (Lotharius and Brundin 2002, Burré et al. 2010). Together with heat shock chaperone Hsc 70 and SNAP25, aSyn is active in the assembly of the SNARE (soluble N-ethylmaleimide-sensitive-factor attachment receptor) complex, and in synaptic vesicle exocytosis and reciprocal endocytosis (Burré et al. 2010). Furthermore, aSyn participates in cargo sorting and protein degradation as it is involved in endosome trafficking, autophagy and chaperone-mediated autophagy (CMA) (Abeliovich et al. 2000, Cuervo et al. 2004, Ebrahimi-Fakhari et al. 2011). At cellular level, aSyn is present in different structural forms, while in LBs is mostly in a fibrillary state, which results from reciprocal interactions of aSyn monomers. In neurodegenerative diseases like PD, monomeric aSyn assembles into soluble oligomers or protofibrils, a process shown to be enhanced by the A30P and A53T mutations (Conway et al. 2000). The formation of these protofibrils ultimately leads to the generation of insoluble amyloid fibrils. In addition it has been reported that aSyn oligomers are prone to be secreted via exosomes (Danzer et al. 2012) as cells and neurons can secrete aSyn via exocytosis (Emmanouilidou et al. 2010, Bellingham et al. 2012). The exact mechanisms underlying aSyn exocytosis are still under deep investigation, but this cell-to-cell transfer has been proposed to explain the spreading of LB pathology in experimental models and support the prion-like hypothesis of PD (Braak et al. 2003, Luk et al. 2012, Olanow and Brundin 2013). Furthermore, it has been reported that LB pathology spreads from affected host cells to grafted “healthy” neurons, and transplanted neurons display LB-like structures staining positive for aSyn and ubiquitin (Kordower et al. 2008, Kordower et al. 2008).

This prion hypothesis has gained momentum from research in PD showing that exogenous aSyn assemblies seed and propagate LB-like neuropathology in neuronal and animal models (Volpicelli-Daley et al. 2011, Luk et al. 2012). This was supported by parallel evidence that inclusion formation and cell death could result from neuron-to-neuron transmission of aSyn (Desplats et al. 2009), possibly as a consequence of exosomal release of pathologic forms of the protein (Danzer et al. 2012). The involvement of exosomes contributed to the increasing emphasis on the endosome-lysosome and autophagy-lysosome systems as cellular processes underlying disease onset, spreading and progression. Exosomes are vesicles released by cells in a process tightly linked to intracellular endosomal function, with their content being representative of the disease state (Tofaris 2017). Importantly, aSyn is a lysosomal substrate (Cuervo et al. 2004) and its aggregated forms resist autophagic degradation with consequent

cellular accumulation (Tanik et al. 2013). In addition, aSyn overexpression is known to lead to an increased number of autophagosomes, but this increase is not paralleled by an increased degradative capacity in cell lines (Tanik et al. 2013). Moreover, literature evidence shows that pathological aSyn reduces autophagy and causes lysosomal depletion in PD brains, cell and animal models (Chu et al. 2009, Dehay et al. 2010). Physiologically, aSyn is degraded by both the ubiquitin proteasome system (UPS) and autophagy-lysosome pathway (ALP) (Ravikumar et al. 2002, Klucken et al. 2012), but high molecular weight species of the protein, like aggregates, are specifically degraded by the ALP (Cuervo et al. 2004).

1.2.2 LRRK2

Leucine-rich repeat kinase 2 (LRRK2) is a multifunctional protein composed of a catalytic GTPase and kinase core and several protein binding domains (Paisan-Ruiz et al. 2013). It derives its name from the presence of leucine-rich repeats (LRR) and a kinase domain in its structure. The LRRK2 protein is well characterized, consisting of 2527 amino acids and 51 exons, which give rise to a 268 kDa protein (Singleton et al. 2013). The GTPase domain consists of a Ras of complex (ROC) and a C-terminal of Roc (COR) domain. Other domains occurring in the LRRK2 protein are protein-protein interaction domains (armadillo, ankyrin and LRR domains) at the N-terminal, which suggest a scaffolding function of the protein, in addition to the enzymatic activities (Marín 2006, Lin and Farrer 2014). The kinase domain (serine/threonine kinase) and the WD40 domain are located at the C-terminal. Nonetheless, the exact relationship between kinase and GTPase functions is still unresolved and one of the main controversial issues about LRRK2 biology (Islam and Moore 2017). The LRRK2 protein is able to self-interact, to form dimers, to phosphorylate substrates and to autophosphorylate (Abou-Sleiman et al. 2006, Greggio et al. 2008).

LRRK2 is expressed in different brain regions, including the substantia nigra, striatum and other cortical regions, and is present at the synapse. Several are the cellular functions modulated by LRRK2, with a strong indication for synaptic transmission (Piccoli et al. 2011, Beccano-Kelly et al. 2014, Volta and Melrose 2017), vesicle trafficking (Cookson 2016) and autophagy (Manzoni and Lewis 2017). Interestingly, these pathways might converge in neuronal biology and function (Inoshita et al. 2017). Furthermore, LRRK2 is involved in neurite outgrowth in primary cultures and *in vivo* (Plowey et al. 2014) (Biskup et al. 2006). Neurons derived from

iPSCs carrying the G2019S LRRK2 mutation display reduced neurite outgrowth, increased sensitivity to stress and defects in autophagy, contributing to increased aSyn protein levels (Reinhardt et al. 2013). LRRK2 orthologs in *D. melanogaster* and *C.elegans* were also shown to participate in synaptic vesicle trafficking (Lin and Farrer 2014). Both upregulation and downregulation of LRRK2 kinase activity have an impact on vesicle trafficking at nerve terminals, which indicates a tight regulation of LRRK2 kinase function in synaptic vesicle trafficking (Esposito et al. 2012).

As mentioned earlier, LRRK2 has been proposed to directly phosphorylate several putative substrates, including LRRK2 itself, suggesting multiple roles for the protein (Islam and Moore 2017). Recent work revealed that members of the Ras analog in brain (Rab) family of small GTPases are the true *bona fide* substrates for LRRK2 (Steger et al. 2016, Lis et al. 2018). Rab proteins are the largest group among the Ras superfamily and are known to be key regulators of intracellular membrane trafficking. They are expressed in all cell types, but where first discovered in brain tissue (Zhen and Stenmark 2015, Pfeffer 2017). LRRK2 interacts with different Rab GTPases, indicating its contribution in intracellular trafficking. Rab5b, a protein known to regulate endocytic vesicular transport, co-localizes with LRRK2 on synaptic vesicles, supporting a role of LRRK2 in synaptic vesicle trafficking (Shin et al. 2008). Rab7L1, nominated in PD GWAS, was found to interact with LRRK2, impacting neurite outgrowth and vesicle trafficking directed to the Golgi apparatus (MacLeod et al. 2013). More recently, it has been reported that Rab7L1 activates LRRK2 and downstream phosphorylation of Rab10 and Rab8a (Purlyte et al. 2018).

The LRRK2 gene was identified to be located at the PARK8 locus in 2004 and was linked to autosomal-dominant inherited familial late-onset PD. Patients with LRRK2 mutations show a clinical phenotype similar to idiopathic patients and generally respond well to L-DOPA therapy (Wallings et al. 2015). The discovery of LRRK2 was the first evidence that a genetic defect could be found in familial and sporadic PD (Kalinderi et al. 2016). All mutations occur in the enzymatic core of LRRK2 (e.g. G2019S and I2020T in the kinase domain and R1441C/G/H, R1628P and Y1699C in the GTPase domain) (West et al. 2005, Gloeckner et al. 2006, Daniels et al. 2011, Wallings et al. 2015, Shu et al. 2016). About 6% of familial and 3% of sporadic PD cases in Europe and North America are associated to the G2019S mutation and up to 30% of PD cases in specific populations (Lesage et al. 2006, Ozelius et al. 2006, Lin and Farrer 2014,

Kalinderi et al. 2016). People carrying this mutation have a higher risk of developing PD (28% higher at age 60 and 74% higher at age 79). The G2019S mutation is the most common genetic cause of PD (Trinh and Farrer 2013) and exerts its pathogenicity through an increase of kinase activity (about 3-fold), causing neurite degeneration and neuronal cell death (Smith et al. 2006). Therefore, new therapeutic approaches, based on kinase inhibition or silencing have been proposed for PD (Greggio et al. 2006, Lees et al. 2009, Lin and Farrer 2014). On the other hand, kinase-dead variants of LRRK2 or pharmacological treatment with kinase inhibitors lead to peripheral dysfunctions, suggesting that LRRK2 function is important in cellular homeosthasis and cannot be completely ablated (Cookson 2015). Adjacent to the G2019S substitution, a second mutation (I2020T) was discovered (Zimprich et al. 2004). Both mutations are associated with a toxic gain of function, resulting in an increased kinase activity (West et al. 2005). The other LRRK2 mutations are far less frequent. Mutations located in the ROC/COR domains (R1441C/G/H) lead to a decrease in the GTPase activity of the protein (Lewis et al. 2007) and affect the same Arginine residue, defining this codon as a hotspot for PD (Tsika and Moore 2013). The differences in disease development and the end-stage pathologies caused by the different mutations could be attributed to changing genetic and environmental factors and indicate that LRRK2 is implicated in multiple signaling pathways (Kalinderi et al. 2016).

Numerous studies have reported an involvement of LRRK2 and its mutants in the modulation of ALP machinery and autophagic process, also suggesting that kinase activity plays a key role in autophagy (Alegre-Abarrategui et al. 2009, Manzoni et al. 2013, Saez-Atienzar et al. 2014, Manzoni and Lewis 2017, Eguchi et al. 2018, Schapansky et al. 2018, Wallings et al. 2019). Mutant LRRK2 produces an aberrant autophagic function, specifically impairing CMA and macroautophagy and the processing of aSyn (Bravo-San Pedro et al. 2013, Manzoni et al. 2013, Orenstein et al. 2013, Beilina et al. 2014, Ho et al. 2019). LRRK2 favors the accumulation of pathological aSyn (Volpicelli-Daley et al. 2016, Zhao et al. 2017) and LRRK2 kinase inhibition is beneficial against this neuropathology (Volpicelli-Daley et al. 2016). LRRK2 also affects lysosome biology in different models, causing reduced lysosome function (MacLeod et al. 2013, Henry et al. 2015, Hockey et al. 2015, Schapansky et al. 2018). Specifically, the overexpression of LRRK2 causes an increase in lysosomal size and number in human fibroblasts and astrocytes (MacLeod et al. 2006, MacLeod et al. 2013, Henry et al. 2015, Hockey et al. 2015). In contrast, Schapansky et al showed a reduction in lysosomal size in G2019S LRRK2 knock-in primary

neurons (Schapansky et al. 2018). A possible explanation for these opposite results could lie in the different models used. However, the increase in the number of lysosomes per cell seems to be consistent in all cell models analyzed. One explanation might be the upregulation of lysosome biogenesis, taking place as a compensatory mechanism. These data indicate that LRRK2 functions as a negative regulator of the lysosomal system and that G2019S mutation exacerbates this function leading to lysosomal impairment (Henry et al. 2015). The regulation of ALP by LRRK2 is a common and accepted process, however precise mechanisms are still unknown.

1.3 Autophagy

In cells, two different pathways mediate the removal of unwanted materials, including proteins: autophagy and the UPS/unfolded protein response (UPR) (Cortes and La Spada 2014). Autophagy is divided into three types, based on how the cargo is delivered to the lysosome (the common effector): macroautophagy, microautophagy and CMA. During macroautophagy a double-membrane sequestering compartment forms in the cytosol, matures to an autophagosome and ultimately fuses with the lysosome, forming the autolysosome (Feng et al. 2014). In microautophagy cytoplasmic content is directly engulfed by the lysosome (Li et al. 2012). CMA is a highly selective process in which proteins with a specific amino acid motif (KFERQ-like motif) are recognized by chaperone proteins and transported directly to the lysosome (Kon and Cuervo 2010). Macroautophagy, the best characterized type of auotophagy, is a powerful evolutionarily conserved catabolic process that mediates the degradation of unnecessary and dysfunctional proteins or organelles. Autophagy is widely studied, since the process or its dysregulation is relevant in many diseases (Ravikumar et al. 2010, Choi et al. 2013) and it is highly dynamic and can be modulated at different levels (Klionsky et al. 2016). The term autophagic flux refers to the whole process, roughly divided in inclusion of the cargo, trafficking to the lysosome and final degradation of the cargo into the lysosome. The process of autophagy begins with the formation of a double-membrane vesicle, termed autophagosome, through the extension of an isolation membrane (phagophore). This process can be broadly divided in nucleation and elongation of the isolation membrane, which are regulated by distinct sets of autophagy-related (Atg) genes. Over two decades ago, the first Atg genes were identified in yeast (Tsukada and Ohsumi 1993) (Klionsky et al. 2003). The ULK (Unc-51 Like

Kinase)/Atg1 kinase complex and the autophagy-specific phosphatidylinositide 3-kinase complex are important for the nucleation step, while Atg12- and Atg8/LC3-conjugation systems are essential for elongation. Once Atg8/LC3 is lipidated and incorporated into the phagophore membrane, the growing membrane engulfs cytoplasmic content destined for degradation. The newly formed autophagosome has an average size of 0,5 to 1,5 μm in mammals (Pfeifer 1978). The autophagosome might fuse with endosomes (to form amphisomes) or directly fuse with lysosomes to form autolysosomes, where the degradation of the cargo into amino acids and other small molecules takes place (Mizushima et al. 2011). The acidic lysosomal lumen and hydrolyases degrade first the inner membrane of the autophagosome and then the cargo, which are recycled and provide building blocks for the cells to produce new molecules (Yorimitsu and Klionsky 2005). A hierarchical analysis of ATGs indicated that ULK1, ATG14, WIPI1, LC3 and ATG16L1 are required to form the ULK complex, being the most upstream complex (Itakura and Mizushima 2010).

Autophagosomes often converge with endocytic vesicle trafficking and the movement of the organelles depends on microtubules and motor proteins (Monastyrska et al. 2009). Autophagy is regulated by a wide range of cellular signals, such as cellular stress, nutrient starvation, growth factors, hypoxia or ER stress. Induction of autophagy via mTOR is dependent on nutrient availability and the increase of unfolded proteins can induce autophagy, through induction of ER stress (He and Klionsky 2009). The coordinated lysosomal expression and regulation (CLEAR) network regulates lysosome and autophagosome biogenesis (Palmieri et al. 2011) and TFEB is the master regulator of this network, inducing the expression of ATG genes (Settembre et al. 2011). TFEB activity is regulated by its cellular localization: activation leads to translocation from the cytoplasm to the nucleus, where TFEB promotes the transcription of genes involved in lysosomal biogenesis (Settembre and Ballabio 2011). Unspecific bulk degradation is a feature of autophagy, although autophagy can also be directed towards specific cargos/organelles, such as peroxisomes (pexophagy), mitochondria (mitophagy) and ubiquitinated proteins (Kim et al. 2007, Weidberg et al. 2011, Till et al. 2012). Ubiquitinated proteins are recognized by SQSTMq/p62, which is one adapter protein interacting with LC3 (Vadlamudi et al. 1996, Bjorkoy et al. 2005). This type of cargo specificity is of importance in diseases, where aggregated (ubiquitinated) proteins accumulate, such as PD.

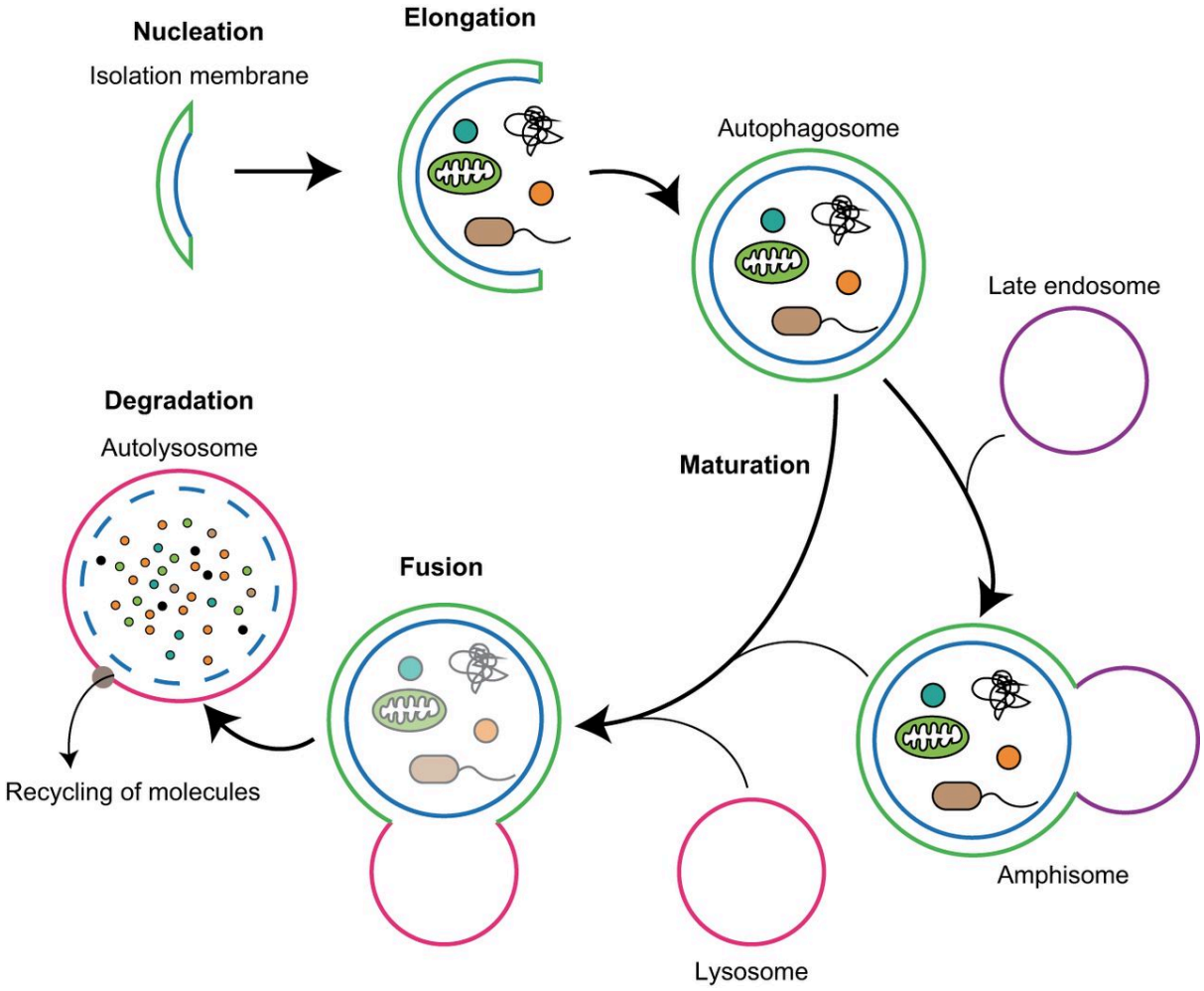

Figure 2: Overview of macroautophagy. Upon induction of autophagy, cargos (protein aggregates, organelles, etc.) are sequestered by a double-membrane structure, called autophagosome. These autophagosomes fuse with late endosomes to become amphisomes and finally with lysosomes to become autolysosomes, where cargo is finally degraded and recycled (Nakamura and Yoshimori 2017).

1.3.1 Autophagy in PD

Generally, the steady-state levels of cellular proteins is controlled by their rates of production and degradation (Hetz and Glimcher 2011). Therefore, either reducing production or stimulating degradation appeared to be promising strategies to prevent or reverse uncontrolled aSyn accumulation (Devine et al. 2011). In PD research, ALP is emerging as the process mostly involved in the clearance of pathological aSyn (Cuervo et al. 2004, Chu et al. 2009). In recent years, autophagy has been accepted as a cellular process deeply involved in the pathogenesis of both familial and idiopathic PD. Consistently, deletion of autophagic genes in mice caused locomotor defects, accumulation of polyubiquitinated proteins and neurodegeneration (Hara et

al. 2006). In addition, post-mortem evidence showed perturbation of autophagy markers in different neurodegenerative disorders (Anglade et al. 1997, Sasaki 2011, Piras et al. 2016). Observations in PD brain tissues suggest an aberrant regulation of autophagy associated with the aggregation of aSyn (Dehay et al. 2010). Moreover, an important role for autophagy in brain is highlighted by the observation that this organ is the most severely affected in lysosomal storage disorders (Nixon 2013). The most significant evidence of the negative impact of lysosome dysfunction emerged from the finding that heterozygous mutations in the *GBA* gene, encoding the lysosomal hydrolase Glucocerebrosidase (GCase), compromise its function and augment the risk of developing PD by approximately 20-fold (Sidransky et al. 2009). Additionally, it is known that the autophagic machinery becomes less efficient with aging in the healthy brain and stimulation of autophagy promotes longevity in some animal species (Lipinski et al. 2010, Rubinsztein et al. 2011).

Furthermore, PD-related proteins are being combined into a common pathway, related to the ALP. For example, LRRK2 mutations enhance protein levels of the lysosomal cation pump ATP13A2 (Henry et al. 2015). Loss of function mutations in its coding gene are associated with parkinsonian Kufor-Rakeb syndrome and trigger alkalinisation of lysosomes (Appelqvist et al. 2013). The G2019S mutation induces lysosomal deficits in different cell models (Sanchez-Danes et al. 2012) and upregulation of ATP13A2 could represent a compensatory mechanism as overexpression of ATP13A2 is thought to rescue lysosome dysfunction (Dehay et al. 2012). Another example is the ATP6V0A1 gene that was recently associated with PD by GWAS (Chang et al. 2017). Furthermore, it has been recently demonstrated that both WT and G2019S LRRK2 bind to ATP6V0A1, which is abolished by the R1441C mutation (Wallings et al. 2019).

1.4 RIT2

Variability in the *RIT2* (Ras-like without CAAX 2) gene locus has been first associated with an increased risk of developing PD in 2012, and then replicated in several GWAS studies (Pankratz et al. 2012, Nalls et al. 2014, Nalls et al. 2019). In addition, the *RIT2* locus was replicated in several smaller population GWAS (Emamalizadeh et al. 2014, Liu et al. 2015, Nie et al. 2015). Furthermore, the *RIT2* gene has been reported to be associated with Autism Spectrum Disorders and schizophrenia (Glessner et al. 2010, Hamedani et al. 2017). Two patients presenting with

speech limitations and seizures displayed deletions in the chromosomal region containing the *RIT2* gene, among others (Bouquillon et al. 2011).

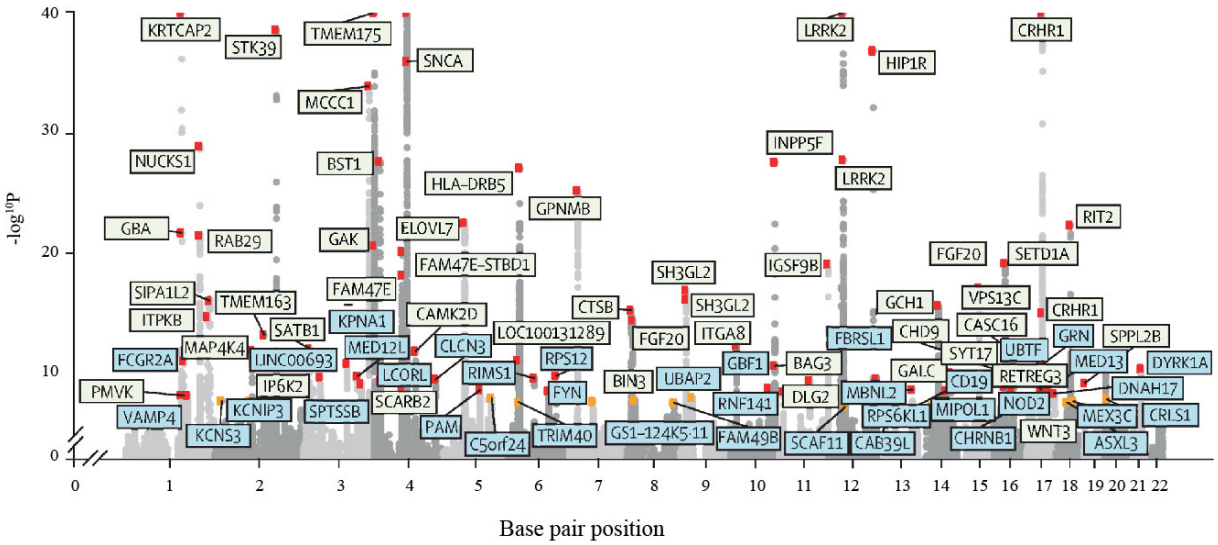

Figure 3: Manhattan plot summarizing results of the latest PD GWAS. The nearest gene to each of the 90 significant variants is labelled (green for previously identified loci, blue for novel loci). Variant points are colour-coded red and orange, with orange representing significant variants at $p=5 \times 10^{-8}$ and 5×10^{-9} and red representing significant variants at $p<5 \times 10^{-9}$. The X-axis represents the base pair position of variants from smallest to largest per chromosome (1–22) (Nalls et al. 2019).

RIT2 codes for the protein Rin, a member of the novel Rit subfamily of Ras-like small GTPases together with its homolog Rit (coded by the *RIT1* gene) (Shi et al. 2013). Both of them are localized at the plasma membrane despite the lack of C-terminal lipidation, a modification usually required for membrane association (Spencer et al. 2002). Ras proteins are implicated in a plethora of cellular processes, where they function as molecular switches between an active guanosine triphosphate- (GTP)-bound and an inactive guanosine diphosphate (GDP)-bound state (Simanshu et al. 2017). The cycle between active and inactive states is regulated by the interaction of Ras proteins with specific guanine nucleotide exchange factors (GEFs) and GTPase-activating proteins (GAPs) (Bos et al. 2007, Cherfils and Zeghouf 2013). Both Rit and Rin participate in mitogen-activated protein kinase (MAPK) signaling via activation of p38 and extracellular signal-regulated kinase 1/2 (ERK1/2) to modulate neurite outgrowth and differentiation (Shi and Andres 2005, Shi et al. 2005). A study conducted by Uenaka et al. aiming to identify candidate drugs for PD by using GWAS data and *in silico* databases,

demonstrated that dabrafenib, a B-Raf kinase inhibitor, exerts protective effects in RIT2 KO cells. The protective effect was attributed to an increase in ERK phsosphorylation, however an effect on cell viability is observed only in the presence of RIT2 (Uenaka et al. 2018).

Rit is expressed in all organs and throughout developmental stages, whereas Rin shows specific neuronal expression, which increases throughout postnatal development and peaks in the adult life (Spencer et al. 2002, Shi et al. 2013, Zhang et al. 2013). Disease-associated genetic alterations in *RIT2* may alter its expression levels (Emamalizadeh et al. 2017), possibly via length differences in short tandem repeats within its promoter. The *RIT2* promoter contains one of the longest short tandem repeats (11 repeats) and homozygosity for a 5-repeat allele has been reported to decrease gene expression and has been associated with schizophrenia (Emamalizadeh et al. 2017). Moreover, it has been reported that the POU4 family of transcription factors modulate *RIT2* expression (Zhang et al. 2013). Rin is enriched in rodent DA neurons, indicating it might be involved in the maintenance and survival of DA neurons in the adult rodent brain (Zhou et al. 2011). Moreover, Rin interacts with the DA transporter (DAT) and regulates its internalization (Navaroli et al. 2011). A recent study reported that the conditional KO of *RIT2* decreases DAT levels in the striatum of male mice, indicating a sex-specific role for *RIT2* expression in DA neurons and DA-dependent behavior (Sweeney et al. 2019). Interestingly, the SNc of PD patients presents reduced RIT2 expression (Bossers et al. 2009). It can be speculated that the homolog Rit has its major function in enhancing neuronal survival during oxidative damage through activation of p38 (Cai et al. 2012, Cai et al. 2012), but the precise roles of Rin are mostly unknown. The previously mentioned findings suggest Rin might play an important role in SNc neuron physiology and thus be involved in PD-relevant biological pathways.

2 Materials and methods

2.1 Cell lines and culture methods

SH-SY5Y wildtype (WT) Cell bank IRCCS AOU San Martino IST (Biedler et al. 1973)
SH-SY5Y stably expressing WT LRRK2 and G2019S LRRK2
Department of Neurosciences - KU Leuven (Vancraenenbroeck et al. 2014)

Control SH-SY5Y cells were maintained in DMEM GlutaMAX (Gibco, 10566016) medium, supplemented with 10% fetal bovine serum (FBS; Sigma-Aldrich) and 1% penicillin/streptomycin (Gibco, 15140122). SH-SY5Y neuroblastoma cell lines stably overexpressing WT or G2019S-LRRK2 were maintained in DMEM GlutaMAX with 15% FBS, 1% non-essential amino acids, 50 µg/ml gentamycin (Caelo) and 200 µg/ml hygromycin B (Invitrogen). All cells were incubated at 37°C with 5% CO_2 and passaged two to three times a week depending on confluency using Trypsin-EDTA 0.05% (Gibco, 25300054).

2.1.1 Pharmacological treatments

The LRRK2 kinase inhibitor PF-06447475 (herein, PF-475, Pfizer) was dissolved in DMSO at a concentration of 10mM under sterile conditions. PF-475 was diluted in DMSO and applied to cultured cells for 2h or 6h at 300 or 500 nM, while 0.1% DMSO was used as vehicle control for all experiments.
Chloroquine (CQ; ThermoFisher L10382) in aqueous solution at a stock concentration of 30mM was used to block the fusion of autophagosomes with lysosomes and to evaluate the autophagic flux in cells. CQ was applied for 3 hours at a concentration of 100 µM in complete medium for immunocytochemistry (ICC) experiments and at the same concentration for 6 hours for western blot experiments.

2.1.2 Nucleofection of *RIT2* into G2019S LRRK2 overexpressing cells

Human *RIT2* plasmid (SC118279, Origene) was transfected using the Nucleofector™ technology from Lonza (Walkersville). Cells were detached, counted and 200.000 cells were pelleted for 10 minutes at 200xg. The cell pellet was carefully resuspended in 20 µl of

nucleofection solution (16,4 µl SF Cell Line Solution + 3,6 µl Supplement) containing 800 ng DNA and the cell suspension was then transferred to a 16-well strip and nucleofected using the CA-137 program on the X-unit. After nucleofection the reaction was incubated for 10 minutes at RT and then 80 µl of complete plating medium were added to the well. Cells were plated in an appropriate slide for subsequent experiments, which were carried out 72 hours after nucleofection.

2.2 Western blotting

Western blotting was used to investigate protein levels under different conditions or treatments. Cells were lysed in RIPA lysis buffer (ThermoFisher) containing protease inhibitors (cOmplete tablets; Roche) and phosphatase inhibitors (PhosSTOP; Roche) and incubated on ice for 30 minutes. Then, lysates were sonicated for 10 seconds at 10% intensity, centrifuged at 10.000xg for 10 minutes at 4°C and the supernatant transferred to a new tube. Protein concentration of the lysates was determined against a bovine serum albumin (BSA) standard curve (2.000, 1.000, 750, 500, 250, 125, 25 µg/ml Albumin Standard in ddH_2O) using the Pierce™ bicinchoninic acid (BCA) Protein Assay Kit (ThermoFisher). Samples, blank control and standards (10 µl each) were pipetted in a transparent 96-well plate. To each well 200 µl of BCA working reagent (50 parts of BCA Reagent A with 1 part of BCA Reagent B) were added and then the plate was incubated for 30 minutes at 37°C. Absorbance was measured using the Envision plate reader (Perkin Elmer) at 562 nm. Protein concentration was determined using a linear regression of the standard curve.

Cell lysates containing the same amount of protein (15 µg for total protein, 30 µg for phosphorylated proteins) were heated in LDS sample buffer (NuPAGE) containing 50 mM dithiothreitol (DTT) at 95°C for 5 min and loaded onto a NuPAGE™ 4-12% Bis-Tris Protein Gels (Invitrogen). Dependent on the size of the protein of interest, MOPS (for high molecular weight proteins like LRRK2; over 100 kDa) or MES (low molecular weight proteins like LC3B) running buffer (Invitrogen) was used and 500 µl of NuPAGE™ Antioxidant (Invitrogen) was added to the inner electrophoresis chamber. Samples were separated for 5 minutes at 100 V and then about 60 minutes at 150V. After gel electrophoresis the proteins were transferred onto a polyvinylidene difluoride (PVDF) membrane (BioRad): high molecular weight proteins were

transferred overnight at 100 mA at 4°C, whereas low molecular weight proteins were transferred during three hours at 300 mA at 4°C. Transfer efficiency was controlled with Ponceau S staining (5 minutes incubation), then membranes were washed in ddH2O and finally in 1x TBS, before they were blocked in 5% milk in 1x TBS-Tween 1% (TBS-T) for one hour. Primary antibodies were incubated in 5% milk in TBS-T overnight at 4°C on an orbital shaker. After three washing steps in TBS-T, the secondary antibody was incubated in 5% milk for two hours at RT. Then membrane was washed three times in TBS-T and chemiluminescence images were acquired using Chemidoc Touch (BioRad) and relative band intensity levels were calculated using ImageLab software (BioRad).

Primary antibodies:

rabbit anti-LC3B	1:2.000	Cell Signaling Technologies, # 3868
rabbit anti-LRRK2	1:250	Abcam, ab133474
rabbit anti-pS1292 LRRK2	1:1.000	Abcam, ab203181
rabbit anti-pS935 LRRK2	1:1.000	Abcam, ab133450
Mouse anti-aSyn	1:2.000	Abnova, MAB5383
Mouse anti-β-actin	1:6.000	Sigma, A2228

Secondary antibodies:

rabbit anti-mouse IgG Antibody, HRP conjugate	1:10.000	Millipore, AP160P
mouse anti-rabbit IgG Antibody, HRP conjugate	1:10.000	Millipore, AP188P

2.3 Immunofluorescence (IF), confocal imaging and image analyses

Cells, plated on glass coverslips (12 mm), were fixed in 4% paraformaldehyde (PFA) in 1x PBS for 20 minutes at RT and then washed 3x5 minutes in 1x PBS. Then cells were permeabilized for 5 minutes with 0,5% Triton X-100 in 1x PBS at RT and then blocked in 3% BSA in 1x PBS for 30 minutes at RT. After blocking, cells were incubated with primary antibodies diluted in 0,05% Triton X-100 in 1x PBS shaking overnight at 4°C. The following day, after 3x 5 minutes washing with 1x PBS, cells were incubated with secondary fluorescent antibodies in 0,05% Triton X-100 in 1x PBS for 2h at RT. Cells were washed 3x 5 minutes in 1x PBS and in the last

wash step NucBlue™ Fixed Cell ReadyProbes™ Reagent (ThermoFisher, R37606) was added to stain nuclei. Coverslips were mounted using fluorescent mounting medium (Dako) and then sealed with nail polish.

Primary antibodies:

rabbit anti-LC3B	1:2.000	Molecular Probes, L10382
mouse anti-pS129-aSyn	1:2.000	Abcam, ab184674
rabbit anti-LRRK2	1:250	Abcam, ab133474

Secondary antibodies:

Donkey anti-Rabbit Secondary Antibody, Alexa Fluor 488	1:1.000	A-21206, Life Technologies
Donkey anti-Mouse Secondary Antibody, Alexa Fluor 488	1:1.000	A-21202, Life Technologies
Donkey anti-Mouse Secondary Antibody, Alexa Fluor 555	1:1.000	A31570, Life Technologies

Visualization of IF was performed using a Leica SP8-X confocal laser scanning microscope system equipped with a 63x oil immersion objective. Images were analysed as projected stacks with custom pipelines in CellProfiler (Kamentsky et al. 2011).

2.4 Lysotracker Deep Red staining

To investigate lysosome morphology and number, the Lysotracker Deep Red dye (Molecular Probes, L12492) was used. Cells were plated in slides for live imaging (µ-Slide, Ibidi) and treated accordingly to the experimental plan. On the day of experimentation cells were washed twice with 1x HBSS (Gibco) and then incubated with Lysotracker dye at a final concentration of 50nM in HBSS for 20 min at 37°C. After the incubation cells were washed twice more with HBSS and then imaged in complete medium containing DAPI for live imaging (Invitrogen, R37605). Cells were visualized live on the confocal microscope at 63X magnification, using the

resonant function. Single stacks were reconstructed in Imaris software (BitPlane) to a 3D structure and number and diameter of lysosomes quantified by the software.

2.5 DQ-Red-BSA assay

To study the proteolytic activity of lysosomes, the fluorescent DQ-Red-BSA (Frost et al. 2017) (Molecular Probes, D12051) was used. DQ Red BSA powder was dissolved at a concentration of 1 mg/ml in sterile PBS and covered with foil. Cells were plated in slides for live imaging and on the day of experimentation, cells were incubated with the DQ-Red-BSA in complete medium for 120 min at 37°C. After the incubation cells were washed 3x with PBS and then imaged in complete medium containing DAPI for live imaging. Images were acquired using the confocal microscope at 63X magnification. Projected stack images were then analysed with CellProfiler to quantify the number of fluorescent spots.

2.6 Analysis of autolysosome formation with GFP-LC3-mCherry reporter

To assess autolysosome formation, a GFP-LC3-mCherry reporter construct, where GFP fluorescence is pH-sensitive, was employed. In the cytosol and in autophagosomes, both GFP and mCherry fluorophores are active and both green and red fluorescence are detected. Upon fusion of the autophagosome with the lysosome and formation of the autolysosome, the pH of the vesicle turns acidic and quenches the GFP signal. Thus, autolysosomes are defined as mCherry-positive spots in confocal images. The GFP-LC3-mCherry construct was transfected in WT-, G2019S-LRRK2 and SH-SY5Y cells using FuGene HD (Promega). 150.000 cells were plated in 24-well plates on glass coverslips. The next day cells of one well were transfected using 800 ng of the GFP-LC3-mCherry plasmid. DNA was diluted in 40 µl of OptiMEM (Gibco) and then 4,16 µl of Fugene HD were added directly to the solution. Transfection mix was incubated for 15 minutes at RT and then added dropwise to the cells. After 48 hours of expression, cells were fixed with 4% PFA. Images were acquired with the confocal microscope and analysed with CellProfiler, determining the turnover from autophagosomes to autolysosomes (red/green ratio) and the total number of autolysosomes (red spots).

2.7 RNA extraction

Total RNA was extracted from cells using the RNeasy Plus Mini kit (Qiagen). The cell pellet (about $2x10^6$ cells) was resuspended in 600 µl RLT Plus buffer containing β-mercaptoethanol (1%) and then transferred to a gDNA Eliminator spin column and centrifuged for 30 seconds at 8000 x g. The flow through was then mixed with one volume of 70% ethanol and applied to the RNA extraction column and centrifuged for 30 seconds at 8000 x g. Flow through was discarded, 700 µl of wash buffer RW1 were applied to the column and centrifuged for 30 seconds at 8000 x g. Two washing steps with RPE buffer followed, flow through was discarded each time and after the second step the centrifugation time was increased to 2 minutes to dry the RNA-binding membrane. Total RNA was eluted in 30 µl of nuclease free water. RNA concentration was determined using Nanodrop and RNA quality was assessed using the Experion device (BioRad).

2.8 Reverse transcription of RNA

The SuperScript® VILO™ cDNA Synthesis Kit (Invitrogen) was used to generate first-strand cDNA out of single-stranded RNA. The RT+ reaction mix, which contained all components and which was then used for further reactions was prepared as follows:

5x VILO reaction mix	4 µl
10x Superscript enzyme mix	2 µl
Total RNA	1 µg
Nuclease-free water	up to 20 µl

As negative control (RT-) the reaction was prepared without the 10x Superscript enzyme mix. This mix was prepared as follows:

5x VILO reaction mix	4 µl
10x Superscript enzyme mix	0 µl
Total RNA	400 ng
Nuclease-free water	up to 20 µl

Reverse transcription cycling conditions (Thermocycler Mastercycler® pro; Eppendorf) were:

25°C	10 min
42°C	60 min
85°C	5 min
4°C	∞

2.9 Quantitative PCR

Quantitative real-time PCR (qPCR) allows to detect and quantify the different expression levels of genes of interest. qPCR primer and the All-in One qPCR mix from GeneCopoeia were used in combination for the quantification of mRNA expression levels. The relative quantification was calculated using a reference or housekeeping gene (β-actin).

The reaction was prepared as follows:

2x All-in-One™ qPCR Mix	10 µl
All-in-One™ qPCR Primer	0,2 µM
cDNA Mix	16 ng
Nuclease-free water	up to 20 µl

cDNA mix from reverse transcription was first distributed on a 96-well plate (Hard-Shell®PCR plate GRN/WHT, Bio-Rad), then the reaction mix for each gene of interest (containing qPCR mix, primer and water) was added to the selected wells. Plate was sealed with a microseal® B (Bio-Rad) and spun down briefly. A 3-step detection method was used.

Pre-denature	95°C	10 min		
Denature	95°C	10 sec		
Annealing	60°C	20 sec		40x cycles
Extension	72°C	15 sec	*detection*	
Melting curve				
72°C – 95°C	0,5°C/step	6 sec/step	*detection*	
30°C		30 sec		

Data were examined using the Bio-Rad CFX manager. Expression levels data (Ct values) were analysed as follows. Each sample was run in triplicates, the geometric mean calculated and used for further calculations. To quantify the differences in gene expression the Livak Method (Livak and Schmittgen 2001) was used, which assumes that the amplification efficiency is 100% and determines the relative difference between reference and target gene expression. In relative quantification the Ct values of the tested sample are compared to that of a calibrator to identify differences in gene expression. This provides a relative value of change in the expression level of a gene.

$\Delta(test\ or\ Calibrator) = mean\ Ct(gene\ of\ interest) - mean\ Ct(reference)$

$\Delta\Delta Ct = \Delta(test) - \Delta Ct(Calibrator)$

$Fold\ Change = 2 - \Delta\Delta Ct$

The reference gene was selected using the NormFinder software (Andersen et al. 2004). NormFinder estimates both the intragroup and intergroup variance and identifies the most stable reference gene, which was selected out of a set of four housekeeping genes (*ACTB, GAPDH, HPRT, TBP*). The NormFinder Excel macro processes data provided in a linear scale and Ct values were converted using the following equation:

$RQ = ½(Ct - Ct\ min)$

Ct min is the lowest Ct value for a target gene across the sample set and Ct is the Ct for the same target in all other samples.

2.10 Digital droplet PCR (ddPCR)

Absolute *RIT2* mRNA gene expression was assessed using 9 ng of cDNA for each reaction (Hs01046671_m1, FAM, BioRad) and multiplexed with a housekeeping gene (RPP30, 10031243, HEX, BioRad). PCR was carried out as indicated by the manufacturer using ddPCR Supermix for probes (BioRad, 11969064001). For droplet formation, Droplet Generation Oil for probes was used (BioRad, cat# 1863005). Droplet formation and PCR readout were carried out in BioRad systems for ddPCR. PCR reaction mix was prepared as follows:

2x Supermix for probes	11 µl
RPP30 probe	0,55 µl
Rit2 probe	1,1 µl
cDNA 1ng/µl	9,35 µl

PCR program:

95°C	10 min	
94°C	30 sec	x 40 cycles
60°C	1 min	
98°C	10 min	
4°C	∞	

After PCR amplification, the plate was analyzed in the QX200 Droplet Reader. Experiment Type was "ABS" (absolute quantitation) and fluorescence was read in FAM/HEX channels. Data was analyzed using QuantaSoft^{TM} software from BioRad. Amplitude threshold in Channel 1 and 2 was set individually for each channel. Results are reported as Ratio or Fractional abundance of gene of interest with respect to housekeeping gene.

2.11 Autophagy gene expression array

Total RNA was extracted using the RNeasy Plus Mini Kit (described in 2.7). RNA concentration was quantified with QuantiFluor® RNA System (Promega). 1x Tris-EDTA (TE) buffer was prepared from 20x TE stock. Working solution was prepared by diluting QuantiFluor® RNA Dye 1:400 in 1X TE. RNA standard curve was obtained by serial dilution of QuantiFluor® RNA Standard (100ng/µl):

Standard	Final RNA concentration [ng/µl]
A	50
B	25
C	12,5
D	6,25
E	3,125
F	1,56
G	0,78

200µl of QuantiFluor® RNA Dye working solution were pipetted into single wells of a black 96-well plate. 10µl of the standard curve were dispensed in duplicate to the plate, 10 µl of 1x TE were used as blank and 1 µl of sample were added to the RNA dye working solution. The plate was mixed using a plate shaker and then incubated for 5 minutes at RT, protected from light.

Fluorescence was measured (492 nm Ex/540nm Em) using the EnVision system. RNA concentration was calculated using linear regression of the standard curve values, by subtracting blank value as background and taking into account the dilution factor. Using RNA concentration, first strand cDNA was synthesized from total RNA using the RT2 First Strand Kit (Qiagen) according to the manufacturers protocol. 500 ng of RNA were mixed with 2 µl of GE buffer in a total volume of 10 µl. This genomic DNA elimination mix was then incubated for 5 minutes at 42°C in a thermocycler (Eppendorf) and put on ice immediately for at least 1 minute. Then the retrotranscription mix was prepared as follows:

5x Buffer BC3	4 µl
Control P2	1 µl
RE3 Reverse Transcriptase Mix	2 µl
RNase-free water	3 µl

10 µl of the reverse-transcription mix were added to each tube containing 10 µl genomic DNA elimination mix and mixed gently by pipetting up and down. Retrotranscription mix was incubated for 15 minutes at 42°C and then the reaction was stopped by incubating for 5 minutes

at 95°C. 91 µl RNase-free water were added to the reaction, which could then be used for the real-time PCR protocol. Reaction was prepared as follows:

2x RT2 SYBR Green Mastermix	1350 µl
cDNA synthesis reaction	102 µl
RNase-free water	1248 µl

25 µl of the final mix were then dispensed to each well of the RT2 Profiler PCR Array (PAHS-084Z). Quantitative PCR was performed in a CFX96 Touch™ Real-Time PCR Detection System (BioRad). Analysis was carried out with the webtool provided by Qiagen (https://www.qiagen.com/it/shop/genes-and-pathways/data-analysis-center-overview-page/).
An Excel file with CT values was uploaded to the website. Samples were assigned to control and test groups and CT values were normalized based on the geometric mean of five housekeeping genes (*ACTB*, *B2M*, *GAPDH*, *HPRT1* and *RPLP0*). The webtool calculates fold change using the Delta Delta C_T method. Genes with CT values greater than 35 were assigned as non-expressed genes and excluded from further analysis.

2.12 RIT2 promoter analysis

2.12.1 Cloning of the *RIT2* promoter construct

To study the activity of the RIT2 promoter, the 2.1 kbp genomic DNA sequence upstream from the *RIT2* transcription initiation site was amplified using Q5 High-Fidelity DNA Polymerase (New England Biolabs). Genomic DNA (gDNA) VM0029 was obtained from the MICROS study collection (Pattaro et al. 2007).

Reaction mix:

gDNA	200 ng
Forward primer	0,5 µM
Reverse primer	0,5 µM
dNTPs	10 mM
Q5 buffer	1x
Q5 polymerase	0,25 µl
ddH_20	up to 25 µl

RIT2 Forward oligo

CAGATATCCTAGGATGAATTGAGCACTGTG

RIT2 Reverse oligo

GGGGTACCCCCCACTTCAATTGCTTCCA

PCR program:

98°C	3 min	
98°C	10sec	
55°C	30 sec	40x cycles
72°C	2,5 min	
72°C	2 min	
4°C	∞	

The PCR product was then directly cloned in the Zero Blunt® TOPO® PCR Cloning Kit (Invitrogen).

Reaction mix:

PCR Product	1 µl
Salt Solution	1 µl
pCR™-Blunt II-TOPO®	1 µl
Sterile Water	3 µl

The reaction was incubated for 5 minutes at RT and then transformed in Top10 competent bacteria (Invitrogen). Bacteria were thawed on ice and incubated with the cloning reaction for 30 minutes on ice and then immersed in a 42°C waterbath for 30 seconds. After addition of SOC medium (Invitrogen) bacterial suspension was incubated for 1 hour at 37 °C in an orbital shaker and then plated on Kanamycin (20 µg/ml) containing agar plates. The plates were incubated overnight at 37°C and the next day colonies were screened using colony PCR using the primers that were used for amplification of the promoter from gDNA. Single colonies were resuspended in 10 µl of ddH_2O and AmpliTaq Gold™ DNA Polymerase (Applied Biosystems) was used to amplify the product of interest.

Reaction mix:

10x Gold buffer	3 µl
dNTP´s	200 µM
Forward Primer	0,5 µM
Reverse Primer	0,5 µM
Bacterial colony in H_2O	1 µl
$MgCl_2$	1,5 mM
Betaine solution	1,5 M
Taq Gold Polymerase	0,3 µl
Nuclease free water	up to 30 µl

Colony PCR program:

95°C	10 min	
94°C	10 sec	
55 °C	30 sec	x40 cycles
72°C	2 min	
72°C	5 min	
4°C	∞	

The PCR products were analysed on an agarose gel and one positive colony expanded in liquid culture (starting from colony resuspended in ddH_2O). Plasmid DNA was extracted using the NucleoSpin® Plasmid kit (Machery Nagel). 5 ml of bacterial suspension were centrifuged for 30 seconds at 11000xg in a benchtop centrifuge (Eppendorf). The supernatant was discarded and the bacterial pellet dissolved in 250 µl of A1 resuspension buffer. 250 µl of A2 lysis buffer were added and the tube inverted 6-8 times and then incubated for 5 minutes at RT. After the incubation, 300 µl of A3 neutralization buffer were added and the tube again inverted 6-8 times and then the lysate was clarified for 5 minutes at 11000xg. The supernatant was loaded onto the column and centrifuged for 60 seconds at 11000xg. The membrane was washed with 600 µl wash buffer followed by centrifugation at maximum speed for 2 minutes to dry the membrane. Plasmid DNA was eluted in 30 µl of nuclease-free water and then cut with two restriction enzymes (EcoRV and KpnI), in parallel with the pGLuc basic vector. Insert and plasmid were ligated using the T4 DNA ligase (New England Biolabs).

Reaction mix:

pGLuc basic vector	1 µl
RIT2 promoter	3 µl
Ligase buffer 10x	1 µl
T4 Ligase	0,5 µl
ddH_2O	4,5

Ligation reaction was incubated overnight at 16 °C and then transformed directly in DH5α competent bacteria. Bacteria were thawed on ice and incubated on ice for 30 minutes with the ligation reaction, followed by a heat shock at 42°C for 45 seconds. After addition of SOC medium (Invitrogen), bacterial suspension was incubated for 1 hour at 37 °C in an orbital shaker and then plated on Ampicillin (50 µg/ml) containing agar plates. A colony PCR (as described above) was carried out to screen for positive colonies and one positive colony was expanded in liquid culture for plasmid DNA extraction, as described above. The final plasmid (pGLuc basic 2 vector containing the *RIT2* promoter) was fully sequenced on both strands.

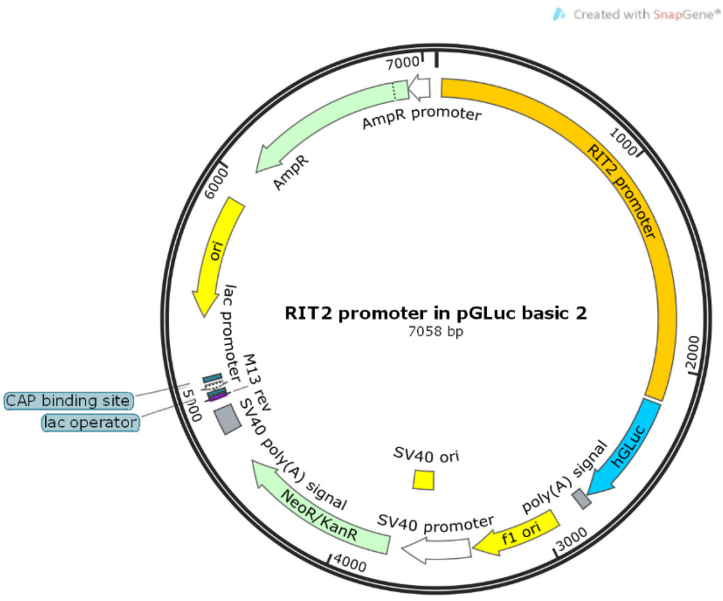

Figure 4: Map of human *RIT2* promoter cloned in front of the *Gaussia* luciferase in the pGLuc basic 2 vector. NeoR/KanR=Neomycin resistance/Kanamycin resistance, AmpR=Ampicillin resistance, ori=origine of replication

2.12.2 Nucleofection of the promoter reporter construct in SH-SY5Y cells

The construct was transfected using the Nucleofector™ technology from Lonza (Walkersville). Cells were detached, counted and 200.000 cells were pelleted for 10 minutes at 200xg. The cell pellet was carefully resuspended in 20 µl of nucleofection solution (16,4 µl SF Cell Line Solution + 3,6 µl Supplement) containing 800ng DNA (64 ng of pTK-CLuc plasmid and 736 ng of pGLuc basic vector or reporter construct for *RIT2*) and the cell suspension was then transferred to a 16-well strip and nucleofected using the CA-137 program on the X-unit. After nucleofection the reaction was incubated for 10 minutes at RT and then 80 µl of complete plating medium were added to the well. Cell suspension was plated in 5 wells of a 96-well plate and after 72 hours of reporter expression the medium was collected. 20µl of each medium sample were transferred to a black OptiPlate for luciferase assessment.

2.12.3 Luciferase reporter gene assay

The reporter gene construct containing the *RIT2* promoter and the reporter luciferase *Gaussia*, was co-transfected with a vector containing the reporter luciferase *Cypridina* (pTK-CLuc, New England Biolabs), which was used for normalization of *Gaussia* luciferase signal across

experimental samples. For assaying 100 samples, 50 µl of BioLux GLuc/CLuc substrate were added to 5 ml BioLux GLuc/CLuc assay buffer. *Gaussia* assay solution could be used immediately after preparation, *Cypridina* assay solution had to be incubated for 30 minutes at room temperature protected from light. The EnVision system (Perkin Elmer) was used for dispensing the substrate and plate reading. The plates were examined using the following protocol:

Dispensing speed	200 µl/s
Dispensing volume	50 µl
Shake duration	2 s
Shake speed	500
Shake Diameter	2 mm
Shake mode	Linear
US-Lum 10s (Label)	7000009
Measurement height	0.2 mm
Measurement time	10 s
Aperture	96 Plate US Luminescence aperture (height:4.2 mm, diameter: 6mm)

Each sample was assessed for *Gaussia* and *Cypridina* signal intensity. Average signal of non-transfected cells was subtracted to all other values for both luciferases, representing the assay baseline. Each value of the *Gaussia* luciferase was then normalized using its relative *Cypridina* luciferase data. The value of the *RIT2* promoter sample was then normalized on the intensity of the empty pGLuc-basic 2 vector, obtaining the fold expression of the promoter with respect to the pGLuc-basic 2 vector.

2.13 Animal handling and behavioural tests

Heterozygous DAT-Ires-Cre mice (The Jackson Laboratory, Stock No: 006660) aged between two and three months were used (males and females). Housing, breeding and procedures were approved by the CPAUL (Comité de protection des animaux de l'Université Laval) and the CCPA (Comité canadien de protection des animaux).

2.13.1 Open field

Open field testing was carried out at baseline and 16 weeks after injection. One hour prior to testing, mice were brought to the room for habituation and were then placed in the open field for 60 minutes. The activity of the mice was recorded automatically with the VersaMax software. The total distance traveled (cm), the horizontal activity (number of beam breaks) and the vertical activity (number of beam breaks) were analyzed.

2.13.2 Cylinder and rotation test

Cylinder test was carried out at baseline and 16 weeks after injection. One hour prior to testing, mice, were brought to the room for habituation and were then placed in a glass cylinder with a diameter of 10 cm and recorded by video. For the cylinder and rotation tests, mice were placed in the cylinder for 5 minutes. Forepaw use and complete rotations were analyzed manually by an investigator.

2.14 Stereotactic surgery

Mice were deeply anesthetized with isoflurane (3-4% for induction and 2% for maintenance with 0.5% oxygen). Adeno-associated virus(AAV)-emCBA-GFP-Flex, AAV-CMVie-hSynP-synA53T, AAV-CAG-Flex-Rit2-EGFP (7,5E12 GC/ml) were unilaterally injected in the right substantia nigra in the following combinations:

- AAV-emCBA-GFP-Flex,
- AAV-emCBA-GFP-Flex + AAV-CMVie-hSynP-synA53T
- AAV-CAG-Flex-Rit2-EGFP
- AAV-CMVie-hSynP-synA53T + AAV-CAG-Flex-Rit2-EGFP

A total volume of 1ul was injected at 2nl/sec at the following coordinates: -3,5mm (AP); -1mm (ML) from bregma; +4mm (DV) from skull. Mice were euthanized 4 months after surgery. For histological studies, mice were perfused with 50 ml of PBS 1X and 50 ml of 4% PFA, brains were removed, post-fixed overnight in 4% PFA and placed in sucrose 30% for cryoprotection overnight. Brains were frozen in OCT on dry ice and then cut at the Cryostat in 60 μm thick sections.

2.15 Immunohistochemistry

Immunohistochemistry (IHC) was performed on 60µm thick brain sections. Free floating sections were blocked in PBS 1X with 1% Normal donkey serum and 0.2% Triton X-100 for 60 min with agitation. Then sections were incubated overnight at 4°C with primary antibodies in blocking solution. The next day, after 3x 5 minutes washing in 1x PBS, the sections were incubated with the secondary antibodies for 60 minutes at RT and then mounted with Fluoroshield mounting medium. For the survival quantification, sections of midbrain (at 4 sections interval) were stained with NeuN and TH antibodies, followed by incubation with Cy3 and Alexa Fluor 647 respectively. Both NeuN and TH positive neurons from the VTA and SNpc regions were counted using a stereology software employing the optical fractionator method (Stereo Investigator, mbf bioscience). For fluorescence quantification of the striatal dopamine terminals, sections were labeled with a TH antibody and incubated with Alexa Fluor 647. Images were acquired with a confocal microscope (LSM700, Zeiss). The fluorescence quantification was obtained by using Corrected Total Cell Fluorescence on a selected region of the striatum with ImageJ software.

Primary antibodies:

Mouse anti-NeuN	1:500	Millipore, MAB377
Sheep anti-TH	1:1.000	Pel-Freez Biologicals, P60101

Secondary antibodies:

Donkey anti-sheep Secondary Antibody, Alexa Fluor 647	1:400	A-21448, Life Technologies
Donkey anti-mouse Secondary Antibody, Cy3	1:200	Jackson Immuno research, 715-165-150

2.16 Proximity ligation assay (PLA)

60 µm thick sections were used for PLA staining. Sections were washed twice in 1x PBS and then blocked for 60 minutes in blocking solution (1x PBS +1% NDS + 0,2% Triton X100) at RT. Then primary antibodies (pS1292 LRRK2, Abcam ab203181; total LRRK2, UC Davis #75-

253) were diluted 1:500 in Duolink II Antibody Diluent (1x) and incubated overnight at 4°C shaking. After 2 washes of 5 minutes in 1x PBS + 0,1% Triton-X100, sections were incubated with PLA probes (Duolink II anti-Mouse MINUS and Duolink II anti-Rabbit PLUS) 1:5 in Antibody Diluent and incubated for 90 min at 37°C shaking. Washes in 1x PBS + 0,1% Triton-X100 were repeated and then sections were incubated in ligation solution (1x Duolink II Ligation stock + Ligase 1:40) for 45 min at 37°C shaking. After ligation sections were washed 2x 5 min in 1x PBS and then incubated with amplification solution (1x Duolink II Amplification stock + Polymerase 1:80) for 100 min at 37°C shaking. After amplification sections were washed twice in 1x PBS for 10 min and then mounted using Fluoroshield mounting medium. Images were acquired with a confocal microscope (LSM700, Zeiss) and analysis of PLA spots was carried out using the "Particle Analysis" function in ImageJ.

2.17 Statistical analyses

Statistical analyses were performed using GraphPad Prism 8. One-way ANOVA followed by the Bonferroni´s *post-hoc* test for pairwise comparisons was used in experiments comparing three or more groups. Two-way ANOVA followed by Bonferroni´s *post-hoc* test for pairwise comparisons was used to analyse the influence of two different categorical independent variables. When comparing two experimental groups, the unpaired, two-tailed Student´s t-test was utilized for normally distributed data. If normality distribution was negative, a non-parametric test was carried out. Data are expressed as the mean ± standard error of the mean (SEM). All experiments in cell lines were performed in a minimum of three independent biological replicates. In imaging experiments 10 single images were acquired for each condition. For *in vivo* experiments, the number of animals is reported. In imaging experiments 10 single images were acquired for each slice (minimum of 2 slices/animal). For all analyses, the threshold for significance was set at $p<0.05$.

3 Results

3.1 Characterization of recombinant LRRK2 cell lines

Recombinant neuroblastoma cell lines (SH-SY5Y) were cultured as described in 2.1 and cell lysates were used for Western blot analysis of total and phosphorylated LRRK2 levels. SH-SY5Y cells showed low levels of endogenous LRRK2, when compared to the overexpressing LRRK2 lines. WT LRRK2 and G2019S LRRK2 cells showed a ~70-fold and ~20-fold overexpression of LRRK2 with respect to control SH-SY5Y cells, respectively (Figure 5 B). Phosphorylation levels of two distinct Serine residues of LRRK2 were also assessed with Western blotting. SH-SY5Y cells showed no detectable amount of pS1292 LRRK2, whereas WT and G2019S LRRK2 cells displayed a clear band. G2019S LRRK2 cells demonstrated a 4-fold increase of pS1292 phosphorylation, when compared to WT LRRK2 cells (phosphorylation normalized on total protein levels; Figure 5 C). SH-SY5Y cells again showed no detectable levels of pS935 LRRK2, but G2019S LRRK2 cells displayed a significant decrease of S935 phosphorylation, with respect to WT LRRK2 cells (Figure 5 D).

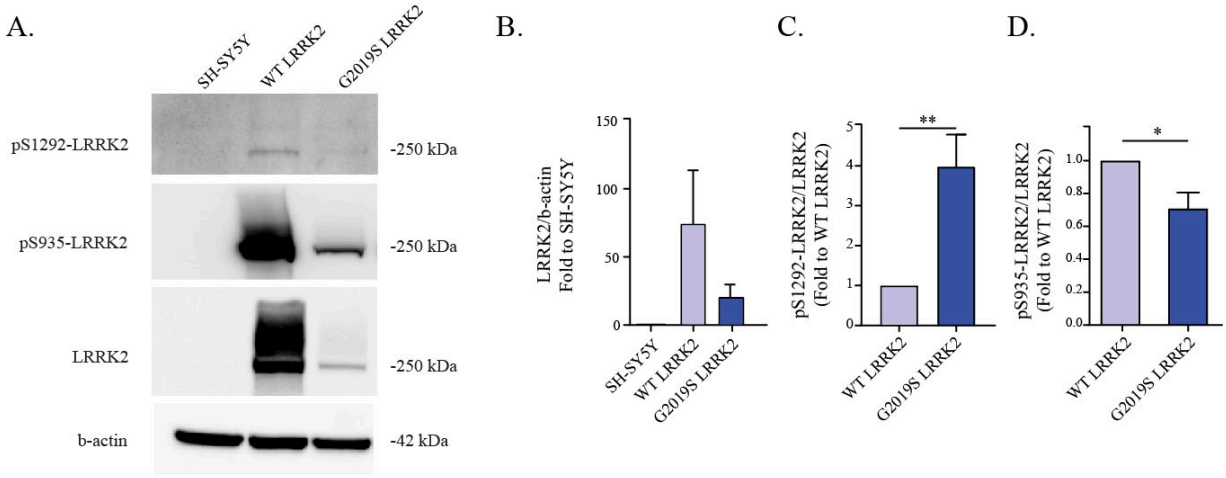

Figure 5: LRRK2 protein levels in recombinant LRRK2 cells lines. A. Representative western blot of LRRK2 protein levels - total LRRK2 (n=5), phospho-S1292 (n=4), phospho-S935 (n=6) in recombinant SH-SY5Y cells. B. Quantification of LRRK2 levels, total LRRK2 was normalized to β-actin, phospho-LRRK2 levels were normalized to total LRRK2 protein levels and expressed as fold-changes relative to WT LRRK2 cells. *p<0.05, **p<0.01, unpaired two-tailed Student`s t-test.

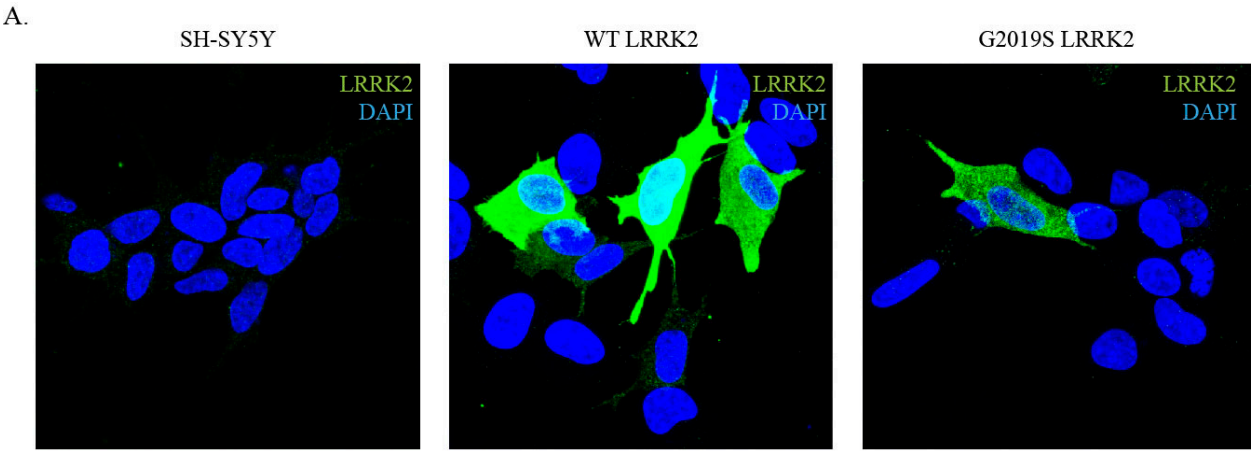

Figure 6: ICC for LRRK2 protein levels. A. ICC for total LRRK2 on SH-SY5Y, WT and G2019S LRRK2 overexpressing cells was used to monitor overexpression of LRRK2.

To confirm Western blot results, ICC was run on the same cell lines, confirming the overexpression of LRRK2. WT LRRK2 showed a dramatic overexpression of LRRK2 protein, whereas G2019S LRRK2 cells displayed a mild overexpression level (Figure 6).

3.2 LRRK2 alters autophagy-related transcriptome

General alterations in the ALP system in WT and G2019S-LRRK2 cells were assessed using an unbiased approach based on transcriptome analysis of genes related to this pathway. Specifically, 84 genes related to the autophagy pathway were screened for mRNA level changes in the different cell lines. The genes and the respective protein products act at different ALP levels, e.g. autophagy induction and initiation, vesicle formation, lysosome fusion and activity. The results of the screen indicated that a vast number of genes were differentially expressed in the three cell lines (Figure 7). SH-SY5Y cells showed an overall different expression pattern when compared to LRRK2 overexpressing cell lines. In about half genes, WT LRRK2 cells showed opposite expression patterns with respect to G2019S cells, indicating a mutation-dependent effect of LRRK2 on the ALP transcriptome. Specifically, G2019S LRRK2 cells displayed differential expression of genes related to lysosomes, such as proteases (*CTSD, CTSS*), and also to the initiation of the autophagy process (*WIPI1*, *MTOR*, *AMBRA1*, *ULK1*). Highlighting some of the differentially expressed genes, *WIPI1* mRNA levels have been shown

to correlate directly to autophagy function and are an indicator of autophagosome formation (Tsuyuki et al. 2014). *WIPI1* gene expression was downregulated in both WT and G2019S LRRK2 cells with a stronger reduction in the latter (fold-change relative to SH-SY5Y cells: WT LRRK2, 0.73; G2019S LRRK2, 0,25). In addition, the MAP1LC3B gene, coding for the LC3B protein, showed increased expression levels in both LRRK2 overexpressing cell lines (fold-change relative to SH-SY5Y cells: WT LRRK2, 1.30; G2019S LRRK2, 1.44;). Fold-changes for all genes can be found in Supplementary data (Supplementary Table 1). Overall, the results from the autophagy array suggested a strong effect of the G2019S LRRK2 mutation on the ALP, which is distinct from WT LRRK2 overexpression.

Figure 7: Clustergram (non-supervised hierarchical clustering of the entire dataset to display a heat map) of RT-PCR array indicating co-regulated genes across groups or individual samples. mRNA levels of 84 genes in the ALP were assessed via qPCR in SH-SY5Y, WT and G2019S LRRK2 cells (2N). 78 genes showed measurable expression levels and are represented in green (fold-change reduction) and red (fold-change increase) relative to SH-SY5Y cells.

3.3 Investigation of the autophagic flux in LRRK2 overexpressing cells

3.3.1 The G2019S LRRK2 mutation increases LC3B-II levels

The analysis of the transcriptome of ATG genes indicated possible malfunctions at different stages of the ALP in LRRK2 cell lines. Gene expression levels are not always indicative of protein abundance, specifically for highly dynamic processes as autophagy. The autophagic flux was investigated in protein lysates of the three cell lines probing for LC3B in Western blot. Cell lines were either treated with CQ or vehicle to assess the dynamics of the process. Vehicle-treated G2019S LRRK2 cells displayed significantly increased levels of LC3B-II with respect to SH-SY5Y cells, whereas WT LRRK2 cells displayed a trend for increase (Figure 8 B). Increased levels of LC3B-II are indicative of a larger proportion of LC3B-II integrated in the autophagosome membrane and therefore indicate an increased number of autophagosomes. CQ treatment inhibits the fusion of the autophagosome to the lysosome and in CQ-treated cells the ratio between LC3B-II and LC3B-I was not changed in the different cell lines (Figure 8 C). This indicates that the overall autophagic flux is not affected by WT or mutant LRRK2 overexpression (Klionsky et al. 2016).

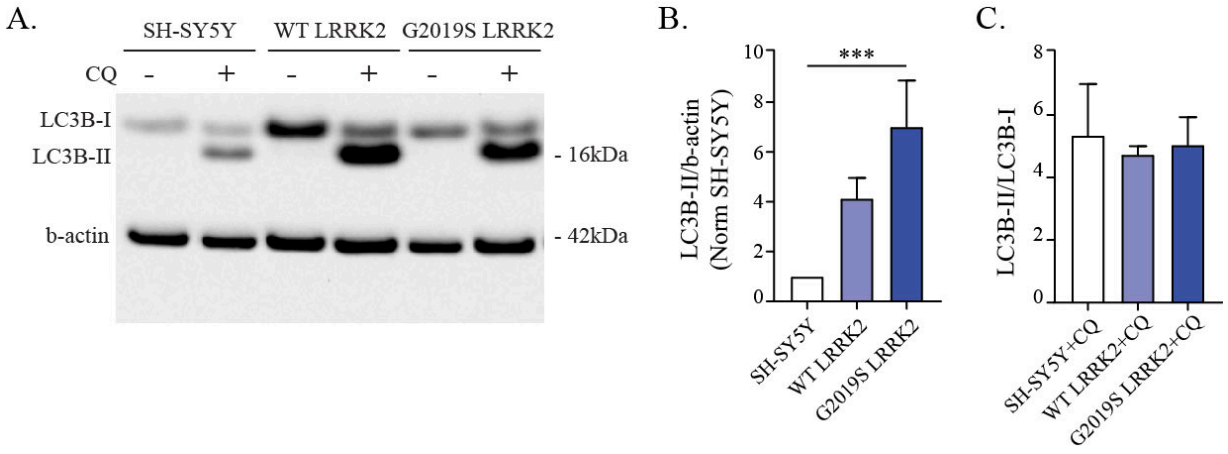

Figure 8: Alterations of the autophagic flux in recombinant LRRK2 cells. A. The autophagic flux was assessed in SH-SY5Y, WT and G2019S LRRK2 cells blotting for endogenous LC3B upon treatment with CQ (100 µM, 3 h). B. Quantification of LC3B-II levels, normalized to β-actin housekeeping gene in non-treated cells. LC3B-II levels are increased in G2109S LRRK2 cells, relative to SH-SY5Y cells (n=7). C. Quantification of LC3B-II levels normalized to LC3B-I levels in CQ-treated cells, indicative of the overall autophagic flux. No difference could be observed indicating no difference in autophagic flux (n=3). ***p<0.001, one-way ANOVA followed by the Bonferroni´s post-hoc test.

3.3.2 The G2019S mutation increases the accumulation of LC3B

Western blot analysis does not provide information on the spatial distribution of proteins within the cellular environment, therefore ICC analysis of endogenous LC3B levels was carried out. The overexpression of WT LRRK2 did not affect the number of LC3B-positive puncta, but the G2019S LRRK2 cell line showed a strong increase in puncta (Figure 9 B), which Figure 9 is consistent with the results from Western blot analysis. Together, this indicates that the G2019S mutation leads to an increase in the number of the cellular LC3B-positive autophagosomes.

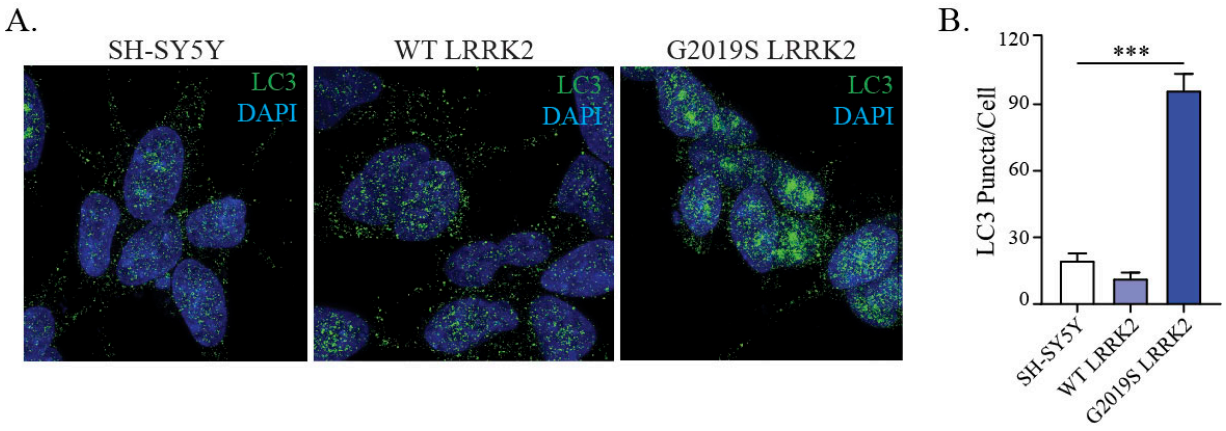

Figure 9: ICC staining of endogenous LC3B levels in SH-SY5Y, WT and G2019S LRRK2 cells. A. LC3B ICC was used to visualize autophagosome number and distribution. B. Quantification of LC3B-positive puncta in the cell lines revealed an increase of LC3B-positive puncta in G2019S LRRK2 cells (n=4). ***p<0.001, one-way ANOVA followed by the Bonferroni´s post-hoc test.

3.3.3 WT LRRK2 but not G2019S LRRK2 increases autolysosome formation

An increased number of autophagosomes can be the result of an increased production or of an impaired degradation. The autophagosome fusion with the lysosome leads to the formation of the autolysosome, degeneration of the vesicle content and re-mobilization of LC3B into the cytosol. Western blot analysis showed no significant difference in the overall autophagic flux in the different cell lines, indicating a possible defect in the fusion of autophagosomes with lysosomes. Autolysosome formation was assessed using a double-tagged LC3 reporter construct (GFP-LC3-mCherry), where mCherry is always expressed but GFP fluorescence is quenched in acidic environments. These pH-dependent fluorescence differences enable to distinguish autophagosomes (double GFP- and mCherry-positive) from autolysosomes (only mCherry-positive). The construct was transfected, cells were fixed after 48 hours, imaged and the GFP

and mCherry positive puncta were counted. The ratio of GFP and mCherry was significantly increased in WT LRRK2 cells, indicating an increased autolysosome formation, which was not matched by the G2019S LRRK2 cells (Figure 10 B). Furthermore, WT LRRK2 cells also displayed an elevated number of mCherry-positive autolysosomes, with respect to SH-SY5Y and G2019S LRRK2 cells (Figure 10 C). Both results suggest that LRRK2 modulates the fusion of autophagosomes with lysosomes, and the G2019S mutation impairs this process.

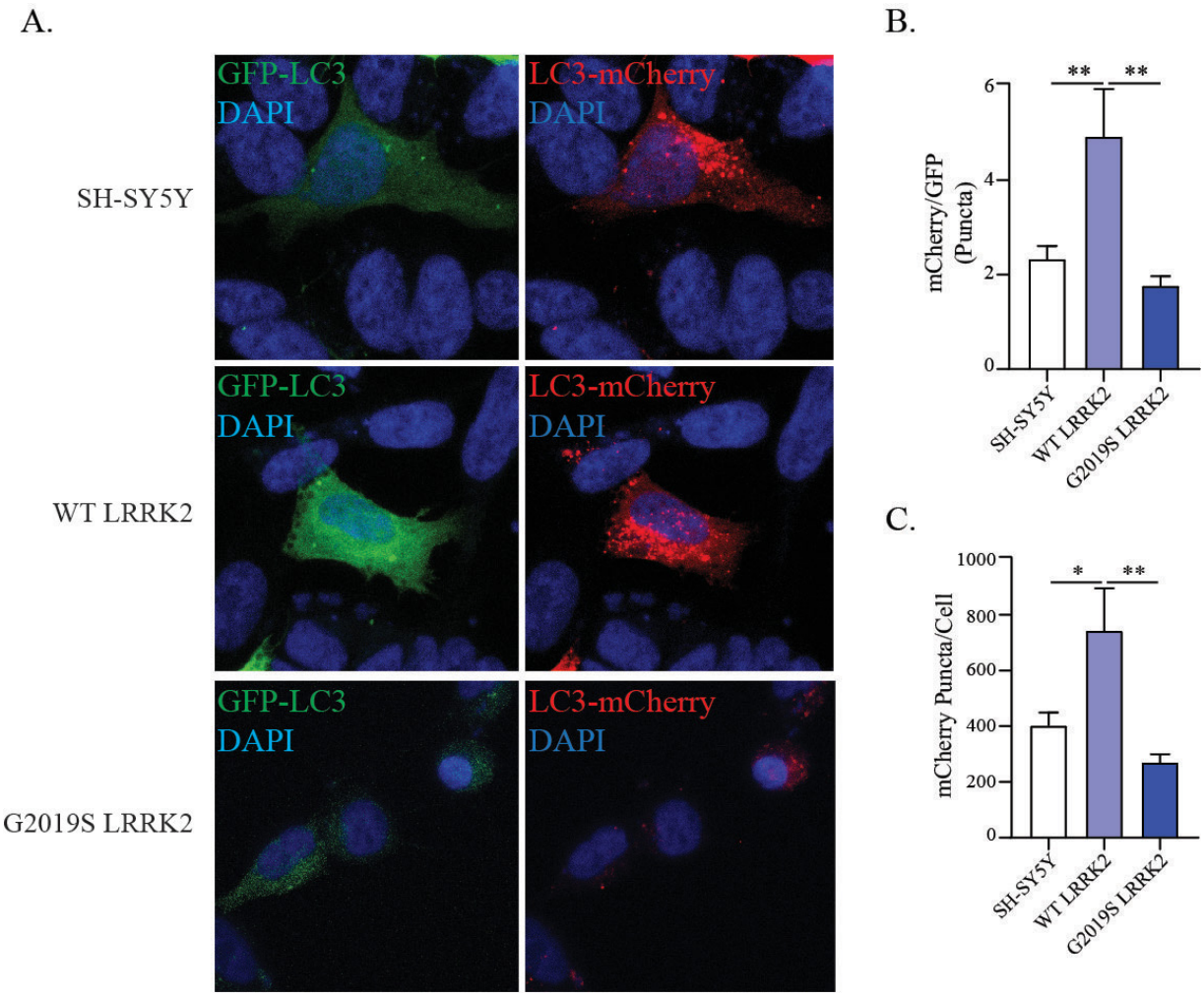

Figure 10: Impaired formation of autolysosomes in G2019S LRRK2 cells. A. The LC3 reporter construct was transfected into SH-SY5Y, WT and G2019S LRRK2 cells to monitor autolysosome formation and number of autolysosomes. B. WT LRRK2 cells displayed an increased mCherry to GFP ratio, indicating increased formation of autolysosomes with respect to SH-SY5Y, which was not observed in G2019S LRRK2 cells (n=6). C. WT LRRK2 cells display an increased number of mCherry puncta, which was prevented by the G2019S mutation (n=6). *p<0,05, **p<0,01, one-way ANOVA followed by Bonferroni´s post-hoc test.

3.3.4 LRRK2 overexpression impacts lysosomal morphology and number

Lysotracker staining was used to assess the number and morphology of lysosomes, which are the final effectors in the ALP process. Cells were incubated with the dye and imaged in live conditions. Both the number and the size of lysosomes were affected by the overexpression of WT and G2019S LRRK2. WT and mutant LRRK2 overexpressing cells showed a significant decrease in the number of lysosomes (Figure 11 B) and a concomitant increase in their size (Figure 11 C). These morphological changes could indicate a dysregulation of the degradative capacity of lysosomes.

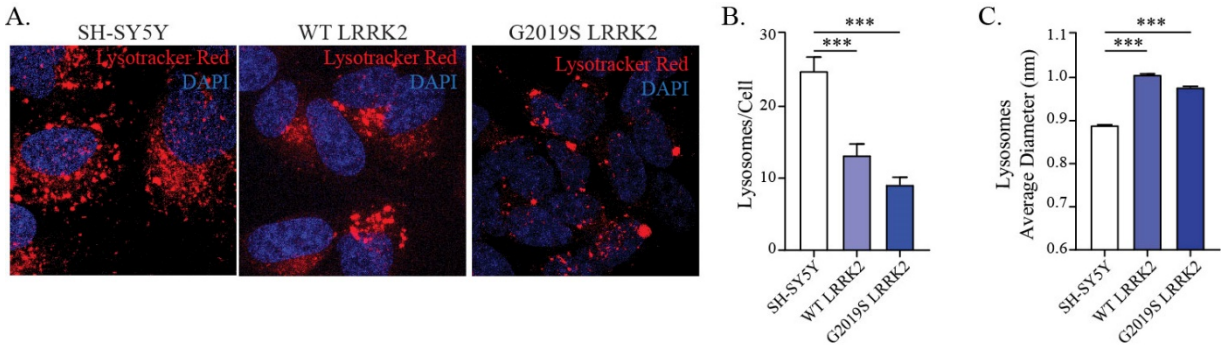

Figure 11: Lysotracker Deep Red staining in SH-SY5Y, WT and G2019S LRRK2 cells. A. Lysotracker staining in the different cell lines. B. Quantification of lysosome number per cell (n=4) revealed a significant decrease of lysosomes in WT and G2019S LRRK2 cells. C. Quantification of average size of lysosomes (n=4) showed a significant increase of lysosomal size in WT and G2019S LRRK2 cells. ***p<0.001, one-way ANOVA followed by the Bonferroni´s post-hoc test.

3.3.5 LRRK2 overexpression alters proteolytic activity of lysosomes

The defects observed in lysosome morphology and autolysosome formation are not sufficient to inform on the functionality of the lysosome. The proteolytic activity of this organelle was investigated using the DQ-Red-BSA assay (Frost et al. 2017). The BSA protein is packed with several fluorophores that auto-quench themselves, because they are in close proximity to each other. When the protein is trafficked to the lysosome it gets cleaved, fluorophores are not in proximity anymore and therefore emit fluorescence. An increase of the fluorescent signal represents a higher proteolytic activity of the cellular lysosomes. Both WT and G2019S LRRK2 cells displayed an increase in the number of DQ-Red-BSA puncta, indicating that overexpressed LRRK2 increases the functionality of lysosomes (Figure 12 B). However, G2019S LRRK2 cells

showed a significantly reduced proteolytic activity with respect to WT LRRK2 cells, pointing again to a mutation-dependent effect of LRRK2 on the ALP, in line with the results obtained with the GFP-LC3-mCherry reporter construct.

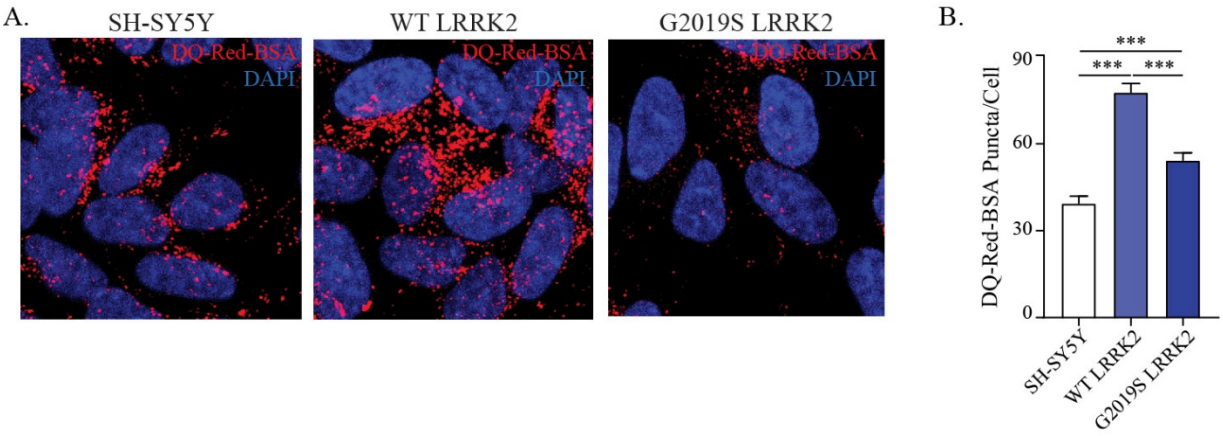

Figure 12: DQ Red BSA assay in SH-SY5Y, WT and G2019S LRRK2 cells A. DQ Red BSA signal in SH-SY5Y, WT and G2019S LRRK2 cells. B. Quantification of fluorescent puncta per cell (n=5) showed a significant increase of proteolytic activity in WT LRRK2 cells, which was not matched by G2019S LRRK2 cells. ***p<0.001, one-way ANOVA followed by the Bonferroni´s post-hoc test.

3.4 G2019S-LRRK2 overexpressing cells contain inclusions positive for phosphorylated aSyn

The DQ-Red-BSA assay is informative on the general capacity of cells to degrade protein cargoes via the lysosomes, but does not indicate the specific cargo substrate(s) involved. PD patients with G2019S mutation predominantly exhibit LB pathology (Kalia et al. 2015, Volta et al. 2015) and in experimental models this mutation has been shown to promote accumulation of pathological aSyn (Volpicelli-Daley et al. 2016). In addition, one of the genes showing an altered expression in the qPCR autophagy array was *CTSB*, encoding for the lysosomal protease Cathepsin B, which plays an essential role in aSyn degradation (McGlinchey and Lee 2015). SH-SY5Y, WT LRRK2 and G2019S LRRK2 cells were probed for pS129-aSyn, which is one of the major pathological posttranslational modifications of aSyn as well as the preponderant form of aSyn present in LBs. In SH-SY5Y and WT LRRK2 cells, only weak and diffuse staining was observed, whereas in G2019S LRRK2 cells evident inclusion-like structures positively marked for pS129-aSyn and located mostly around the nucleus were evidenced (Figure 13 A).

Quantification of the fluorescence signal revealed a strong increase of both the number of spots and intensity of pS129-aSyn staining in G2019S LRRK2 cells (Figure 13 B;C) with respect to SH-SY5Y and WT LRRK2 cells.

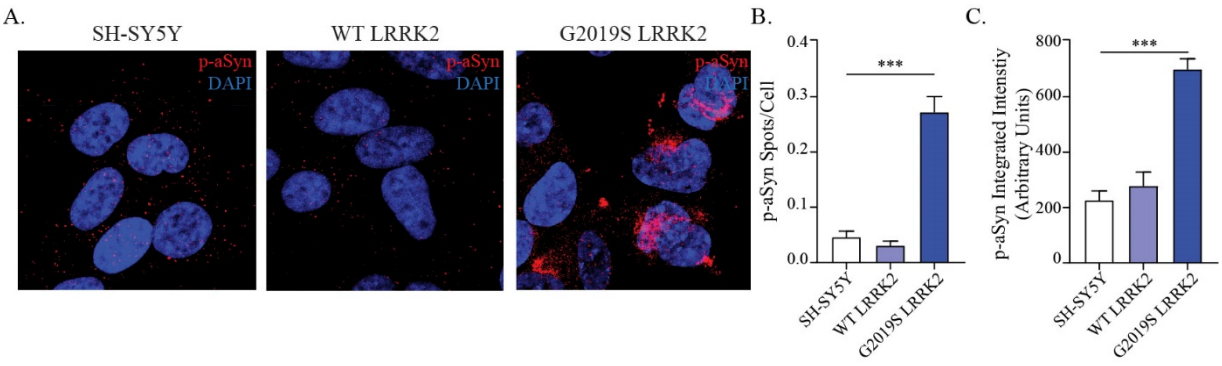

Figure 13: G2019S LRRK2 cells display pS129-aSyn-positive inclusions. A. ICC for pS129-aSyn was used to investigate the presence of intracellular inclusions of aSyn. B. Quantification of the pS129-aSyn-positive inclusions per cell in SH-SY5Y, WT and G2019S LRRK2 cells showed a significant increase of spots per cell in G2019S LRRK2 cells. C. Quantification of integrated intensity of the ICC signal showed a significant increase in G2019S LRRK2 cells (n=6). ***p<0.001, one-way ANOVA followed by the Bonferroni´s post-hoc test.

3.5 Pharmacological LRRK2 kinase inhibition with PF475

The G2019S mutation has been linked to an increase of LRRK2 kinase activity (Figure 5 C) (West et al. 2007), which drives LRRK2 toxicity, and therefore has led to the development of selective LRRK2 kinase inhibitors as disease-modifying agents in PD. As described in 3.1, the G2019S LRRK2 overexpressing cells displayed an about 4-fold increase in pS1292-LRRK2 phosphorylation. The ability of different concentrations (300, 500 and 1000 nM) of the LRRK2 inhibitor PF-475 to dephosphorylate LRRK2 at S935 and S1292 was investigated. Close-to-maximal dephosphorylation was observed already at 300 nM, therefore, 300 and 500 nM PF475 were used in subsequent experiments (Figure 14 B;C). The LRRK2 kinase inhibitor was applied only to G2019S LRRK2 cells, because the mutation leads to a toxic increase in kinase activity and only G2019S LRRK2 cells display pS129-aSyn positive inclusions. Pharmacological kinase inhibition did not affect the autophagy-related transcriptome, tested with the qPCR autophagy array (Supplementary Table 2). This might be due to the fact that the inhibitor was applied for a limited period of time (max 6 hours).

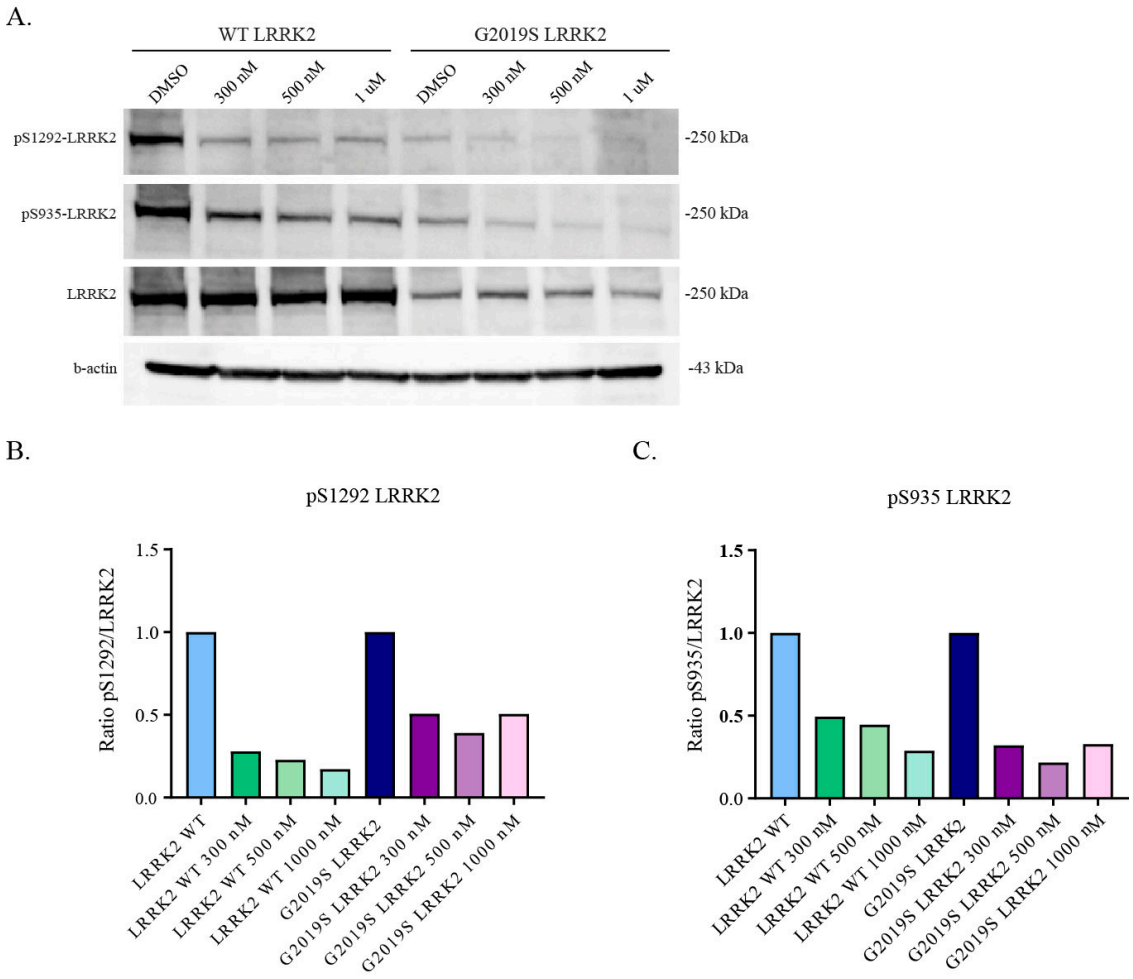

Figure 14: Concentration-dependent dephosphorylation of LRRK2 at S935 and S1292 upon treatment with PF475. A. Phosphorylation levels of S935 and S1292 of LRRK2 after PF475 treatment in WT and G2019S LRRK2 cells were assessed and normalized to total LRRK2 protein levels. B. Quantification of pS935 and pS1292 levels in WT and G2019S LRRK2 cells revealed similar reduction of phosphorylation levels with different concentrations of PF475 (n=1).

3.6 LRRK2 kinase inhibition rescues ALP-related defects

3.6.1 LRRK2 kinase inhibition in cells does not alter autophagic flux

The effect of LRRK2 kinase inhibition in G2019S LRRK2 cells was first assessed by Western blotting for LC3B. PF475 was applied at 300 and 500 nM for 2 hours and then cell lysates were subjected to Western blot analysis (Figure 15 A). The conversion of LC3B-I to LC3B-II was not affected, indicating that the overall autophagic flux was not changed (Figure 15 B). Conversely, LC3B-II levels were significantly reduced by PF-475 at a concentration of 500 nM

(Figure 15 C). This indicates a reduction of the number of autophagosomes in G2019S LRRK2 cells when treated with LRRK2 kinase inhibitor.

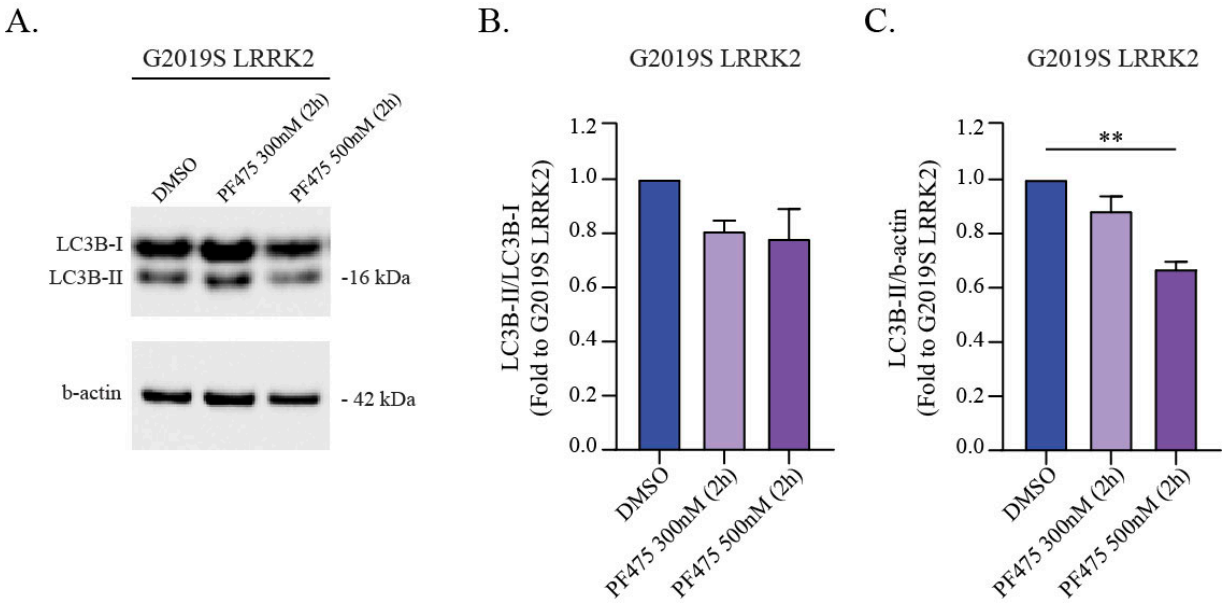

Figure 15: Alterations of the autophagic flux in PF475-treated G2019S LRRK2 cells. A. The autophagic flux was assessed in G2019S LRRK2 cells blotting for endogenous LC3B upon treatment with PF475 (300 or 500nM, 2h). B. Quantification of LC3B-II levels normalized to LC3B-I levels, indicates that the overall autophagic flux is not changed (n=3). C. Quantification of LC3B-II levels, normalized to b-actin in PF475-treated cells. LC3B-II levels are decreased upon PF475 treatment (n=3). **p<0,01, one-way ANOVA followed by Bonferroni´s post-hoc test.

3.6.2 LRRK2 kinase inhibition reduces autophagosome number

To confirm the results from Western blot analysis, G2019S LRRK2 cells were subjected to ICC staining for endogenous LC3B after treatment with PF475. Two hours treatment with 300 or 500 nM significantly reduced the number of LC3B-positive puncta in a concentration-dependent manner (Figure 16 B). This result is consistent with the protein level analyses, confirming that LRRK2 kinase inhibition led to a depletion of autophagosomes.

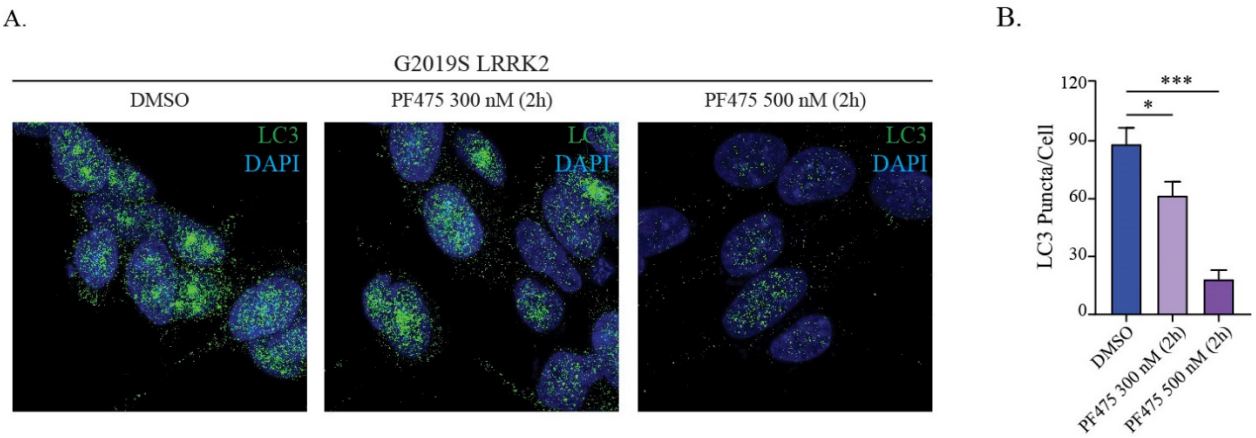

Figure 16: ICC staining of endogenous LC3B levels in G2019S LRRK2 cells treated with PF475 (300 or 500 nM, 2h). A. LC3B ICC was used to visualize autophagosome number and distribution. B. Quantification of LC3B-positive puncta in the G2019S LRRK2 cells revealed a concentration-dependent decrease of LC3B-positive puncta in G2019S LRRK2 cells, when treated with PF475 (n=3). *p<0.05. ***p<0.001, one-way ANOVA followed by the Bonferroni´s post-hoc test.

3.6.3 LRRK2 kinase inhibition increases autolysosome formation

PF475 treatment showed positive effects on the autophagosome number, so G2019S LRRK2 cells were transfected with the GFP-LC3B-mCherry reporter construct to investigate the rate of autophagosome to lysosome fusion and if this event is dependent on kinase activity of LRRK2. After 2 days of construct expression, cells were treated for 6 hours with 300 or 500 nM PF475, then GFP- and mCherry-positive puncta were counted. The mCherry/GFP ratio was increased in a concentration-dependent manner by PF-475, indicating an increase in autophagosome processing and reinstatement of the correct fusion to the lysosome (Figure 17 B). Consistently, the number of mCherry-positive autolysosomes was strongly increased by PF-475, reaching statistical significance at 500 nM (Figure 17 C).

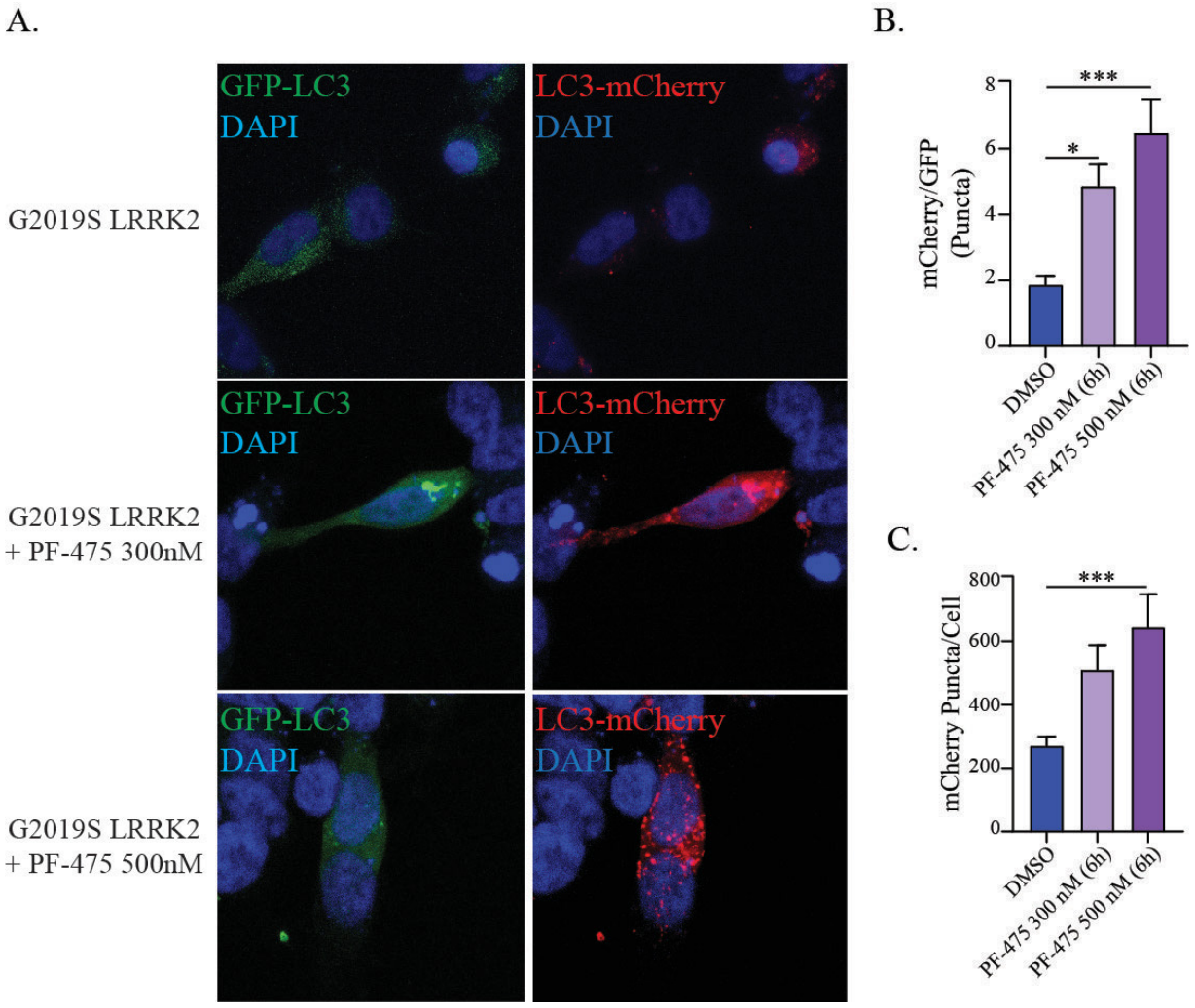

Figure 17: PF475 rescues impaired autolysosome formation in G2019S LRRK2 cells. A. The LC3 reporter construct was transfected into G2019S LRRK2 cells treated with PF475 (300 or 500 nM, 6h) to monitor autolysosome formation and number of autolysosomes. B. PF475 treatment increases mCherry to GFP ratio, indicating increased formation of autolysosomes (n=5). C. PF475 treatment increases in a concentration-dependent manner the number of mCherry puncta (n=6). *p<0,05, ***p<0,001, one-way ANOVA followed by Bonferroni´s post-hoc test.

3.6.4 LRRK2 kinase inhibition rescues lysosomal morphology defects

The effect of LRRK2 kinase inhibition on the morphology of lysosomes was assessed as well. The overexpression of G2019S LRRK2 led to a reduction in number and increase in size of these organelles. G2019S LRRK2 cells were treated for 2 hours with 300 or 500 nM PF475 and then stained with the Lysotracker Deep Red dye (Figure 18 A). The number of lysosomes per cell was significantly increased by the 500 nM concentration of PF475, whereas both the 300

and 500 nM concentrations of PF475 were effective in reducing the size of lysosomes (Figure 18 B;C).

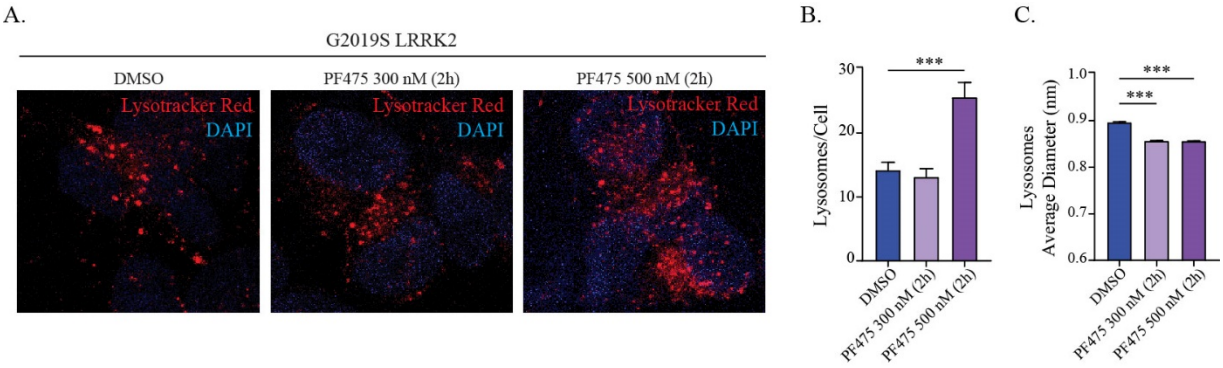

Figure 18: Lysotracker Deep Red staining in PF475-treated G2019S LRRK2 cells. A. Lysotracker staining in G2019S LRRK2 cells. B. Quantification of lysosome number per cell revealed a significant increase of lysosomes with the 500 nM concentration of PF475 (n=3). C. Quantification of average size of lysosomes showed a significant decrease of lysosomal size in PF475-treated G2019S LRRK2 cells (n=3). ***p<0.001, one-way ANOVA followed by the Bonferroni´s post-hoc test.

3.6.5 LRRK2 kinase inhibition enhances proteolytic function of lysosomes

LRRK2 kinase inhibition showed beneficial effects on several ALP stages, and DQ-Red-BSA was used to investigate the impact of PF475 on the proteolytic function of lysosomes in G2019S LRRK2 cells (Figure 19 A). This compound was applied at 300 or 500 nM for 6 hours and during the last 2 hours of incubation, the DQ-Red-BSA was co-applied. Both concentrations were able to significantly enhance the number of fluorescent spots per cell, indicating that kinase inhibition rescued the proteolytic defects in G2019S LRRK2 cells (Figure 19 B).

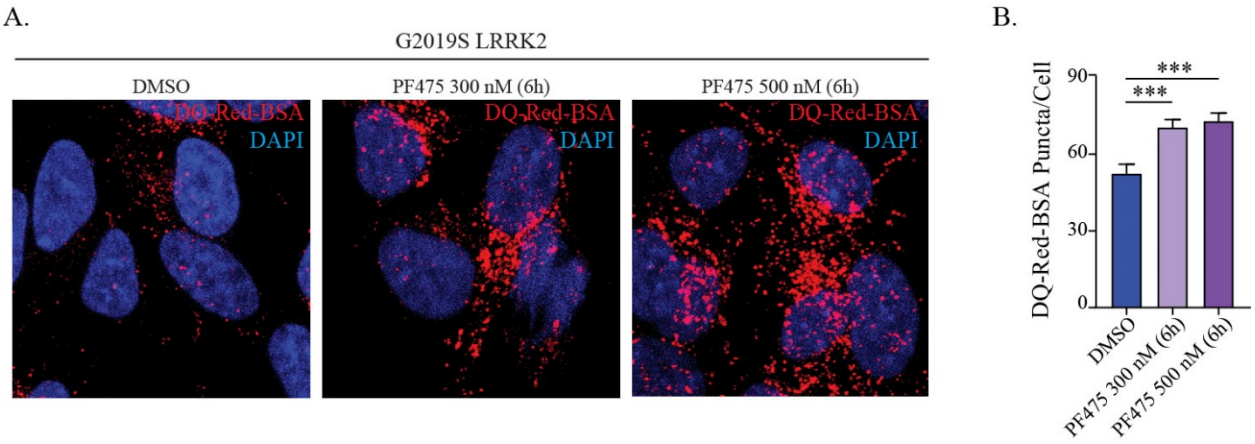

Figure 19: DQ-Red-BSA assay in G2019S LRRK2 cells treated with PF475. A. DQ-Red-BSA staining in PF475-treated G2019S LRRK2 cells. B. Quantification of fluorescent puncta per cell showed a significant increase of proteolytic activity in G2019S LRRK2 cells, upon treatment with PF475 (300 or 500 nM, 6h) (n=4). ***p<0.001, one-way ANOVA followed by the Bonferroni´s post-hoc test.

3.6.6 LRRK2 kinase inhibition reduces pS129-aSyn inclusions

The LRRK2 kinase inhibitor was effective in rescuing several ALP-related phenotypes, therefore PF475 treatment was applied to G2019S LRRK2 cells to investigate if treatment had also an effect on the pS129-aSyn-positive inclusions. G2019S LRRK2 cells were treated with 300 or 500 nM PF475 for 2 hours and then processed for pS129-aSyn ICC staining. In DMSO-treated control cells, organized structures of pS129-aSyn were detected. LRRK2 kinase inhibition led to a reduction of pS129-aSyn-positive spots at both concentrations (Figure 20 A). Moreover, the overall staining was more diffuse when compared to DMSO-treated cells. Specifically, both 300 and 500 nM concentrations of PF475 significantly reduced the number of pS129-aSyn spots and the integrated intensity of the fluorescent signal (Figure 20 B;C). This result indicates that LRRK2 kinase inhibition not only improved ALP, but was also able to reduce pS129-aSyn positive inclusion in G2019S LRRK2 cells.

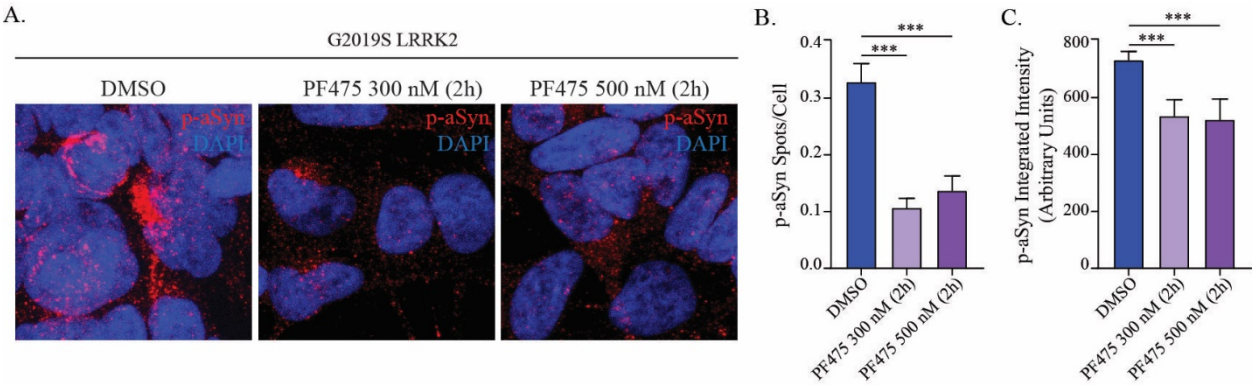

Figure 20: pS129-aSyn-positive inclusions in G2019S LRRK2 cells are reduced by PF475 treatment (300 or 500 nM, 2h). A. ICC for pS129-aSyn was used to investigate the presence of intracellular inclusions of aSyn. B. Quantification of the pS129-aSyn-positive inclusions per cell in PF475-treated G2019 LRRK2 cells showed a significant decrease of spots per cell (n=4). C. Quantification of integrated intensity of the ICC signal showed a significant decrease with PF475 treatment (n=4). ***p<0.001, one-way ANOVA followed by the Bonferroni´s post-hoc test.

3.6.7 The beneficial effect of LRRK2 kinase inhibition on pS129-aSyn inclusions depends on correct fusion of autophagosomes with lysosomes

So far, the results suggested that G2019S LRRK2 induces abnormalities in ALP and leads to accumulation of pS129-aSyn-positive inclusions in a kinase-dependent manner. Specifically, data obtained with the LC3B double-reporter construct indicate that the impairment in the autophagic flux occurs at the autophagosome to lysosome fusion step. To determine if the effect of PF475 treatment on pS129-aSyn inclusions depends on the interference with this fusion step, the process was pharmacologically inhibited with CQ, which impairs the fusion of the autophagosome with the lysosome (Mauthe et al. 2018). G2019S LRRK2 cells were preincubated with CQ (100 µM, 3 hours), then treated with PF475 at 500 nM for 2 hours and processed to ICC analysis for pS129-aSyn (Figure 21 A). The reduction of inclusions after treatment with the inhibitor alone was confirmed, and the treatment with CQ alone induced a non-significant trend towards an increased number of inclusions. Importantly, LRRK2 kinase inhibition in CQ-pretreated cells lost its effect and did not alter the number of pS129-aSyn inclusions (Figure 21 B). The same effects were observed when measuring the intensity of the immunosignal, demonstrating that PF475 reduces aSyn inclusions by acting on the fusion step of the autophagy process (Figure 21 C). Thus, pharmacological blockade of the fusion of autophagosomes with lysosomes prevented the beneficial effect of LRRK2 kinase inhibition on autophagic degradation.

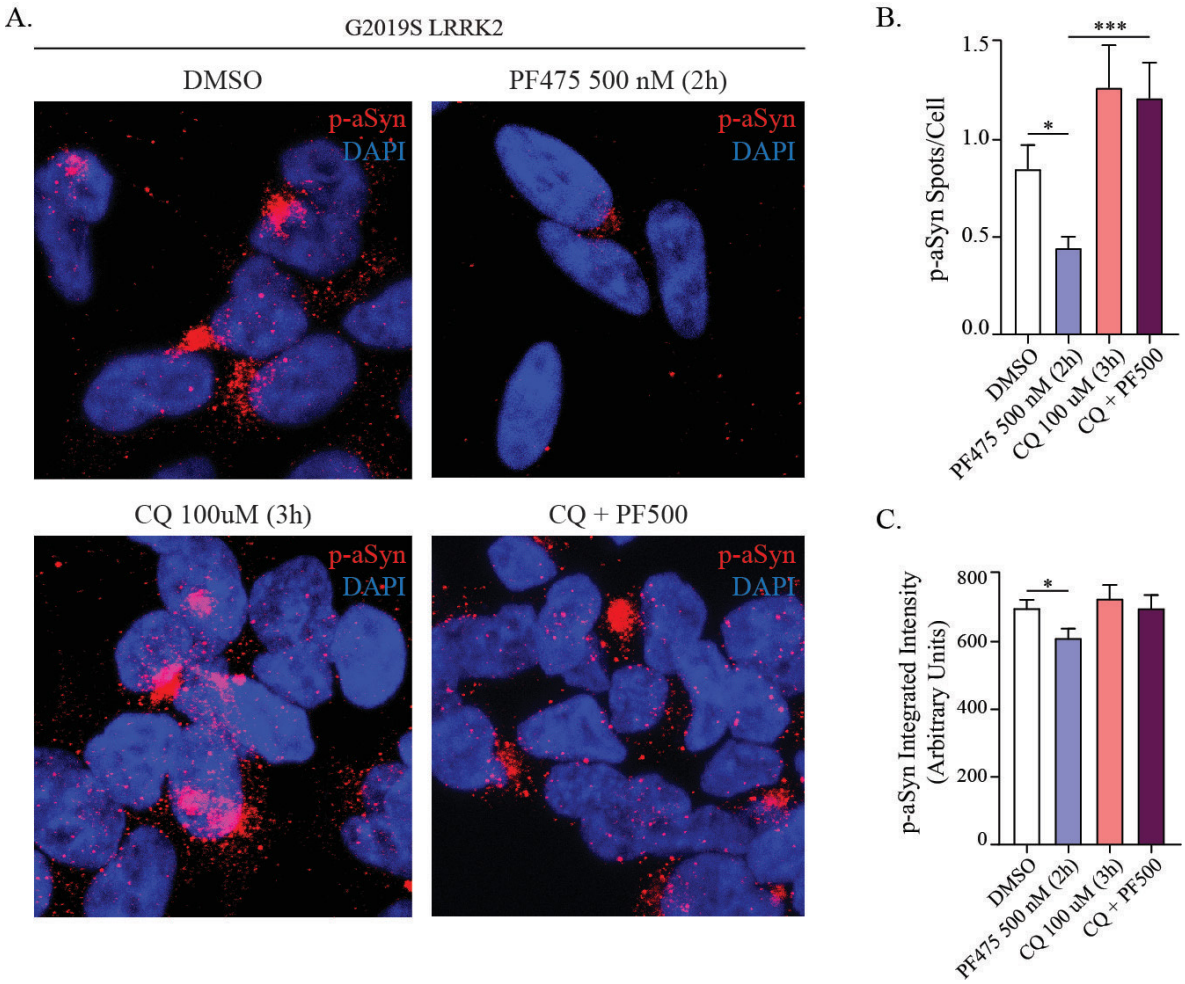

Figure 21: Reduction of pS129-aSyn-positive inclusions in G2019S LRRK2 cells by PF475 treatment (300 or 500 nM, 2h) depends on autophagosome to lysosome fusion. A. ICC for pS129-aSyn was used to investigate the presence of intracellular inclusions of aSyn upon treatment with PF475 (500 nM, 2h), CQ (100 µM, 3h) or CQ+PF475. B. Quantification of the pS129-aSyn-positive inclusions per cell in PF475-treated G2019 LRRK2 cells showed a significant decrease of spots per cell, which was abolished by co-treatment with CQ. CQ alone did not alter the number of pS129-aSyn inclusions (n=3). C. Quantification of integrated intensity of the ICC signal showed a significant decrease with PF475 treatment (n=3). *p<0.05, ***p<0.001, one-way ANOVA followed by the Bonferroni´s post-hoc test.

3.7 *RIT2* mRNA levels are decreased in LRRK2 overexpressing cells

Alterations in the promoter region of the *RIT2* gene have been associated to PD and are hypothesized to alter gene expression (Bossers et al. 2009, Latourelle et al. 2012). Therefore, *RIT2* mRNA levels were assessed in SH-SY5Y cell lines using ddPCR. RNA was extracted from cell lines, quantified and retrotranscribed into cDNA to be used for the reaction. Quantification of the mRNA levels showed that the overexpression of both WT and mutant

LRRK2 caused a reduction of *RIT2* mRNA levels with respect to SH-SY5Y cells and normalized to a housekeeping gene (Figure 22 B;C).

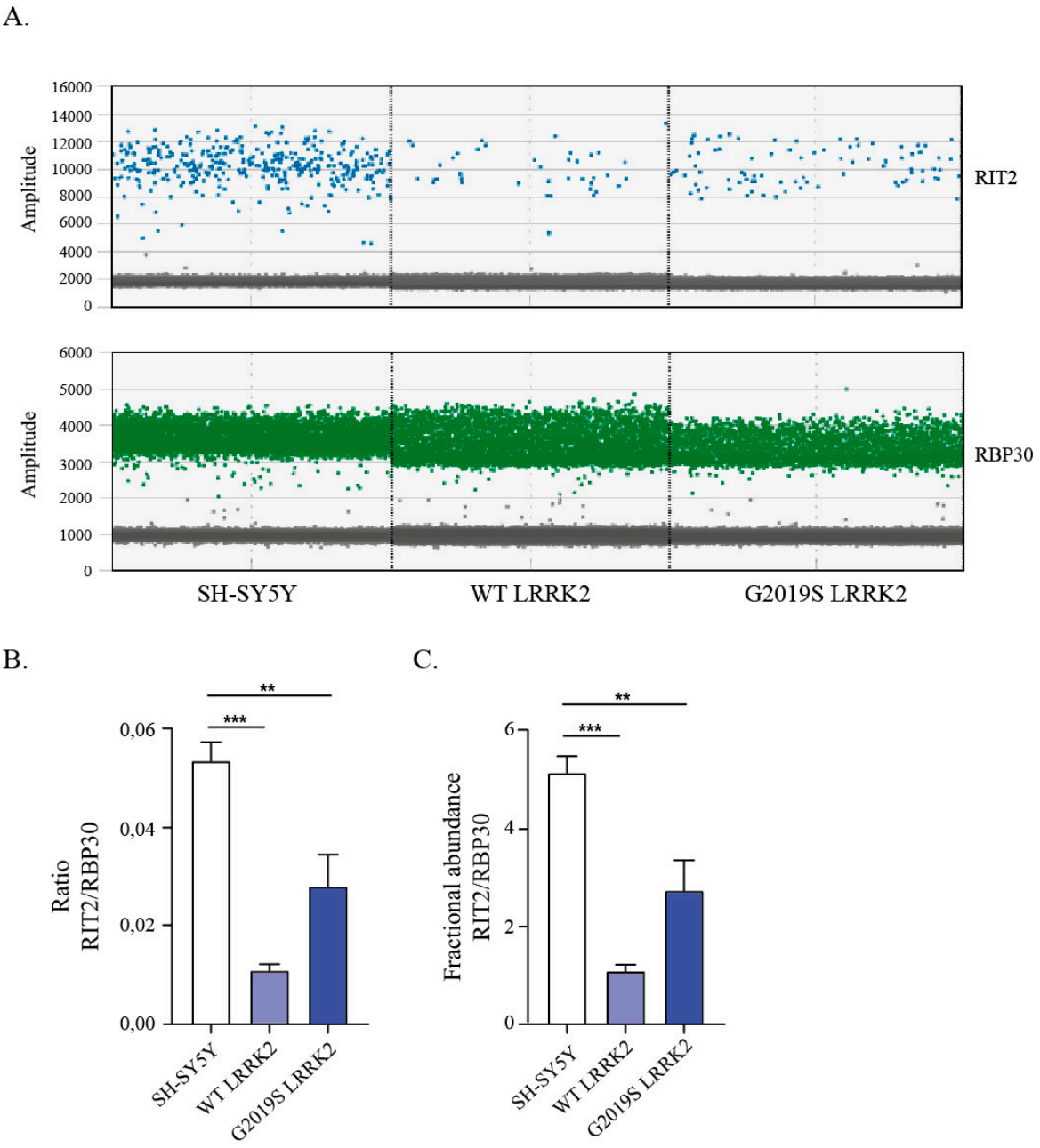

Figure 22: *RIT2* mRNA levels are decreased in WT and G2019S LRRK2 cells. A. Amplitude view of ddPCR reaction for *RIT2* and *RBP30* in SH-SY5Y, WT and G2019S LRRK2 cells. B. Ratio of *RIT2* on *RBP30* expression levels (n=3) is reduced in WT and G2019S LRRK2 cells. C. Fractional abundance (a/(a+b)) of *RIT2* mRNA normalized to *RBP30* (n=3) is reduced in WT and G2019S LRRK2 cells. **p<0.01, ***p<0.001, one-way ANOVA followed by Bonferroni´s post-hoc test.

3.7.1 *RIT2* promoter activity is decreased in LRRK2 overexpressing cells

RIT2 promoter activity was investigated using a luciferase-based gene reporter assay. Cells were nucleofected with the reporter construct containing the *RIT2* promoter sequence and a luciferase. Luciferase production is driven by the promoter activity and was measured after 72 hours of expression. Luciferase production was normalized to a second housekeeping luciferase and expressed as fold-change relative to SH-SY5Y cells. In SH-SY5Y cells, luciferase production was reduced by overexpression of WT and G2019S LRRK2 (~60% and ~40%, respectively) (Figure 23). The downregulation of *RIT2* mRNA levels and the reduced promoter activity in LRRK2 overexpressing cells built the rationale to reestablish Rin protein levels in these cells. In detail, a plasmid construct containing the open reading frame of *RIT2* was transiently nucleofected into G2019S LRRK2 cells. The 4D-Nucleofector™ X Unit from Lonza (Walkersville) was used to deliver the construct into the cells with high efficiency (Figure 24).. RIT2 was expressed for 72 hours before the subsequent experiments were carried out.

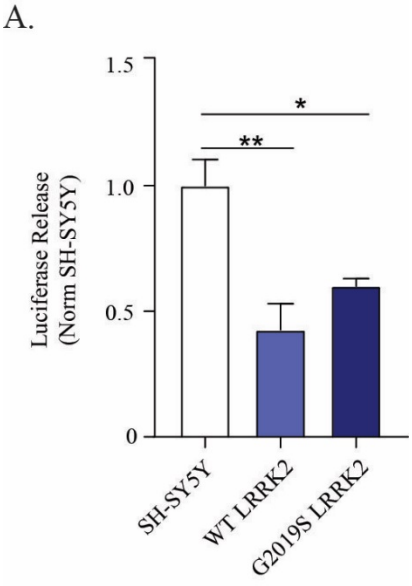

Figure 23: Decreased *RIT2* promoter activity in WT and G2019S LRRK2 cells. A. Luciferase levels were reduced in WT and G2019S LRRK2 cells, when compared to SH-SY5Y cells (n=3). *p<0.05, **p<0.01, one-way ANOVA followed by the Bonferroni´s post-hoc test.

A.

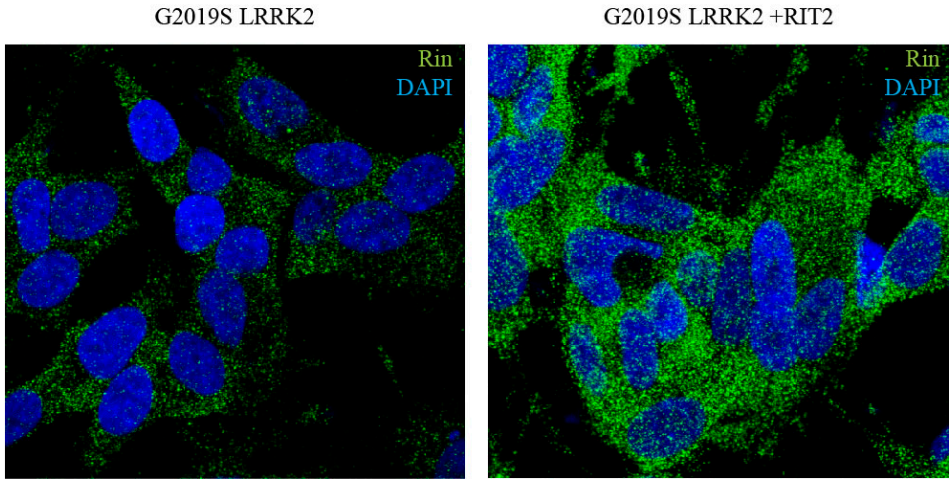

Figure 24: ICC staining for Rin protein in G2019S LRRK2 and G2019S LRRK2+RIT2 cells. A. Rin ICC was used to control for nucleofection efficiency.

3.8 Overexpression of *RIT2* rescues ALP-related defects

3.8.1 *RIT2* overexpression does not affect autophagic flux

The effect of *RIT2* overexpression in G2019S LRRK2 cells was first assessed by Western blotting for LC3B. After transient expression of *RIT2*, cells were collected, lysed and subjected to Western blot analysis. The conversion of LC3B-I to LC3B-II and the total levels of LC3B-II (normalized to β-actin) were significantly increased in G2019S LRRK2 cells, as previously reported (see 3.3.1). *RIT2* overexpression induced a trend to reduce both LC3B-II to LC3B-I and LC3B-II to β-actin ratios, albeit not reaching statistical significance (Figure 25 B;C). This indicates that *RIT2* does not affect the overall autophagic flux in G2019S LRRK2 cells. In addition, the transcriptome of autophagy-related genes was assessed in G2019S LRRK2 cells transfected with *RIT2* (Supplementary Table 3). Specifically, *WIPI1* and *DRAM1* gene expression levels were impacted by *RIT2* overexpression. *WIPI1* was shown to promote autophagy and autophagosome formation (Tsuyuki et al. 2014, Xiao et al. 2018), whereas *DRAM1* is implicated in the processes of lysosomal acidification, clearance of autophagosomes and fusion of autophagosomes with lysosomes (Zhang et al. 2013). Autophagic flux was not affected by *RIT2* overexpression, but the mRNA level differences of genes involved in specific steps of ALP prompted us to investigate the autophagy process at those specific stages.

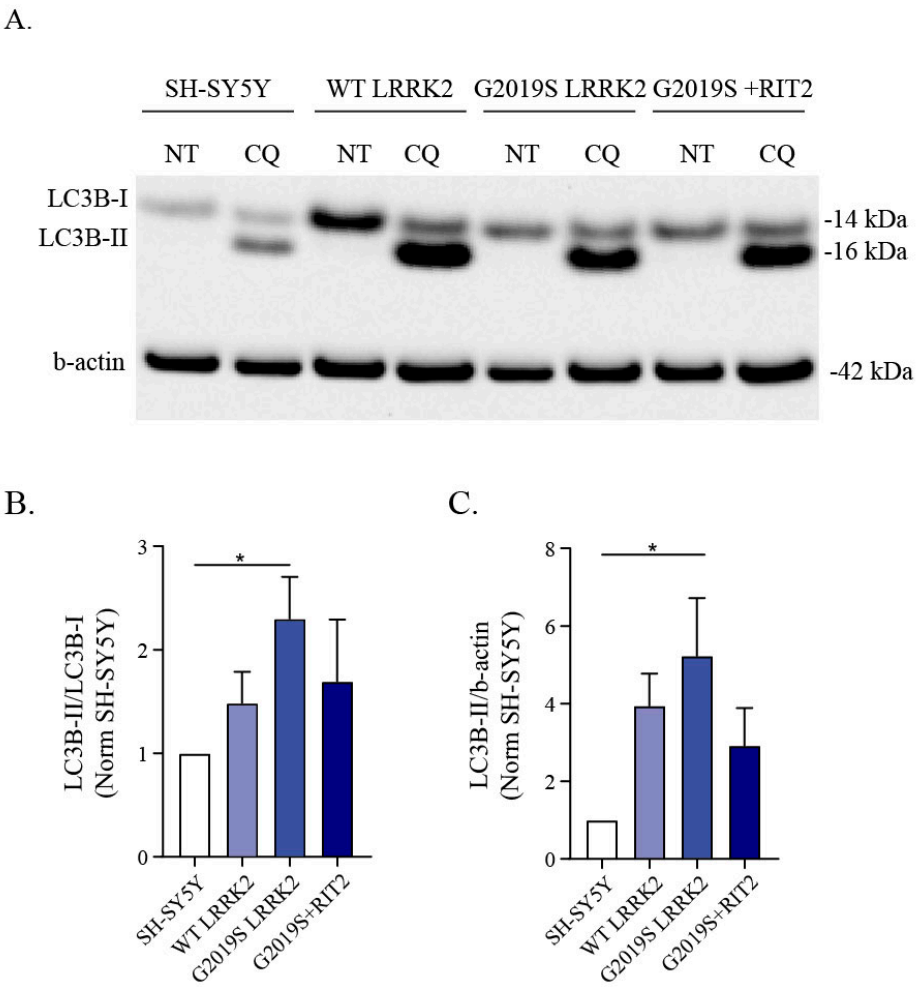

Figure 25: Alterations of the autophagic flux in SH-SY5Y, WT LRRK2, G2019S LRRK2 and G2019S+RIT2 cells. A. The autophagic flux was assessed in SH-SY5Y, WT LRRK2, G2019S LRRK2 and G2019S+RIT2 cells blotting for endogenous LC3B. B. Quantification of LC3B-II levels normalized to LC3B-I levels revealed that the overall autophagic flux is higher in G2019S LRRK2 cells (n=4). C. Quantification of LC3B-II levels, normalized to β-actin housekeeping gene in SH-SY5Y, WT LRRK2, G2019S LRRK2 and G2019S+RIT2: *RIT2* overexpression does not significantly affect the number of autophagosomes (n=4). *p<0.05, one-way ANOVA followed by the Bonferroni´s post-hoc test.

3.8.2 *RIT2* overexpression reduces autophagosome number

To complete the investigation of LC3B levels, cells were subjected to ICC staining for endogenous LC3B with or without *RIT2* nucleofection (Figure 26 A). Cells were plated, and *RIT2* overexpression was maintained for 72 hours before cells were fixed, stained and imaged. The transient overexpression of *RIT2* significantly reduced the number of LC3B-positive puncta (Figure 26 B). On the other hand, *RIT2* overexpression increased the intensity of LC3B staining

(Figure 26 C). These results indicate that *RIT2* overexpression is acting on endogenous LC3B levels and is leading to a reduction in the number of autophagosomes.

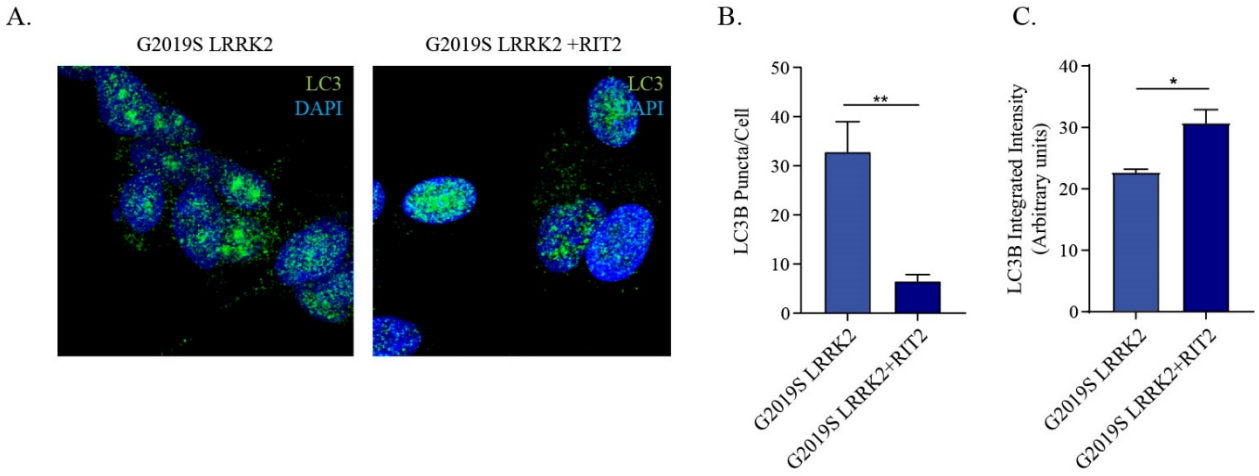

Figure 26: ICC staining of endogenous LC3B levels in G2019S LRRK2 cells transfected with RIT2. A. LC3B ICC was used to visualize autophagosome number and distribution. B. Quantification of LC3B-positive puncta revealed a decrease of LC3B-positive puncta in G2019S LRRK2 cells, when transfected with RIT2 (n=4). C. Quantification of integrated intensity of the immune signal revealed an increase of the intensity of the staining in G2019S LRRK2 cells, when transfected with RIT2 (n=4). *p<0.05. **p<0.01, unpaired two tailed Student`s t-test.

3.8.3 *RIT2* overexpression rescues lysosome morphology

The effect of transient *RIT2* overexpression on morphology and number of lysosomes in G2019S LRRK2 cells was assessed using the Lysotracker Deep Red dye. When compared to SH-SY5Y cells, G2019S LRRK2 cells displayed a decrease in number (Figure 27 B) and an increase in size of lysosomes (Figure 27 C). Thus, the overexpression of *RIT2* rescued the morphological defects induced by the G2019S LRRK2 mutation.

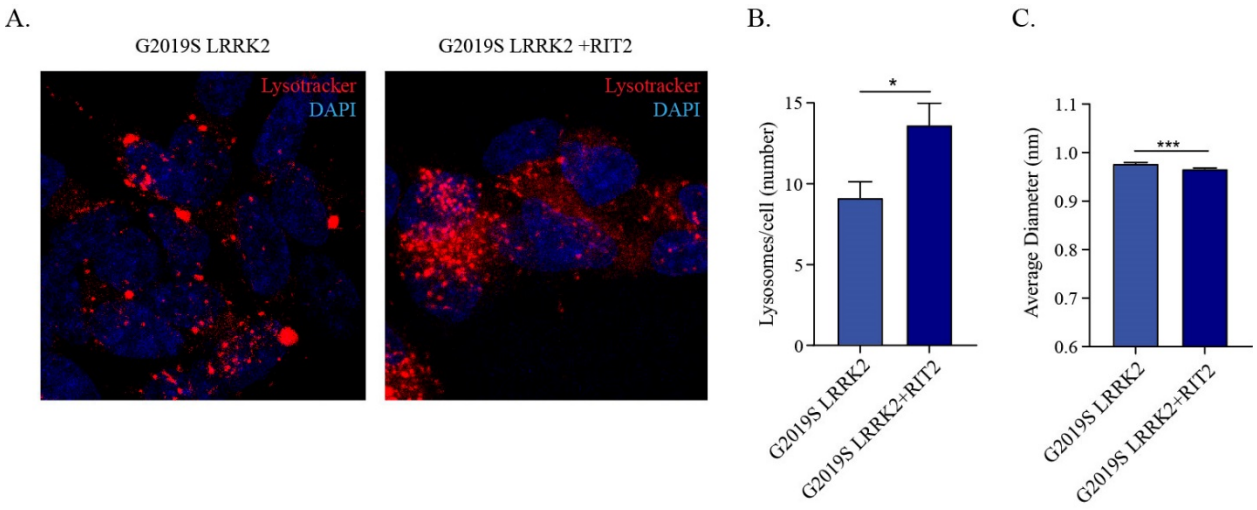

Figure 27: Lysotracker Deep Red staining in G2019S LRRK2 cells transfected with RIT2. A. Lysotracker staining in G2019S LRRK2 cells with or without *RTI2* transfection. B. Quantification of lysosome number per cell revealed a significant increase after *RIT2* transfection (n=3). C. Quantification of average size of lysosomes showed a significant decrease after *RIT2* transfection (n=3). *p<0.05, ***p<0.001, unpaired two tailed Student`s t-test.

3.8.4 *RIT2* overexpression increases proteolytic activity of lysosomes

Given the rescue of the morphological defects, the DQ-Red-BSA assay was used to investigate the proteolytic function of lysosomes in G2019S LRRK2 cells, upon transfection with *RIT2*. After 72 hours of *RIT2* expression, cells were incubated with DQ-Red-BSA and imaged. The overexpression of *RIT2* significantly enhanced the number of fluorescent spots per cell (Figure 28 B), indicating an increase in the proteolytic function. This demonstrated that *RIT2* not only acts on the morphology and number of autophagosomes and lysosomes, but also on the functionality of lysosomes.

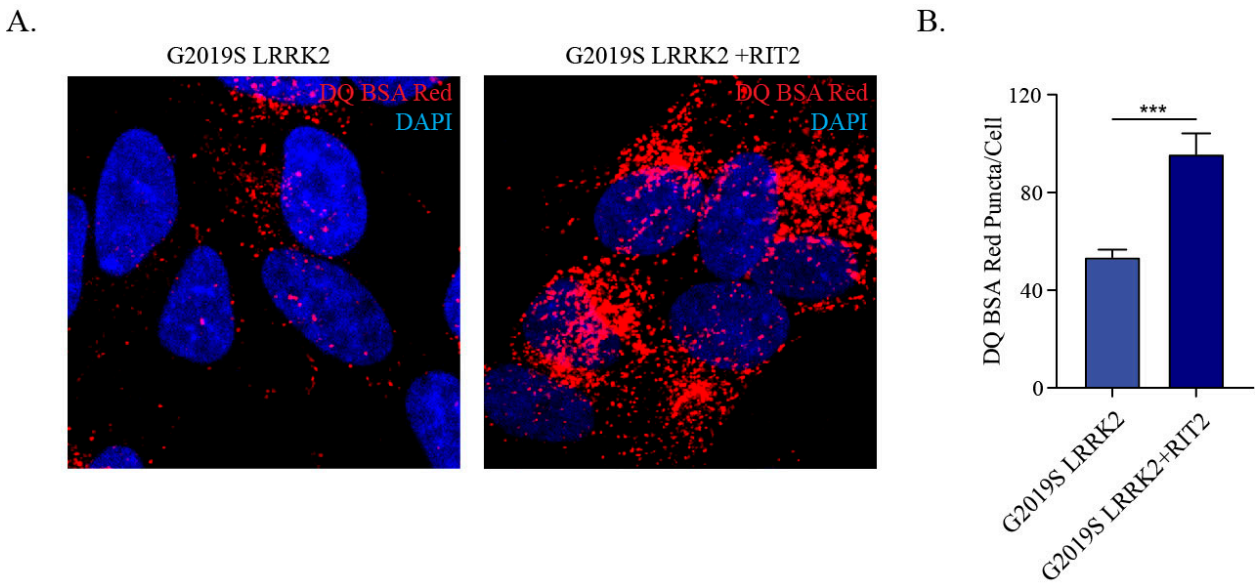

Figure 28: DQ-Red-BSA assay in G2019S LRRK2 cells transfected with *RIT2*. A. DQ-Red-BSA signal in G2019S LRRK2 cells and cells transfected with RIT2. B. Quantification of fluorescent puncta per cell (n=3) showed a significant increase of proteolytic activity in G2019S LRRK2 cells, upon *RIT2* transfection. ***p<0.001, unpaired two tailed Student`s t-test.

3.9 *RIT2* overexpression reduces pS129-aSyn inclusions

So far, the results suggested that the G2019S mutation in LRRK2 induces abnormalities in ALP and leads to an accumulation of pS129-aSyn-positive inclusions. Moreover, LRRK2 kinase inhibition in G2019S LRRK2 cells was able to rescue ALP-related defects and, more importantly, to reduce the number of pS129-aSyn-positive inclusions. The overexpression of RIT2 phenocopied the effects elicited by the application of the LRRK2 kinase inhibitor, therefore, the effect of *RIT2* overexpression on pS129-aSyn inclusions was assessed. G2019S LRRK2 cells were nucleofected with *RIT2* and after 72 h fixed and processed for pS129-aSyn staining. *RIT2* overexpression led to a significant reduction of pS129-aSyn-positive inclusions (Figure 29 B). This result indicates that LRRK2 kinase inhibition and RIT2 overexpression not only have beneficial effects on different stages of the ALP, but also reduce the number of pS129-aSyn inclusion in G2019S LRRK2 cells.

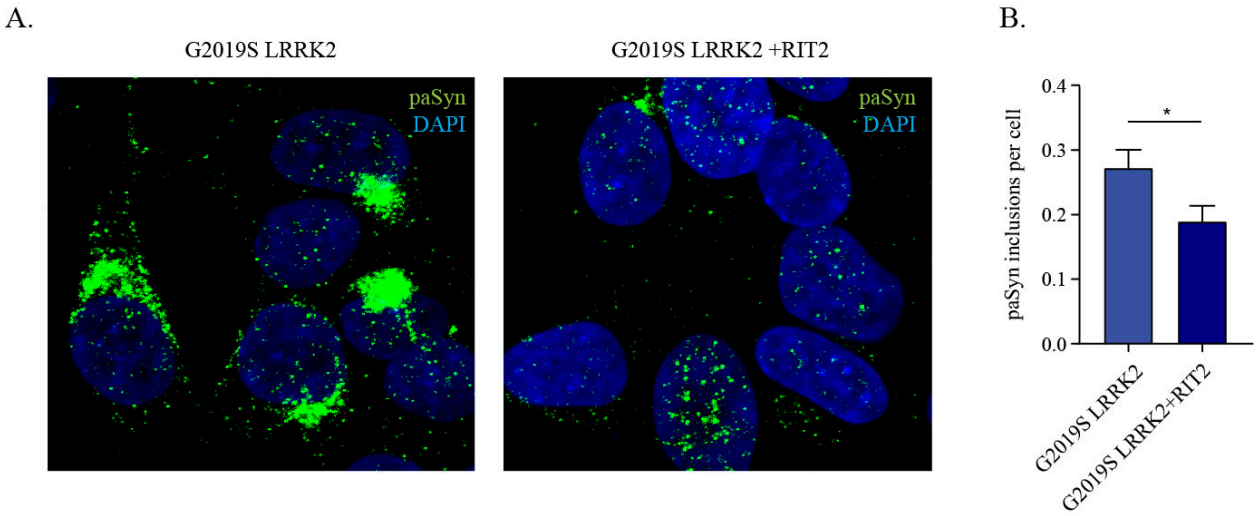

Figure 29: pS129-aSyn-positive inclusions in G2019S LRRK2 cells are reduced after *RIT2* transfection. A. ICC for pS129-aSyn was used to investigate the presence of intracellular inclusions of aSyn. B. Quantification of the pS129-aSyn-positive inclusions per cell in G2019 LRRK2 cells transfected with *RIT2* showed a significant decrease of spots per cell (n=4). *p<0.05, unpaired two tailed Student`s t-test.

3.10 LRRK2 inhibitor treatment does not affect *RIT2* gene expression levels

Our results indicate that RIT2 overexpression in G2019S LRRK2 cells phenocopies the pharmacological inhibition of LRRK2 kinase activity. We hypothesized that LRRK2 and RIT2 might be involved in a common molecular mechanism. We first explored the possibility that LRRK2 inhibitor treatment influenced *RIT2* mRNA levels. SH-SY5Y, WT and G2019S LRRK2 cells were treated with 300 and 500 nM PF475 for 6 hours, RNA was extracted and retrotranscribed. *RIT2* mRNA levels were then assessed using qPCR. No difference in *RIT2* gene expression was observed upon PF475 treatment (Figure 30), possibly due to the short application time of the LRRK2 inhibitor. Moreover, we have no evidence that LRRK2, either directly or indirectly, activates specific transcription factors.

A.

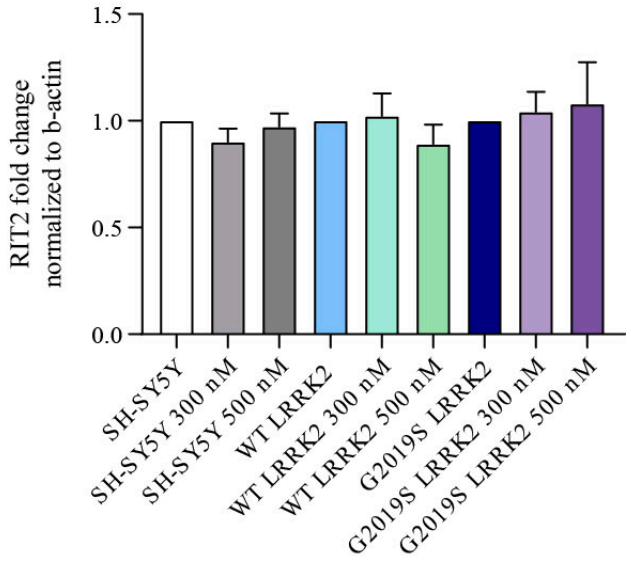

Figure 30: *RIT2* mRNA levels upon PF475 treatment in SH-SY5Y, WT and G2019S LRRK2 cells. A. *RIT2* mRNA levels (normalized on *ACTB* housekeeping gene and non-treated cells) were not changed upon PF475 treatment (300 or 500 nM, 6h; n=3)

3.11 *RIT2* overexpression reduces S1292, but not S935 phosphorylation of LRRK2

Since the LRRK2 inhibitor treatment did not affect *RIT2* mRNA expression levels, the opposite mechanistic hypothesis, i.e. that *RIT2* overexpression would inhibit LRRK2 kinase activity, was considered. Thus, LRRK2 phosphorylation levels at two distinct residues (S935 and S1292), which are responsive to pharmacological LRRK2 inhibition, were measured (shown in 3.5 and (Kluss et al. 2018)). G2019S LRRK2 cells were nucleofected with *RIT2*, lysed 72h later and processed for Western blot analysis. The overexpression of RIT2 in G2019S LRRK2 cells led to a significant decrease of S1292 phosphorylation (Figure 31 B), when compared to non-nucleofected G2019S LRRK2 cells.

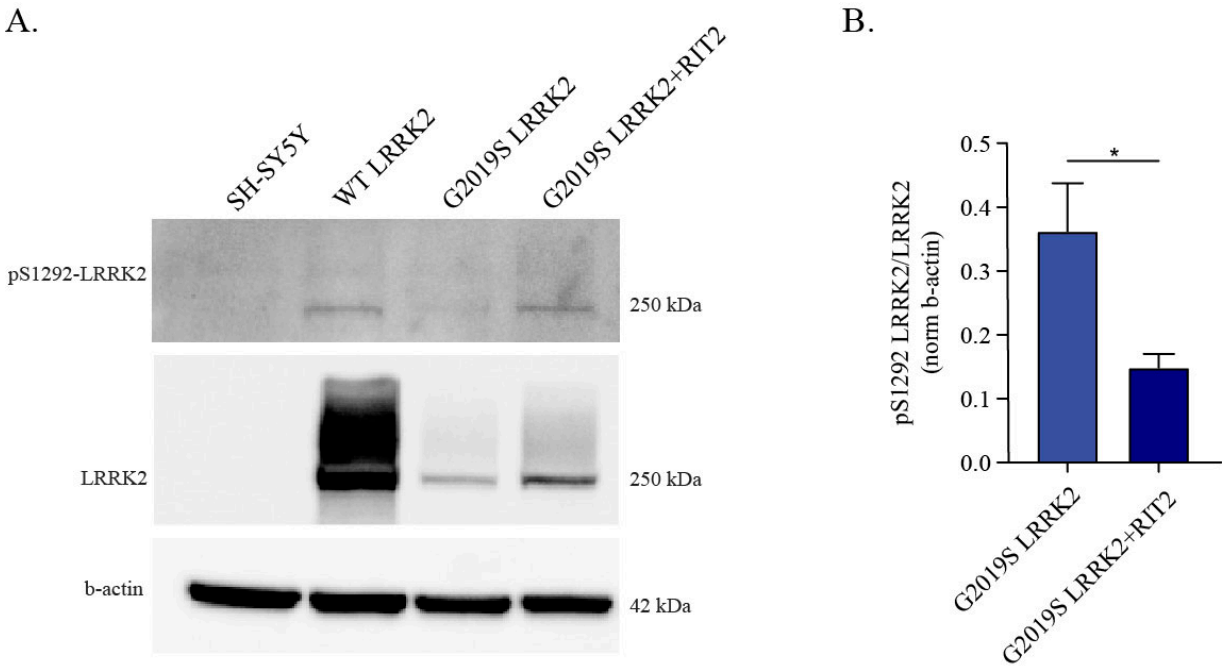

Figure 31: LRRK2 phosphorylation levels in SH-SY5Y, WT LRRK2, G2019S LRRK2 and G2019S+RIT2 cells. A. Phosphorylation of S1292 was assessed in SH-SY5Y, WT LRRK2, G2019S LRRK2 and G2019S+RIT2 cells blotting for pS1292, total LRRK2 and β-actin (n=5). B. pS1292 LRRK2 levels, normalized to total LRRK2, were reduced after *RIT2* overexpression. *p<0.05, unpaired two tailed Student`s t-test.

At the same time and distinct from LRRK2 kinase inhibitor treatment, pS935 levels were not decreased. Oppositely, a significant increase of S935 phosphorylation was observed with RIT2 overexpression in G2019S LRRK2 cells (Figure 32 B). Moreover, total LRRK2 levels (normalized to β-actin) in G2019S LRRK2 cells transfected with *RIT2* were slightly increased (Figure 32 C). Again, this effect is distinct from LRRK2 kinase inhibitors, which have been demonstrated to downregulate LRRK2 through destabilization of the protein (Lobbestael et al. 2016).

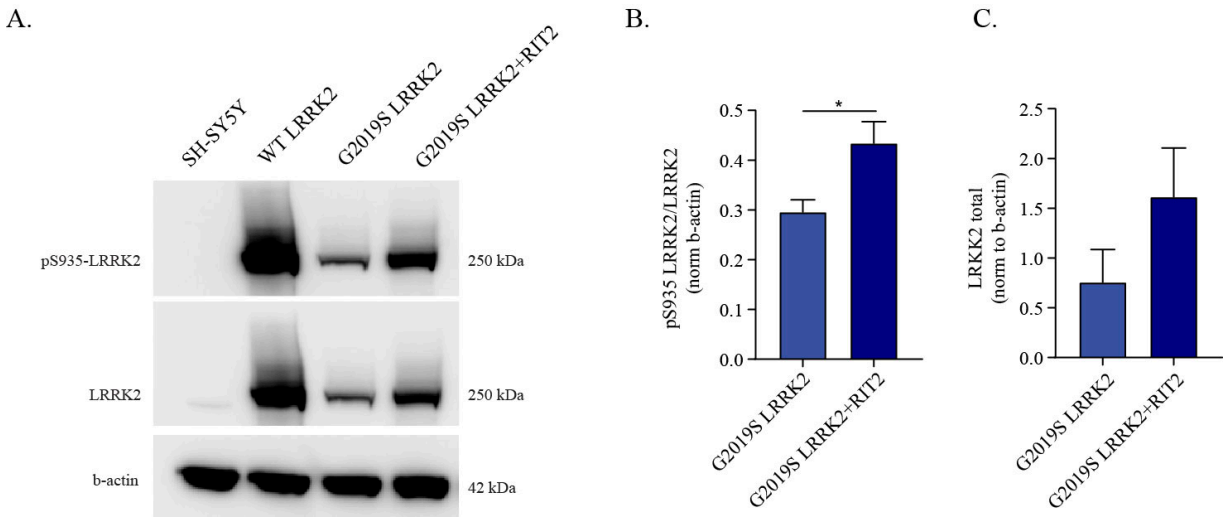

Figure 32: LRRK2 phosphorylation levels in SH-SY5Y, WT LRRK2, G2019S LRRK2 and G2019S+RIT2 cells. A. Phosphorylation of S935 was assessed in SH-SY5Y, WT LRRK2, G2019S LRRK2 and G2019S+RIT2 cells blotting for pS935, total LRRK2 and b-actin. B. pS935 LRRK2 levels, normalized to total LRRK2, are significantly increased after *RIT2* overexpression (n=5). C. RIT2 transfection led to a trend of increased total LRRK2 levels, normalized on β-actin (6N). *p<0.05, unpaired two tailed Student`s t-test.

3.12 Neuroprotective effect of *RIT2* in an *in vivo* PD mouse model

3.12.1 Enhanced *RIT2* expression in the mouse midbrain counteracts aSyn-dependent deficits and DA neuron loss

We modeled PD pathophysiology in the mouse using a unilateral injection of an AAV 2/9 expressing the human mutant A53T aSyn (AAV-CMVie-hSynP-synA53T, AAV aSyn herein) into the substantia nigra of DAT-Ires-Cre mice. This approach has been previously shown to induce progressive SNc neuron loss, aSyn neuropathology and motor deficits (Oliveras-Salva et al. 2013). DAT-Ires-Cre mice express the Cre recombinase specifically in cells expressing DAT, allowing specific gene manipulation in DA neurons. This model allows to relate the observed phenotypes directly to cellular responses in DA neurons. The injection of AAV-aSyn led to an about 4-fold increase of total aSyn protein levels measured by traditional Western blotting (Figure 33 A;B). After 16 weeks of overexpression, the animals developed motor deficits in the rotational test with a propensity to rotate in the direction of the lesion side (ipsilateral) and to use preferably the ipsilateral forepaw (Figure 33 D). In addition, aSyn expression induced a loss of TH positive neurons in the midbrain (Figure 34) coupled to a loss of striatal DA terminals (Figure 35), mimicking the nigrostriatal degeneration observed in PD.

The co-injection of AAV-aSyn with AAV-FLex-RIT2 reduced total aSyn protein levels in midbrain tissue and reversed the aSyn-induced rotation defect, when compared to AAV-Flex-GFP control injection. Open field-testing demonstrated a significant increase in the distance travelled when *RIT2* was co-expressed with aSyn, and also a trend for an increase with AAV-FLex-RIT2 injection alone (Figure 33 C). In addition, the loss of TH-positive neurons in SNc and DA in striatum was attenuated by co-expression of aSyn and *RIT2*.

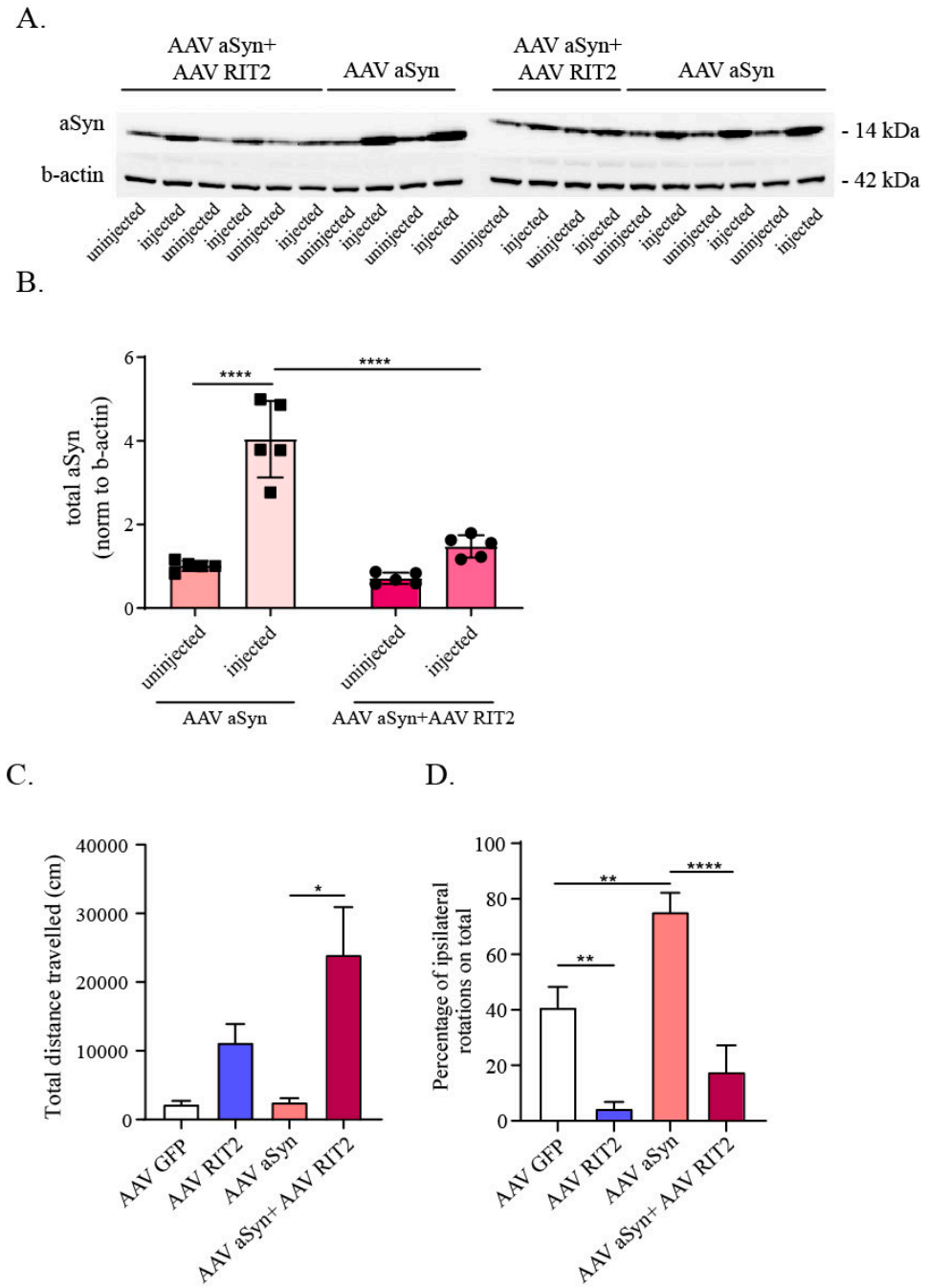

Figure 33: AAV aSyn injection in the mouse SNc increases total aSyn levels and induces motor deficits, which are reversed by co-injection of AAV RIT2. A. Total aSyn levels in mice injected with AAV aSyn alone or in combination with AAV RIT2 were assessed blotting for total aSyn and β-actin. B. Quantification of total aSyn levels, normalized on β-actin (5 animals/group). Co-injection of AAV RIT2 significantly reduces aSyn levels in the injected side. C. Total distance travelled in the open field test, revealed a significant increase of activity in AAV asyn + AAV RIT2 co-injected mice (AAV GFP-7 animals, AAV RIT2-6 animals, AAV aSyn-9 animals, AAV aSyn+AAV RIT2-5 animals). D. AAV aSyn injection induces a significant increase of ipsilateral rotations (on total number of rotations), which is decreased by co-injection of AAV RIT2. AAV RIT2 injection alone significantly decreases the number of ipsilateral rotations (same number of animals as in C). B-****$p<0.0001$, two-way ANOVA followed by the Bonferroni´s post-hoc test. C/D-*$p<0.05$, **$p<0.01$, ****$p<0.0001$, one-way ANOVA followed by Bonferroni´s post-hoc test.

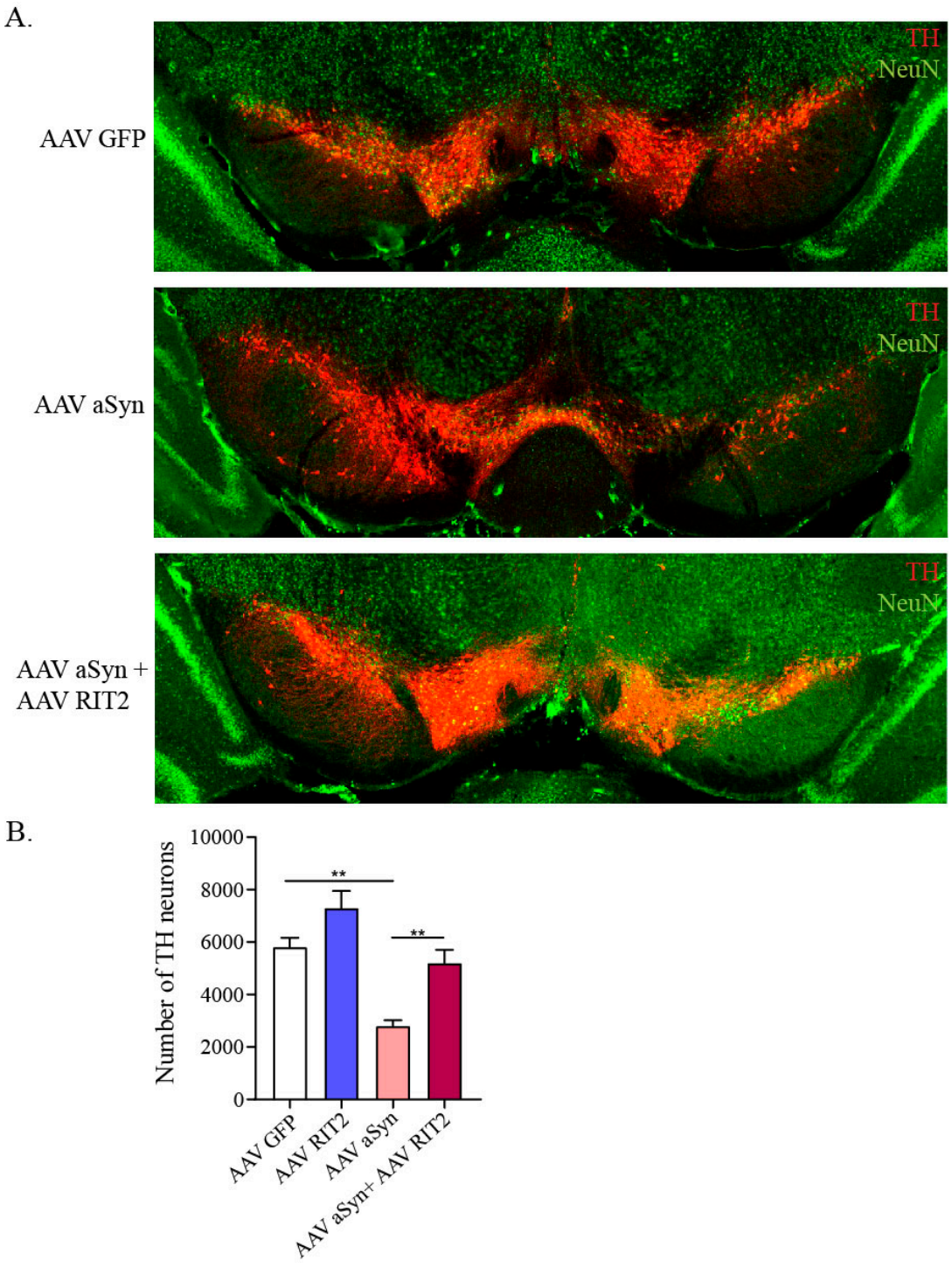

Figure 34: A. IHC staining of TH and NeuN in the midbrain of AAV GFP, AAV aSyn and AAV aSyn + AAV RIT2 injected mice. B. Quantification of TH neurons. AAV aSyn injection significantly reduced the number of TH neurons, which is attenuated by the co-injection of AAV RIT2 (5 animals/group). **p<0.01, one-way ANOVA followed by the Bonferroni´s post-hoc test.

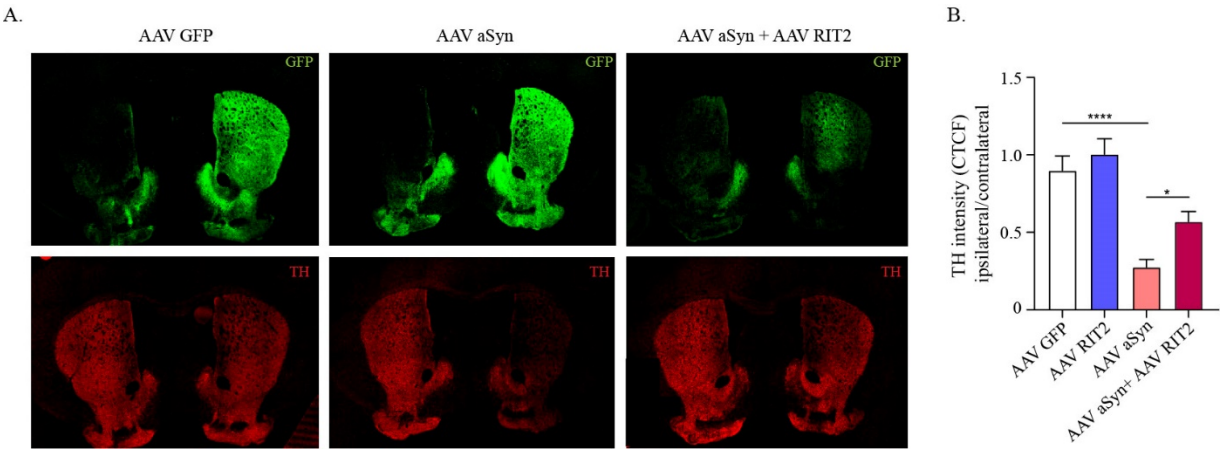

Figure 35: A. IHC staining of TH and GFP in the striatum of AAV GFP, AAV aSyn and AAV aSyn + AAV RIT2 injected mice. B. Quantification of TH intensity. AAV aSyn injection significantly reduced the intensity of TH signal, which is rescued by the co-injection of AAV RIT2 (5 animals/group). **p<0.01, ****p<0.0001, one-way ANOVA followed by the Bonferroni´s post-hoc test.

3.12.2 *In vivo* aSyn overexpression increases endogenous LRRK2 activity, which is prevented by RIT2 overexpression

Viral co-expression of RIT2 with aSyn was shown to ameliorate the aSyn-induced neuronal loss and behavioural deficits in the mouse. A recently published article reported that viral overexpression of aSyn leads to increased LRRK2 kinase activity in the rat (Di Maio et al. 2018). Here, we have shown that RIT2 reduces phosphorylation levels of LRRK2 in cells, thus leading to inhibition of kinase activity. Therefore, the impact of RIT2 on LRRK2 S1292 phosphorylation was assessed *in vivo*. Two antibodies for LRRK2 (one for total protein and one for pS1292 LRRK2) were used for a PLA, which is a method used to identify two epitopes being in close proximity to each other. In this case, both epitopes are on the same protein, thus increasing specificity and decreasing background staining. PLA analysis was carried out on midbrain sections after 8 weeks of viral overexpression. AAV-aSyn injection induced a marked increase in the number of PLA dots, indicating a significant increase of endogenous LRRK2 autophosphorylation and activity. The co-expression of RIT2 with aSyn completely prevented the overactivation of endogenous LRRK2 (Figure 36 D). Importantly, total LRRK2 levels were not changed by AAV aSyn or AAV aSyn + AAV-Flex-RIT2 (Figure 36 B). In summary, viral RIT2 overexpression in the mouse was able to rescue aSyn-induced motor deficits, DA neuron loss and endogenous LRRK2 activation.

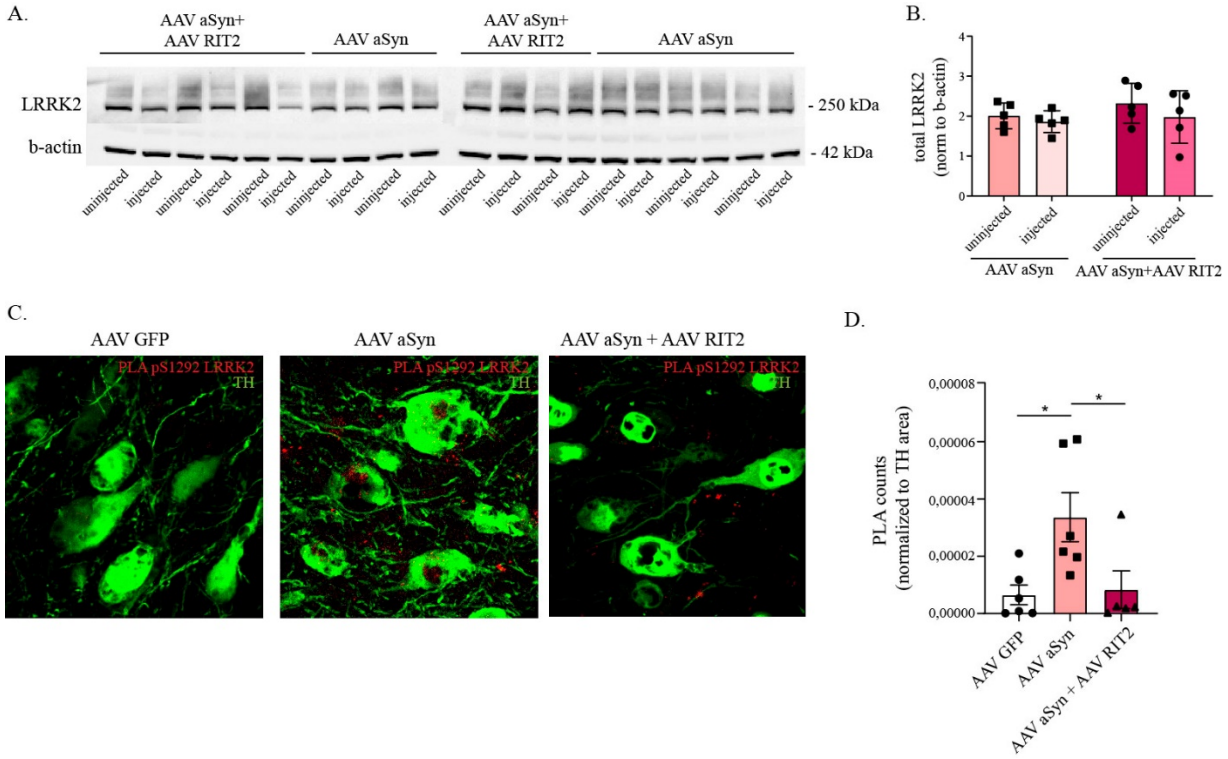

Figure 36: AAV aSyn injection in the mouse SNc increases endogenous LRRK2 kinase activity, which is reversed by co-injection of AAV RIT2. A. Total LRRK2 levels in mice injected with AAV aSyn alone or in combination with AAV RIT2 were assessed by Western blot analysis for total LRRK2 and β-actin. B. Quantification of total LRRK2 levels, normalized on β-actin (5 animals/group). Viral overexpression of aSyn or RIT2 did not affect total LRRK2 levels. C. PLA analysis of AAV GFP, AAV aSyn and AAV aSyn + AAV RIT2 injected mice in TH neurons in the SNc. D. Quantification of PLA counts. AAV aSyn significantly increased the number of PLA counts (normalized on TH area) and the increase was prevented by co-injection of AAV RIT2 (AAV GFP and AAV aSyn-6 animals, AAV aSyn+AAV RIT2-5 animals). *p<0.05, one-way ANOVA followed by the Bonferroni´s post-hoc test.

4 Discussion

4.1 G2019S LRRK2 cells display ALP defects and pS129-aSyn-positive inclusions

LRRK2 mutations, particularly the G2019S substitution, are the most common causes of autosomal dominant PD. In addition, genomic variability in the *Lrrk2* locus has been associated to PD in several GWAS studies, demonstrating its importance in the idiopathic disorder as well (Pankratz et al. 2012, Nalls et al. 2014, Chang et al. 2017, Nalls et al. 2019). Increased LRRK2 kinase activity was recently observed in idiopathic PD (Di Maio et al. 2018), providing a further bridge between familial and idiopathic forms. LRRK2-associated PD presents neuropathological features almost indistinguishable from the idiopathic disease. The G2019S LRRK2 mutation is mostly associated to LB pathology, while other mutations present pleomorphic neuropathology (Zimprich et al. 2004).

In this project, we investigated the effects of G2019S LRRK2 on the ALP and pS129-aSyn-positive inclusion clearance. First, we investigated LRRK2 expression levels in SH-SY5Y cells overexpressing WT and G2019S LRRK2. We showed that recombinant LRRK2 expression levels differ, with WT LRRK2 cells displaying an expression level that is about three times higher than in G2019S LRRK2 cells. LRRK2 overexpression was confirmed by ICC staining for LRRK2 and showed that the protein resides mostly in the cytosol. To conclude the biochemical characterization, we confirmed a 3-4 fold increase of S1292 LRRK2 autophosphorylation in G2019S LRRK2 cells when compared to WT LRRK2 cells, which is consistent with previous observations (West et al. 2005). On the other hand, phosphorylation levels of S935 LRRK2 were decreased in G2019S LRRK2 cells, when compared to WT LRRK2 cells. In our hands, the phosphorylation levels of this Serine residue does not correlate with kinase activity, consistent with previous observations in different tissues from WT and G2019S knock-in mice (Kluss et al. 2018, Mercatelli et al. 2019). LRRK2 plays important roles in regulating different stages of autophagy, but a clear view on the steps specifically affected and the nature of this regulation is currently missing. Many studies show contradicting results, possibly due to different model systems used (Yakhine-Diop et al. 2014, Ho et al. 2018, Schapansky et al. 2018, Ho et al. 2019, Wallings et al. 2019). We first employed an unbiased approach to detect broad alterations in autophagy via the expression levels of related genes in SH-SY5Y, WT LRRK2 and G2019S LRRK2 cell lines. The qPCR-based array of autophagy-

associated genes indicated several genes that were differentially regulated when LRRK2 (WT or G2019S mutant) was overexpressed. Specifically, several genes implicated in autophagosome formation and processing displayed differential modulation by LRRK2 overexpression. Moreover, we also observed a difference in gene expression levels that was dependent on the G2019S LRRK2 mutation. *MAP1LC3A*, *MAP1LC3B* and *WIPI1* particularly attracted our attention, since they are important in autophagosome formation and fusion to the lysosome. These hints led us to further investigate specific steps of ALP,, such as autophagosome formation, autophagosome fusion to the lysosome and lysosomal morphology. Our data show that both WT and G2019S LRRK2 impact autophagosome number, lysosome morphology and functionality. ICC analysis of LC3B demonstrated an increase in LC3B puncta in G2019S LRRK2 cells but not WT LRRK2 cells, which is consistent with the increased *MAP1LC3A* and *MAP1LC3B* mRNA levels. In contrast, lysosome number and morphology were affected in the same manner by WT and mutant LRRK2 overexpression. Only G2019S LRRK2 cells showed a concurrent impairment in autolysosome formation and proteolytic activity of the lysosomes, causing accumulation of endogenous pS129-aSyn-positive inclusions specifically in these cells. Moreover, our transcriptome analysis showed altered mRNA levels of *CTSB*, encoding for the lysosomal protease Cathepsin B, which plays an essential role in aSyn degradation (McGlinchey and Lee 2015). Enhanced cellular levels of WT LRRK2 also have consequences on ALP; however cells appear to be capable of better compensation. In fact, despite similar lysosomal depletion, WT LRRK2 increases proteolytic activity, enhances the autophagosome-lysosome fusion capacity and no detectable pS129-aSyn inclusions are observed. This indicates that the correct advancement of the autophagic process is capable of compensating the lysosomal depletion. However, there is the possibility that pS129-aSyn inclusion clearance and ALP modulation are two partially distinct phenomena. Our evidence indicates that the phenomena are not correlated, but ALP modulation might be the cause of the pS129-aSyn inclusion clearance. In fact, autophagosome to lysosome fusion is a critical step in the autophagic process and, as such, object of intense investigation in not only PD, but also other diseases. The inhibition of autophagosome to lysosome fusion is a promising therapy in the treatment of glioblastoma (Shojaei et al. 2019). In Huntington disease, mutant huntingtin affects the mobility of autophagosomes, resulting in a reduction of autolysosome formation and an increase in the number of autophagosomes (Wong and Holzbaur 2014). The Kufor-Rakeb

syndrome is associated with mutations in the ATP13A2 gene, which is also causative for some early-onset forms of PD. Patient-derived fibroblasts carrying these mutations display an increase in the number of autophagosomes, resulting from a block in the fusion with lysosomes (Ramirez et al. 2006).

Enhanced LRRK2 levels *per se* induce variations in ALP, and the G2019S mutation leads to alterations to LRRK2 functionality that result in specific functional changes. Notably, our gene expression array shows an enhancement of *MAP1LC3A* and *MAP1LC3B* transcription in LRRK2 cells, which might be interpreted as an increased autophagic function. However, more targeted functional assays demonstrated the opposite, calling for caution when interpreting results from a single experimental paradigm (Klionsky et al. 2016). Investigating autophagosome number requires the same level of accuracy: an increase in the number could derive either from an increase in the production of autophagosomes, or a blockade in their degradation. This, again, points to the autophagosome maturation and fusion to the lysosome as critical steps in ALP. In fact, in PD a defective autophagosome to lysosome fusion was shown to increase the number of autophagosomes but, at the same time, exosomal aSyn release was increased as well (Danzer et al. 2012, Ejlerskov et al. 2013, Lee et al. 2013).

It has been demonstrated that autophagosomes are formed at random positions in the cell and are then actively transported towards the center of the cell (Jahreiss et al. 2008, Kimura et al. 2008). In contrast, lysosomes mostly distribute around the nucleus (Pu et al. 2016). This implies that the process of fusion is heavily dependent on the spatial location of autophagosomes and lysosomes, and that the trafficking of autophagosomes and lysosomes can be a critical factor in this process. In fact, the loss of dynein, causing motoneuron disease, leads to an accumulation of LC3-positive structures, resulting from an impaired fusion of autophagosomes to lysosomes (Ravikumar et al. 2005).

In summary, endogenous aSyn accumulates specifically in G2019S-LRRK2 cells, probably due to impaired lysosomal degradation following ineffective formation of autolysosomes. Several previous studies demonstrated that LRRK2 modulates aSyn neuropathology in a kinase-dependent manner and PD-associated mutations, such as G2019S, negatively affect this modulatory action (Daher et al. 2015, Volpicelli-Daley et al. 2016, Zhao et al. 2017, Ho et al. 2019). On the other hand, autophagy impairment can play a causative role in aSyn accumulation (Cuervo et al. 2004, Komatsu et al. 2006, Lynch-Day et al. 2012, Sato et al. 2018). In addition,

alterations in autophagy/lysosome markers are found in PD brain areas affected by LB pathology (Chu et al. 2009, Dehay et al. 2010). However, no direct, experimental link between aSyn accumulation, LRRK2 kinase activity and autophagy has been reported to date.

4.2 LRRK2 kinase inhibition rescues ALP-related defects and reduces pS129-aSyn inclusions in G2019S LRRK2 cells

LRRK2 kinase inhibitors have been developed with the goal of providing a disease-modifying therapeutic strategy based on the etiological involvement of increased kinase activity in LRRK2 PD patients (West 2015). Preclinical models confirmed their potential in rescuing toxic effects of mutant LRRK2 (Atashrazm and Dzamko 2016), providing rationale for clinical trials in familial LRRK2 PD. However, recent evidence demonstrated that LRRK2 silencing or kinase inhibition are also effective against aSyn neuropathology and toxicity (Daher et al. 2014, Daher et al. 2015, Volpicelli-Daley et al. 2016, Zhao et al. 2017). We showed that G2019S LRRK2 overactivated the kinase function in our model system, therefore we next sought to investigate the effects of LRRK2 kinase inhibition on the observed ALP defects. Two different concentrations of the LRRK2 kinase inhibitor PF475 were applied to G2019S LRRK2 cells. In summary, the pharmacological inhibition of LRRK2 attenuated all the observed abnormalities at different stages of autophagy. PF475 treatment decreased LC3B levels in a concentration-dependent manner. In addition, lysosome number was increased and lysosomal size was decreased. Autolysosome formation and number of autolysosomes were rescued, as well as the proteolytic function of lysosomes, measured by the DQ-Red-BSA assay. Most importantly, these effects were accompanied by a reduction of pS129-aSyn-positive inclusions. These results suggest that reduction in lysosome function and formation of autolysosomes are causative of pS129-aSyn accumulation, but still do not prove it. It was recently demonstrated that CQ specifically inhibits the fusion between autophagosomes and lysosomes (Mauthe et al. 2018). The blockade of autophagosome to lysosome fusion by CQ prevented the PF475-dependent reduction of pS129-aSyn inclusions. This indicates that the fusion step might be the target of LRRK2 kinase activity and is required for clearance of pathologic aSyn. On the other hand, we cannot exclude the possibility of LRRK2 kinase activity having effects upstream from the fusion event, which mediate pS129-aSyn degradation. It is known that LRRK2 phosphorylates a variety of substrates, including a subset of Rab GTPases and specifically Rab10 (Steger et al.

2016). The Rab family functions as molecular switches in the fusion and motion of intracellular membranes (Stenmark 2009). The composition of cellular membranes is characteristic of each organelle and one of the diversifying components are Rab GTPases, providing specificity to trafficking events (Stenmark 2009, Zhen and Stenmark 2015). They "identify" different organelles and through the recruitment of effector proteins, they also determine the fate of organelles. Among these downstream effectors, particular relevance is given by SNAREs, of these, especially VAMP7, VAMP8, and VTI1B. These SNARES are specifically implicated in the autophagosome to lysosome fusion, a process impaired in lysosomal storage disorders where cholesterol accumulates in the lysosome. This accumulation sequesters SNAREs in the membrane preventing their recycling (Fraldi et al. 2010). The fusion of autophagosomes to lysosomes depends also on syntaxin 17 (STX17), which is interacting with VAMP8 and SNAP29 and localizes to the outer autophagosome membrane. Interestingly, STX17 is not present on phagophores or other autophagosome precursors, preventing them from fusing with the lysosome at an excessively early stage of maturation (Itakura et al. 2012). The small GTPase Rab7, on the other hand, is recruited to late autophagosomes (Gutierrez et al. 2004) and links autophagosomes to microtubule motors, mediating kinesin-driven movement (Pankiv et al. 2010). It could be hypothesized that LRRK2 phosphorylates Rab7, impacting its function and subsequently the autophagosome to lysosome fusion process. LRRK2 and Rab7L1 are recruited to overloaded, stressed lysosomes, where LRRK2 becomes activated and phosphorylates its substrate Rab10. Phosphorylated Rab10 accumulates on lysosomes, which ultimately leads to suppression of lysosomal enlargement and enhanced lysosomal secretion. The authors of the study suggest that Rab GTPases possibly acquire novel functions under stress conditions that are distinct from their physiological role in endocytic trafficking (Eguchi et al. 2018). These findings might explain the effects of LRRK2 kinase activity on lysosome size and number in our cell models. The differential location of STX17 on phagophores and autophagosomes point to the fact that autophagosomes are organelles that form *de novo* and have to "acquire" the required molecular machinery for the correct fusion process. Therefore, the interactions between LRRK2 and STX17, and generally between LRRK2 and Rab GTPases and SNARES are interesting targets.

4.3 *RIT2* overexpression rescues ALP defects and reduces pS129-aSyn inclusion burden in G2019S LRRK2 cells

In the second part of our project, we propose a novel, underexplored target to combat aSyn neuropathology and associated deficits. We validate the therapeutic potential of the small GTPase RIT2 in complementary models and define the cellular processes involved. We measured *RIT2* mRNA levels in our cell lines using ddPCR, a new and sensitive method to detect expression changes even in low abundance mRNAs. The overexpression of both WT and G2019S LRRK2 dramatically reduced *RIT2* mRNA levels. This result matches with the decrease of *RIT2* promoter activity observed with the luciferase reporter construct, and is consistent with literature evidence of decreased *RIT2* mRNA levels in PD patient brains (Bossers et al. 2009). The downregulation of *RIT2* mRNA constitutes the rationale to transiently restore *RIT2* expression in G2019S LRRK2 cells, which was achieved by high efficiency nucleofection for 72 hours. *RIT2* overexpression was capable to reduce autophagosome number, increase lysosome number and reduce their size. Moreover, *RIT2* was able to rescue the impaired proteolytic function of lysosomes. In summary, the overexpression of *RIT2* provided the same rescue of G2019S-dependent phenotypes as observed with LRRK2 kinase inhibition, leading to the question if LRRK2 and *RIT2* could interact in a common pathway. We first hypothesized that PF475 impacted *RIT2* gene expression, but the treatment had no effect on *RIT2* mRNA levels. Rather, the opposite hypothesis turned to be correct, with *RIT2* overexpression modulating the phosphorylation levels of LRRK2. Importantly, S1292 phosphorylation was reduced by *RIT2* overexpression, whereas S935 phosphorylation was significantly increased, critically differentiating *RIT2*-related effects from those deriving from pharmacological LRRK2 kinase inhibition. In addition, we report that the overexpression of *RIT2* neither reduced LRRK2 total protein levels, an established consequence of treatment with pharmacological LRRK2 kinase inhibitors (Lobbestael et al. 2016). Indeed, the phosphorylation levels of S935 have been associated with 14-3-3 protein binding and a reduction in the pS935 LRRK2 levels was shown to reduce this binding and destabilize LRRK2 protein (Dzamko et al. 2010). The exact mechanisms behind LRRK2 destabilization is not yet understood, but it is thought to rely on LRRK2 kinase activity, since mice expressing a kinase-dead form of LRRK2 display reduced LRRK2 protein levels (Herzig et al. 2011, Mercatelli et al. 2019). LRRK2 KO mice show pathological changes in kidney and lung, whereas the kinase-dead expressing mice displayed

defects only in the kidney (Herzig et al. 2011). In addition, LRRK2 kinase inhibition induces morphological defects in the lung of non-human primates (Fuji et al. 2015). However, LRRK2 destabilization is reversible, if the treatment is withdrawn (De Wit et al. 2019). Understanding the exact regulation of LRRK2 protein degradation is a key point to predict side effects of LRRK2 kinase inhibitors. LRRK2 inhibitors are, in fact, envisaged to be administered not only to LRRK2-PD patients, but also to idiopathic PD patients, as indicated by the increase of pS1292 LRRK2 levels in urinary exosomes and brain tissue (Fraser et al. 2016, Di Maio et al. 2018). Indeed, Denali Therapeutics is testing a LRRK2 kinase inhibitor (DNL201) in a randomized, placebo controlled Phase 1b clinical study in patients with mild to moderate Parkinson's disease, with and without genetic LRRK2 mutations (ClinicalTrials.gov identifier NCT03710707). We demonstrated that *RIT2* overexpression is capable to reduce pS1292 LRRK2 levels, without affecting S935 LRRK2 phosphorylation and LRRK2 protein stability. These findings open the door to novel therapeutic strategies, displaying beneficial effects phenocopying LRRK2 kinase inhibitors, but we predict this approach will avoid undesired peripheral effects.

4.4 Enhanced *RIT2* expression in an *in vivo* PD mouse model is neuroprotective

To validate the findings obtained in our recombinant cell lines, we moved to an *in vivo* mouse model, which consisted of the unilateral injection of an AAV carrying the human A53T aSyn into the SNc of DAT-Ires-Cre mice. This approach has previously been shown to induce progressive SNc neuronal loss, aSyn neuropathology and motor deficits (Oliveras-Salva et al. 2013, Ip et al. 2017, Williams et al. 2018). In fact, we demonstrated that total aSyn protein levels are increased upon viral overexpression, which leads to a loss of TH neurons in the midbrain and a reduction of striatal dopamine terminals. Moreover, AAV-aSyn injected animals displayed motor deficits, which were reversed by the selective expression of *RIT2* in midbrain DA neurons. The co-expression of *RIT2* not only rescued motor impairment, but also attenuated the loss of TH neurons in the midbrain and of the reduction of striatal DA nerve terminals. Notably, the viral overexpression of *RIT2* in DA neurons, independently from aSyn overexpression, induced a marked increase in locomotion, measured in the open field test. Animals displayed a hyperactive phenotype, which might derive from altered DA levels or release dynamics. It has been recently reported that the genetic deletion of DAT in rats increases extracellular DA lifetime, resulting in marked locomotor hyperactivity (Leo et al. 2018). Consistently, DAT KO

mice, display pronounced hyperlocomotion (Giros et al. 1996). The DAT T356M mutation specifically causes reduced transporter function, a reduced rate of DA reuptake from the extracellular space and in homozygosity leads to hyperactivity in mice (DiCarlo et al. 2019). It was previously shown that *RIT2* interacts with DAT and is required for its trafficking, indicating a role for *RIT2* in the regulation of DA release and signaling (Navaroli et al. 2011), suggesting this modulation as the underlying mechanism of the increased locomotion ability. However, further studies specifically looking at DAT protein levels, subcellular localization, DA levels and release are needed to confirm this hypothesis. Interestingly, a recent study showed that the conditional KO of *RIT2* decreases total DAT protein in the male striatum, in the absence of changes of TH or DAT mRNA levels. The reduction of DAT protein in the striatum leads to a defect in DA signaling, which could be a possible explanation for the observed anxiolytic phenotype, detected in the open field and elevated plus maze tests (Sweeney et al. 2019).

The reduction of pS1292 LRRK2 levels *in vitro* and the recent observation that virally overexpressed aSyn increases endogenous LRRK2 kinase activity (Di Maio et al. 2018), led us to investigate LRRK2 kinase function in the AAV-aSyn mouse model, in order to reconcile the molecular mechanism. Indeed, we confirmed the finding from Di Maio et al., showing an increased LRRK2 kinase activity in the mouse midbrain, following AAV-aSyn injection. The co-injection of *RIT2* completely prevented the overactivation of endogenous LRRK2. In summary, viral *RIT2* overexpression in the mouse was able to rescue aSyn-induced motor deficits, DA neuron loss and endogenous LRRK2 activation, confirming the neuroprotective effects of *RIT2* in different model systems. In cell lines, we demonstrate that LRRK2 kinase inhibition (pharmacological and *RIT2*-mediated) is affecting primarily autophagic structures and mechanisms. Further experiments are needed to confirm that the neuroprotective effect of *RIT2* in the aSyn mouse model is also dependent on the regulation of autophagosome and lysosome number and most importantly on the fusion of the autophagosome to the lysosome. Targeting aSyn and its pathological aggregation is currently an intensively studied research field in many neurodegenerative diseases like PD and related synucleinopathies (DLB, MSA) (Dehay et al. 2015, O'Hara et al. 2018). Furthermore, autophagy is a conserved cellular process that functions to remove unwanted cellular material (proteins, whole organelles), and has been implicated in several neurodegenerative proteinopathies (Martinez-Vicente and Cuervo 2007) including PD (Lynch-Day et al. 2012). aSyn is a substrate for autophagy (Cuervo et al. 2004),

but the physiological role and pathological species are still under debate. On the other hand, it has been shown that PD-causing mutations in aSyn impair autophagy and are resistant to degradation (Tanik et al. 2013, Scrivo et al. 2018). Our results demonstrate that impacting ALP can have beneficial effects on aSyn inclusion clearance and therefore could also be an interesting target in different neurodegenerative proteinopathies. In fact, the observed effects of *RIT2* specifically on autophagosome to lysosome fusion might not be restricted to aSyn pathology, but applicable to other diseases, such as Alzheimer´s and Huntington´s.

Lastly, *RIT2*-dependent effects on autophagy can have a possible impact on synaptic vesicle trafficking. It has been demonstrated that autophagy is also active in degrading synaptic vesicles in DA neurons (Hernandez et al. 2012). However, autophagy at the cell body and at the synapse levels are two distinct mechanisms (Maday and Holzbaur 2016, Vijayan and Verstreken 2017). On the other hand, the machinery necessary for autophagy is present at the synapse and include many common proteins. EndophilinA (EndoA) is a presynaptic protein involved in vesicle endocytosis and colocalizes with autophagosomes. The phosphorylation of EndoA induces changes in the protein structure leading to the formation of highly curved membrane zones, which are required at the elongation step of autophagosome formation (Soukup and Verstreken 2017). Interestingly, LRRK2 mediates a phosphorylation cycle on EndoA that regulates endocytosis at the synaptic terminal (Matta et al. 2012). A second example are SNARES, which are key players in membrane fusion, an important mechanism in both autophagy and synaptic vesicle endo- and exocytosis. The neuron-specific synaptic SNARE n-syb (neuronal Synaptobrevin), for example, localizes to synaptic and endosomal vesicles and a loss of n-syb leads to endosomal accumulations and a secondary increase in autophagy (Haberman et al. 2012).

In our study, we specifically focused on macroautophagy since, in our cell models, this major form of autophagy was found to be severely affected. Nevertheless, CMA is also profoundly implicated in LRRK2 biology and aSyn pathology (Cuervo et al. 2004, Orenstein et al. 2013, Ho et al. 2019) and we do not exclude an involvement of CMA and the possibility that parallel pathways might lead to similar cellular consequences. This hypothesis is also supported by the relation and compensatory interaction of macroautophagy and CMA (Kaushik et al. 2008, Patel and Cuervo 2015). Lastly, LRRK2 has direct roles on lysosome biology and function (Eguchi et al. 2018) and we do observe changes in WT LRRK2 cells in lysosome number, but no

accumulation of undegraded autophagosomes and/or aSyn inclusions. This could be explained by the ability of forming autolysosomes and the strong proteolytic activity retained by these cells, which could serve as a compensatory mechanism, in addition to a direct role of LRRK2 on lysosome biology. We could also speculate that CMA might compensate in WT LRRK2 cells but not G2019S LRRK2 cells, maintaining lysosome function.

In conclusion, we demonstrate that *RIT2* acts both on autophagy-related processes and pS129-aSyn clearance. Activation of autophagy has indeed been proposed as a therapeutic strategy in PD and in most neurodegenerative proteinopathies (Menzies et al. 2017, Obergasteiger et al. 2018, Conway et al. 2019, Weber et al. 2019, Zhu et al. 2019). Future studies are required to fully understand the mechanism of action of *RIT2* and specifically the mechanism of *RIT2*-dependent regulation of LRRK2 kinase activity.

5 Supplementary data

5.1 Supplementary tables

Supplementary Table 1: List of fold-changes of gene expression of autophagy array genes in SH-SY5Y, WT LRRK2 and G2019S LRRK2 cells (normalized to SH-SY5Y)

Gene symbol	SH-SY5Y	WT LRRK2	G2019S LRRK2
Autophagic Vacuole Formation:			
AMBRA1 (NYW1)	1,00	1,14	1,32
ATG12	1,00	1,04	0,89
ATG4A	1,00	1,14	0,86
ATG4B	1,00	0,96	1,32
ATG4C	1,00	0,78	0,44
ATG4D	1,00	0,85	0,87
ATG5	1,00	1,11	1,24
ATG9A	1,00	1,23	1,17
ATG9B	1,00	0,80	0,99
BECN1	1,00	0,98	1,09
GABARAP	1,00	1,03	0,81
GABARAPL2	1,00	1,26	1,12
MAP1LC3A	1,00	1,35	1,67
MAP1LC3B	1,00	1,30	1,44
RGS19	1,00	0,92	0,84
ULK1	1,00	1,08	1,06
WIPI1	1,00	0,73	0,25
Vacuole Targeting:			
ATG4A	1,00	1,14	0,86
ATG4B	1,00	0,96	1,32
ATG4C	1,00	0,78	0,44
ATG4D	1,00	0,85	0,87
GABARAP	1,00	1,03	0,81

Protein Transport:			
ATG10	1,00	1,10	0,65
ATG16L2	1,00	0,91	0,56
ATG3	1,00	0,79	0,88
ATG4A	1,00	1,14	0,86
ATG4B	1,00	0,96	1,32
ATG4C	1,00	0,78	0,44
ATG4D	1,00	0,85	0,87
ATG7	1,00	1,50	2,11
ATG9A	1,00	1,23	1,17
GABARAP	1,00	1,03	0,81
GABARAPL2	1,00	1,26	1,12
RAB24	1,00	1,04	0,84
Autophagosome-Lysosome Linkage:			
DRAM1	1,00	1,34	0,62
GABARAP	1,00	1,03	0,81
LAMP1	1,00	1,10	1,29
NPC1	1,00	1,01	0,81
Ubiquitination:			
ATG3	1,00	0,79	0,88
ATG7	1,00	1,50	2,11
HDAC6	1,00	1,46	0,97
Proteases:			
ATG4A	1,00	1,14	0,86
ATG4B	1,00	0,96	1,32
ATG4C	1,00	0,78	0,44
ATG4D	1,00	0,85	0,87
Co-Regulators of Autophagy & Apoptosis:			
AKT1	1,00	1,48	1,29
APP	1,00	1,16	1,14

ATG12	1,00	1,04	0,89
ATG5	1,00	1,11	1,24
ATG7	1,00	1,50	2,11
ATG9A	1,00	1,23	1,17
ATG9B	1,00	0,80	0,99
BAD	1,00	0,95	0,73
BAK1	1,00	0,60	0,60
BAX	1,00	1,14	0,96
BCL2	1,00	1,77	2,65
BCL2L1	1,00	1,22	1,76
BECN1	1,00	0,98	1,09
BID	1,00	0,76	0,70
BNIP3	1,00	0,81	0,68
CASP3	1,00	1,94	2,05
CDKN1B (P27KIP1)	1,00	1,35	0,95
CDKN2A (p16INK4a)	1,00	3,11	6,98
CLN3	1,00	0,76	0,88
CTSB	1,00	2,73	2,44
CXCR4	1,00	9,00	19,34
DAPK1	1,00	0,81	1,02
DRAM1	1,00	1,34	0,62
EIF1AK3	1,00	1,59	0,83
FADD	1,00	0,90	1,44
FAS (TNFRSF6)	1,00	0,86	1,27
HDAC1	1,00	0,87	1,01
HTT	1,00	0,88	0,77
MAPK8 (JNK1)	1,00	1,72	1,82
MTOR	1,00	1,04	0,92
NFKB1	1,00	1,03	1,07
PRKAA1 (AMPK)	1,00	1,37	1,17

PTEN	1,00	1,11	1,48
SNCA	1,00	0,73	0,50
SQSTM1	1,00	1,02	1,20
TGFB1	1,00	0,71	0,73
TGM2	1,00	2,58	0,52
TP53 (p53)	1,00	0,72	0,99
Co-Regulators of Autophagy & the Cell Cycle:			
BAX	1,00	1,14	0,96
CDKN1B (P27KIP1)	1,00	1,35	0,95
CDKN2A (p16INK4a)	1,00	3,11	6,98
PTEN	1,00	1,11	1,48
RB1	1,00	1,10	0,96
TGFB1	1,00	0,71	0,73
TP53 (p53)	1,00	0,72	0,99
Autophagy Induction by Intracellular Pathogens:			
EIF1AK3	1,00	1,59	0,83
LAMP1	1,00	1,10	1,29
Autophagy in Response to Other Intracellular Signals:			
CTSD	1,00	1,20	1,12
CTSS	1,00	0,48	0,19
DRAM2 (TMEM77)	1,00	1,35	1,03
EIF4G1	1,00	0,89	1,33
GAA	1,00	0,91	0,97
HGS	1,00	0,77	1,32
MAPK14 (p38ALPHA)	1,00	1,42	1,37
PIK3C3 (Vps34)	1,00	0,82	1,07
PIK3R4	1,00	0,89	0,98
RPS6KB1	1,00	1,11	1,02
ULK2	1,00	1,16	0,80
UVRAG	1,00	1,26	0,98

Chaperone-Mediated Autophagy:			
HSP90AA1	1,00	1,13	2,09
HSPA8	1,00	0,99	1,87

Supplementary Table 2: List of fold-changes of gene expression of autophagy array genes in G2019S LRRK2 NT and PF475 treated cells (normalized to G2019S LRRK2)

Gene symbol	**G2019S NT**	**G2019S 300 nM**	**G2019S 500 nM**
Autophagic Vacuole Formation:			
AMBRA1 (NYW1)	1,00	0,85	1,00
ATG12	1,00	1,12	1,01
ATG4A	1,00	0,91	0,90
ATG4B	1,00	0,95	1,04
ATG4C	1,00	0,90	0,95
ATG4D	1,00	0,98	1,14
ATG5	1,00	0,99	0,94
ATG9A	1,00	0,94	1,15
ATG9B	1,00	1,03	0,97
BECN1	1,00	0,85	0,90
GABARAP	1,00	0,96	0,97
GABARAPL2	1,00	1,09	0,96
MAP1LC3A	1,00	0,92	1,22
MAP1LC3B	1,00	1,12	1,09
RGS19	1,00	1,01	1,30
ULK1	1,00	1,07	1,09
WIPI1	1,00	0,86	1,04
Vacuole Targeting:			
ATG4A	1,00	0,91	0,90
ATG4B	1,00	0,95	1,04
ATG4C	1,00	0,90	0,95
ATG4D	1,00	0,98	1,14

GABARAP	1,00	0,96	0,97
Protein Transport:			
ATG10	1,00	0,81	0,81
ATG16L2	1,00	0,91	1,18
ATG3	1,00	1,00	1,00
ATG4A	1,00	0,91	0,90
ATG4B	1,00	0,95	1,04
ATG4C	1,00	0,90	0,95
ATG4D	1,00	0,98	1,14
ATG7	1,00	0,94	0,97
ATG9A	1,00	0,94	1,15
GABARAP	1,00	0,96	0,97
GABARAPL2	1,00	1,09	0,96
RAB24	1,00	0,77	0,94
Autophagosome-Lysosome Linkage:			
DRAM1	1,00	1,08	0,96
GABARAP	1,00	0,96	0,97
LAMP1	1,00	0,86	1,00
NPC1	1,00	0,76	0,91
Ubiquitination:			
ATG3	1,00	1,00	1,00
ATG7	1,00	0,94	0,97
HDAC6	1,00	0,98	1,11
Proteases:			
ATG4A	1,00	0,91	0,90
ATG4B	1,00	0,95	1,04
ATG4C	1,00	0,90	0,95
ATG4D	1,00	0,98	1,14
Co-Regulators of Autophagy & Apoptosis:			
AKT1	1,00	0,88	0,98

APP	1,00	0,86	0,94
ATG12	1,00	1,12	1,01
ATG5	1,00	0,99	0,94
ATG7	1,00	0,94	0,97
ATG9A	1,00	0,94	1,15
ATG9B	1,00	1,03	0,97
BAD	1,00	0,88	1,03
BAK1	1,00	1,09	1,13
BAX	1,00	0,88	0,97
BCL2	1,00	0,95	1,06
BCL2L1	1,00	0,89	0,99
BECN1	1,00	0,85	0,90
BID	1,00	1,01	1,03
BNIP3	1,00	0,95	1,01
CASP3	1,00	0,94	1,00
CDKN1B (P27KIP1)	1,00	0,92	1,02
CDKN2A (p16INK4a)	1,00	1,08	0,97
CLN3	1,00	0,93	1,01
CTSB	1,00	0,94	1,02
CXCR4	1,00	0,93	0,92
DAPK1	1,00	0,65	0,78
DRAM1	1,00	1,08	0,96
EIF1AK3	1,00	1,02	1,10
FADD	1,00	0,75	0,93
FAS (TNFRSF6)	1,00	0,64	0,58
HDAC1	1,00	0,90	0,98
HTT	1,00	0,90	1,11
MAPK8 (JNK1)	1,00	0,98	1,00
MTOR	1,00	0,90	1,03
NFKB1	1,00	0,93	1,01

PRKAA1 (AMPK)	1,00	0,93	0,94
PTEN	1,00	0,84	0,81
SNCA	1,00	0,99	0,91
SQSTM1	1,00	1,01	1,17
TGFB1	1,00	0,72	0,99
TGM2	1,00	1,18	0,74
TP53 (p53)	1,00	0,83	0,92
Co-Regulators of Autophagy & the Cell Cycle:			
BAX	1,00	0,88	0,97
CDKN1B (P27KIP1)	1,00	0,92	1,02
CDKN2A (p16INK4a)	1,00	1,08	0,97
PTEN	1,00	0,84	0,81
RB1	1,00	0,87	0,96
TGFB1	1,00	0,72	0,99
TP53 (p53)	1,00	0,83	0,92
Autophagy Induction by Intracellular Pathogens:			
EIF1AK3	1,00	1,02	1,10
LAMP1	1,00	0,86	1,00
Autophagy in Response to Other Intracellular Signals:			
CTSD	1,00	0,85	0,93
CTSS	1,00	0,91	0,80
DRAM2 (TMEM77)	1,00	1,09	1,06
EIF4G1	1,00	0,79	1,19
GAA	1,00	0,80	1,05
HGS	1,00	0,93	1,01
MAPK14 (p38ALPHA)	1,00	0,99	0,98
PIK3C3 (Vps34)	1,00	0,92	0,89
PIK3R4	1,00	0,83	0,88
RPS6KB1	1,00	0,84	0,91
ULK2	1,00	0,90	0,94

UVRAG	1,00	0,84	0,85
Chaperone-Mediated Autophagy:			
HSP90AA1	1,00	0,88	0,98
HSPA8	1,00	1,05	1,00

Supplementary Table 3: List of fold change of gene expression of autophagy array genes in G2019S LRRK2 NT and G2019S +RIT2 cells (normalized to G2019S LRRK2)

Gene symbol	**G2019S NT**	**G2019S + RIT2**
Autophagic Vacuole Formation:		
AMBRA1 (NYW1)	1,00	1,21
ATG12	1,00	1,13
ATG4A	1,00	1,38
ATG4B	1,00	1,06
ATG4C	1,00	1,28
ATG4D	1,00	1,36
ATG5	1,00	0,91
ATG9A	1,00	1,71
ATG9B	1,00	1,48
BECN1	1,00	0,97
GABARAP	1,00	1,27
GABARAPL2	1,00	0,95
MAP1LC3A	1,00	0,97
MAP1LC3B	1,00	0,92
RGS19	1,00	1,14
ULK1	1,00	1,20
WIPI1	1,00	2,05
Vacuole Targeting:		
ATG4A	1,00	1,38
ATG4B	1,00	1,06
ATG4C	1,00	1,28
ATG4D	1,00	1,36

GABARAP	1,00	1,27
Protein Transport:		
ATG10	1,00	1,21
ATG16L2	1,00	1,71
ATG3	1,00	0,94
ATG4A	1,00	1,38
ATG4B	1,00	1,06
ATG4C	1,00	1,28
ATG4D	1,00	1,36
ATG7	1,00	0,94
ATG9A	1,00	1,71
GABARAP	1,00	1,27
GABARAPL2	1,00	0,95
RAB24	1,00	1,23
Autophagosome-Lysosome Linkage:		
DRAM1	1,00	2,36
GABARAP	1,00	1,27
LAMP1	1,00	1,14
NPC1	1,00	1,05
Ubiquitination:		
ATG3	1,00	0,94
ATG7	1,00	0,94
HDAC6	1,00	1,53
Proteases:		
ATG4A	1,00	1,38
ATG4B	1,00	1,06
ATG4C	1,00	1,28
ATG4D	1,00	1,36
Co-Regulators of Autophagy & Apoptosis:		
AKT1	1,00	1,43

APP	1,00	1,09
ATG12	1,00	1,13
ATG5	1,00	0,91
ATG7	1,00	0,94
ATG9A	1,00	1,71
ATG9B	1,00	1,48
BAD	1,00	1,44
BAK1	1,00	0,96
BAX	1,00	1,37
BCL2	1,00	1,07
BCL2L1	1,00	0,99
BECN1	1,00	0,97
BID	1,00	0,97
BNIP3	1,00	1,28
CASP3	1,00	0,92
CDKN1B (P27KIP1)	1,00	1,26
CDKN2A (p16INK4a)	1,00	1,11
CLN3	1,00	1,19
CTSB	1,00	1,19
CXCR4	1,00	1,63
DAPK1	1,00	0,95
DRAM1	1,00	2,36
EIF1AK3	1,00	1,32
FADD	1,00	0,80
FAS (TNFRSF6)	1,00	1,19
HDAC1	1,00	1,06
HTT	1,00	1,61
MAPK8 (JNK1)	1,00	0,96
MTOR	1,00	1,39
NFKB1	1,00	1,20

PRKAA1 (AMPK)	1,00	1,20
PTEN	1,00	0,76
SNCA	1,00	1,18
SQSTM1	1,00	1,18
TGFB1	1,00	1,31
TGM2	1,00	1,37
TP53 (p53)	1,00	1,22
Co-Regulators of Autophagy & the Cell Cycle:		
BAX	1,00	1,37
CDKN1B (P27KIP1)	1,00	1,26
CDKN2A (p16INK4a)	1,00	1,11
PTEN	1,00	0,76
RB1	1,00	1,19
TGFB1	1,00	1,31
TP53 (p53)	1,00	1,22
Autophagy Induction by Intracellular Pathogens:		
EIF1AK3	1,00	1,32
LAMP1	1,00	1,14
Autophagy in Response to Other Intracellular Signals:		
CTSD	1,00	1,58
CTSS	1,00	1,91
DRAM2 (TMEM77)	1,00	1,19
EIF4G1	1,00	1,11
GAA	1,00	1,44
HGS	1,00	0,80
MAPK14 (p38ALPHA)	1,00	1,14
PIK3C3 (Vps34)	1,00	0,93
PIK3R4	1,00	0,95
RPS6KB1	1,00	1,08
ULK2	1,00	1,19

UVRAG	1,00	1,39
Chaperone-Mediated Autophagy:		
HSP90AA1	1,00	0,55
HSPA8	1,00	0,66

6 References

Abeliovich, A., Y. Schmitz, I. Farinas, D. Choi-Lundberg, W. H. Ho, P. E. Castillo, . . . A. Rosenthal (2000). "Mice lacking alpha-synuclein display functional deficits in the nigrostriatal dopamine system." Neuron **25**(1): 239-252.

Abou-Sleiman, P. M., M. M. Muqit and N. W. Wood (2006). "Expanding insights of mitochondrial dysfunction in Parkinson's disease." Nat Rev Neurosci **7**(3): 207-219.

Alegre-Abarrategui, J., H. Christian, M. M. Lufino, R. Mutihac, L. L. Venda, O. Ansorge and R. Wade-Martins (2009). "LRRK2 regulates autophagic activity and localizes to specific membrane microdomains in a novel human genomic reporter cellular model." Hum Mol Genet **18**(21): 4022-4034.

Andersen, C. L., J. L. Jensen and T. F. Ørntoft (2004). "Normalization of real-time quantitative reverse transcription-PCR data: a model-based variance estimation approach to identify genes suited for normalization, applied to bladder and colon cancer data sets." Cancer Res **64**(15): 5245-5250.

Anglade, P., S. Vyas, F. Javoy-Agid, M. T. Herrero, P. P. Michel, J. Marquez, . . . Y. Agid (1997). "Apoptosis and autophagy in nigral neurons of patients with Parkinson's disease." Histol Histopathol **12**(1): 25-31.

Appelqvist, H., P. Waster, K. Kagedal and K. Ollinger (2013). "The lysosome: from waste bag to potential therapeutic target." J Mol Cell Biol **5**(4): 214-226.

Atashrazm, F. and N. Dzamko (2016). "LRRK2 inhibitors and their potential in the treatment of Parkinson's disease: current perspectives." Clin Pharmacol **8**: 177-189.

Beccano-Kelly, D. A., N. Kuhlmann, I. Tatarnikov, M. Volta, L. N. Munsie, P. Chou, . . . A. J. Milnerwood (2014). "Synaptic function is modulated by LRRK2 and glutamate release is increased in cortical neurons of G2019S LRRK2 knock-in mice." Front Cell Neurosci **8**: 301.

Beilina, A., I. N. Rudenko, A. Kaganovich, L. Civiero, H. Chau, S. K. Kalia, . . . M. R. Cookson (2014). "Unbiased screen for interactors of leucine-rich repeat kinase 2 supports a common pathway for sporadic and familial Parkinson disease." Proc Natl Acad Sci U S A **111**(7): 2626-2631.

Bellingham, S. A., B. B. Guo, B. M. Coleman and A. F. Hill (2012). "Exosomes: vehicles for the transfer of toxic proteins associated with neurodegenerative diseases?" Front Physiol **3**: 124.

Benson, D. L. and G. W. Huntley (2019). "Are we listening to everything the PARK genes are telling us?" J Comp Neurol **527**(9): 1527-1540.

Biedler, J. L., L. Helson and B. A. Spengler (1973). "Morphology and growth, tumorigenicity, and cytogenetics of human neuroblastoma cells in continuous culture." Cancer Res **33**(11): 2643-2652.

Birkmayer, W. and O. Hornykiewicz (1961). "[The L-3,4-dioxyphenylalanine (DOPA)-effect in Parkinson-akinesia]." Wien Klin Wochenschr **73**: 787-788.

Biskup, S., D. J. Moore, F. Celsi, S. Higashi, A. B. West, S. A. Andrabi, . . . V. L. Dawson (2006). "Localization of LRRK2 to membranous and vesicular structures in mammalian brain." Ann Neurol **60**(5): 557-569.

Bjorkoy, G., T. Lamark, A. Brech, H. Outzen, M. Perander, A. Overvatn, . . . T. Johansen (2005). "p62/SQSTM1 forms protein aggregates degraded by autophagy and has a protective effect on huntingtin-induced cell death." J Cell Biol **171**(4): 603-614.

Bonifati, V., P. Rizzu, F. Squitieri, E. Krieger, N. Vanacore, J. C. van Swieten, . . . P. Heutink (2003). "DJ-1(PARK7), a novel gene for autosomal recessive, early onset parkinsonism." Neurol Sci **24**(3): 159-160.

Bos, J. L., H. Rehmann and A. Wittinghofer (2007). "GEFs and GAPs: critical elements in the control of small G proteins." Cell **129**(5): 865-877.

Bossers, K., G. Meerhoff, R. Balesar, J. W. van Dongen, C. G. Kruse, D. F. Swaab and J. Verhaagen (2009). "Analysis of gene expression in Parkinson's disease: possible involvement of neurotrophic support and axon guidance in dopaminergic cell death." Brain Pathol **19**(1): 91-107.

Bouquillon, S., J. Andrieux, E. Landais, B. Duban-Bedu, F. Boidein, B. Lenne, . . . B. Delobel (2011). "A 5.3Mb deletion in chromosome 18q12.3 as the smallest region of overlap in two patients with expressive speech delay." Eur J Med Genet **54**(2): 194-197.
Braak, H., K. Del Tredici, U. Rüb, R. A. de Vos, E. N. Jansen Steur and E. Braak (2003). "Staging of brain pathology related to sporadic Parkinson's disease." Neurobiol Aging **24**(2): 197-211.
Bravo-San Pedro, J. M., M. Niso-Santano, R. Gomez-Sanchez, E. Pizarro-Estrella, A. Aiastui-Pujana, A. Gorostidi, . . . R. A. Gonzalez-Polo (2013). "The LRRK2 G2019S mutant exacerbates basal autophagy through activation of the MEK/ERK pathway." Cell Mol Life Sci **70**(1): 121-136.
Brundin, P. and R. Melki (2017). "Prying into the Prion Hypothesis for Parkinson's Disease." J Neurosci **37**(41): 9808-9818.
Burke, R. E., W. T. Dauer and J. P. G. Vonsattel (2008). "A critical evaluation of the Braak staging scheme for Parkinson's disease." Annals of neurology **64**(5): 485-491.
Burré, J., M. Sharma, T. Tsetsenis, V. Buchman, M. R. Etherton and T. C. Südhof (2010). "Alpha-synuclein promotes SNARE-complex assembly in vivo and in vitro." Science **329**(5999): 1663-1667.
Cai, W., S. W. Carlson, J. M. Brelsfoard, C. E. Mannon, C. L. Moncman, K. E. Saatman and D. A. Andres (2012). "Rit GTPase signaling promotes immature hippocampal neuronal survival." J Neurosci **32**(29): 9887-9897.
Cai, W., J. L. Rudolph, T. Sengoku and D. A. Andres (2012). "Rit GTPase regulates a p38 MAPK-dependent neuronal survival pathway." Neurosci Lett **531**(2): 125-130.
Cantuti-Castelvetri, I., C. Keller-McGandy, B. Bouzou, G. Asteris, T. W. Clark, M. P. Frosch and D. G. Standaert (2007). "Effects of gender on nigral gene expression and parkinson disease." Neurobiol Dis **26**(3): 606-614.
Chang, D., M. A. Nalls, I. B. Hallgrimsdottir, J. Hunkapiller, M. van der Brug, F. Cai, . . . R. R. Graham (2017). "A meta-analysis of genome-wide association studies identifies 17 new Parkinson's disease risk loci." Nat Genet **49**(10): 1511-1516.
Chang, D., M. A. Nalls, I. B. Hallgrimsdottir, J. Hunkapiller, M. van der Brug, F. Cai, . . . R. R. Graham (2017). "A meta-analysis of genome-wide association studies identifies 17 new Parkinson's disease risk loci." Nat Genet **49**(10): 1511-1516.
Chartier-Harlin, M. C., J. Kachergus, C. Roumier, V. Mouroux, X. Douay, S. Lincoln, . . . A. Destee (2004). "Alpha-synuclein locus duplication as a cause of familial Parkinson's disease." Lancet **364**(9440): 1167-1169.
Cherfils, J. and M. Zeghouf (2013). "Regulation of small GTPases by GEFs, GAPs, and GDIs." Physiol Rev **93**(1): 269-309.
Choi, A. M., S. W. Ryter and B. Levine (2013). "Autophagy in human health and disease." N Engl J Med **368**(7): 651-662.
Chu, Y., H. Dodiya, P. Aebischer, C. W. Olanow and J. H. Kordower (2009). "Alterations in lysosomal and proteasomal markers in Parkinson's disease: relationship to alpha-synuclein inclusions." Neurobiol Dis **35**(3): 385-398.
Conway, K. A., S. J. Lee, J. C. Rochet, T. T. Ding, R. E. Williamson and P. T. Lansbury, Jr. (2000). "Acceleration of oligomerization, not fibrillization, is a shared property of both alpha-synuclein mutations linked to early-onset Parkinson's disease: implications for pathogenesis and therapy." Proc Natl Acad Sci U S A **97**(2): 571-576.
Conway, O., H. A. Akpinar, V. Rogov and V. Kirkin (2019). "Selective autophagy receptors in neuronal health and disease." J Mol Biol.
Cookson, M. R. (2015). "LRRK2 Pathways Leading to Neurodegeneration." Curr Neurol Neurosci Rep **15**(7): 42.
Cookson, M. R. (2016). "Cellular functions of LRRK2 implicate vesicular trafficking pathways in Parkinson's disease." Biochem Soc Trans **44**(6): 1603-1610.
Cortes, C. J. and A. R. La Spada (2014). "The many faces of autophagy dysfunction in Huntington's disease: from mechanism to therapy." Drug Discov Today **19**(7): 963-971.

Corti, O., S. Lesage and A. Brice (2011). "What genetics tells us about the causes and mechanisms of Parkinson's disease." Physiol Rev **91**(4): 1161-1218.
Cuervo, A. M., L. Stefanis, R. Fredenburg, P. T. Lansbury and D. Sulzer (2004). "Impaired degradation of mutant alpha-synuclein by chaperone-mediated autophagy." Science **305**(5688): 1292-1295.
Daher, J. P., H. A. Abdelmotilib, X. Hu, L. A. Volpicelli-Daley, M. S. Moehle, K. B. Fraser, . . . A. B. West (2015). "Leucine-rich Repeat Kinase 2 (LRRK2) Pharmacological Inhibition Abates alpha-Synuclein Gene-induced Neurodegeneration." J Biol Chem **290**(32): 19433-19444.
Daher, J. P., L. A. Volpicelli-Daley, J. P. Blackburn, M. S. Moehle and A. B. West (2014). "Abrogation of alpha-synuclein-mediated dopaminergic neurodegeneration in LRRK2-deficient rats." Proc Natl Acad Sci U S A **111**(25): 9289-9294.
Damier, P., E. C. Hirsch, Y. Agid and A. M. Graybiel (1999). "The substantia nigra of the human brain. II. Patterns of loss of dopamine-containing neurons in Parkinson's disease." Brain **122 (Pt 8)**: 1437-1448.
Daniels, V., R. Vancraenenbroeck, B. M. Law, E. Greggio, E. Lobbestael, F. Gao, . . . J. M. Taymans (2011). "Insight into the mode of action of the LRRK2 Y1699C pathogenic mutant." J Neurochem **116**(2): 304-315.
Danzer, K. M., L. R. Kranich, W. P. Ruf, O. Cagsal-Getkin, A. R. Winslow, L. Zhu, . . . P. J. McLean (2012). "Exosomal cell-to-cell transmission of alpha synuclein oligomers." Mol Neurodegener **7**: 42.
Dauer, W. and S. Przedborski (2003). "Parkinson's disease: mechanisms and models." Neuron **39**(6): 889-909.
De Wit, T., V. Baekelandt and E. Lobbestael (2019). "Inhibition of LRRK2 or Casein Kinase 1 Results in LRRK2 Protein Destabilization." Mol Neurobiol **56**(8): 5273-5286.
Dehay, B., M. Bourdenx, P. Gorry, S. Przedborski, M. Vila, S. Hunot, . . . W. G. Meissner (2015). "Targeting alpha-synuclein for treatment of Parkinson's disease: mechanistic and therapeutic considerations." Lancet Neurol **14**(8): 855-866.
Dehay, B., J. Bove, N. Rodriguez-Muela, C. Perier, A. Recasens, P. Boya and M. Vila (2010). "Pathogenic lysosomal depletion in Parkinson's disease." J Neurosci **30**(37): 12535-12544.
Dehay, B., A. Ramirez, M. Martinez-Vicente, C. Perier, M. H. Canron, E. Doudnikoff, . . . E. Bezard (2012). "Loss of P-type ATPase ATP13A2/PARK9 function induces general lysosomal deficiency and leads to Parkinson disease neurodegeneration." Proc Natl Acad Sci U S A **109**(24): 9611-9616.
Desplats, P., H. J. Lee, E. J. Bae, C. Patrick, E. Rockenstein, L. Crews, . . . S. J. Lee (2009). "Inclusion formation and neuronal cell death through neuron-to-neuron transmission of alpha-synuclein." Proc Natl Acad Sci U S A **106**(31): 13010-13015.
Deuschl, G., S. Paschen and K. Witt (2013). "Clinical outcome of deep brain stimulation for Parkinson's disease." Handb Clin Neurol **116**: 107-128.
Devine, M. J., K. Gwinn, A. Singleton and J. Hardy (2011). "Parkinson's disease and alpha-synuclein expression." Mov Disord **26**(12): 2160-2168.
Di Fonzo, A., M. C. Dekker, P. Montagna, A. Baruzzi, E. H. Yonova, L. Correia Guedes, . . . V. Bonifati (2009). "FBXO7 mutations cause autosomal recessive, early-onset parkinsonian-pyramidal syndrome." Neurology **72**(3): 240-245.
Di Maio, R., E. K. Hoffman, E. M. Rocha, M. T. Keeney, L. H. Sanders, B. R. De Miranda, . . . J. T. Greenamyre (2018). "LRRK2 activation in idiopathic Parkinson's disease." Sci Transl Med **10**(451).
DiCarlo, G. E., J. I. Aguilar, H. J. Matthies, F. E. Harrison, K. E. Bundschuh, A. West, . . . A. Galli (2019). "Autism-linked dopamine transporter mutation alters striatal dopamine neurotransmission and dopamine-dependent behaviors." J Clin Invest **129**(8): 3407-3419.
Dickson, D. W. (2018). "Neuropathology of Parkinson disease." Parkinsonism & Related Disorders **46**: S30-S33.
Dijkstra, A. A., P. Voorn, H. W. Berendse, H. J. Groenewegen, A. J. Rozemuller and W. D. van de Berg (2014). "Stage-dependent nigral neuronal loss in incidental Lewy body and Parkinson's disease." Mov Disord **29**(10): 1244-1251.

Dzamko, N., M. Deak, F. Hentati, A. D. Reith, A. R. Prescott, D. R. Alessi and R. J. Nichols (2010). "Inhibition of LRRK2 kinase activity leads to dephosphorylation of Ser(910)/Ser(935), disruption of 14-3-3 binding and altered cytoplasmic localization." Biochem J **430**(3): 405-413.
Ebrahimi-Fakhari, D., I. Cantuti-Castelvetri, Z. Fan, E. Rockenstein, E. Masliah, B. T. Hyman, . . . V. K. Unni (2011). "Distinct roles in vivo for the ubiquitin-proteasome system and the autophagy-lysosomal pathway in the degradation of alpha-synuclein." J Neurosci **31**(41): 14508-14520.
Edvardson, S., Y. Cinnamon, A. Ta-Shma, A. Shaag, Y. I. Yim, S. Zenvirt, . . . O. Elpeleg (2012). "A deleterious mutation in DNAJC6 encoding the neuronal-specific clathrin-uncoating co-chaperone auxilin, is associated with juvenile parkinsonism." PLoS One **7**(5): e36458.
Eguchi, T., T. Kuwahara, M. Sakurai, T. Komori, T. Fujimoto, G. Ito, . . . T. Iwatsubo (2018). "LRRK2 and its substrate Rab GTPases are sequentially targeted onto stressed lysosomes and maintain their homeostasis." Proc Natl Acad Sci U S A **115**(39): E9115-E9124.
Ejlerskov, P., I. Rasmussen, T. T. Nielsen, A. L. Bergstrom, Y. Tohyama, P. H. Jensen and F. Vilhardt (2013). "Tubulin polymerization-promoting protein (TPPP/p25alpha) promotes unconventional secretion of alpha-synuclein through exophagy by impairing autophagosome-lysosome fusion." J Biol Chem **288**(24): 17313-17335.
Emamalizadeh, B., J. Jamshidi, A. Movafagh, M. Ohadi, M. S. Khaniani, S. Kazeminasab, . . . H. Darvish (2017). "RIT2 Polymorphisms: Is There a Differential Association?" Mol Neurobiol **54**(3): 2234-2240.
Emamalizadeh, B., A. Movafagh, M. Akbari, S. Kazeminasab, A. Fazeli, M. Motallebi, . . . H. Darvish (2014). "RIT2, a susceptibility gene for Parkinson's disease in Iranian population." Neurobiol Aging **35**(12): e27-e28.
Emamalizadeh, B., A. Movafagh, H. Darvish, S. Kazeminasab, M. Andarva, P. Namdar-Aligoodarzi and M. Ohadi (2017). "The human RIT2 core promoter short tandem repeat predominant allele is species-specific in length: a selective advantage for human evolution?" Mol Genet Genomics **292**(3): 611-617.
Emmanouilidou, E., K. Melachroinou, T. Roumeliotis, S. D. Garbis, M. Ntzouni, L. H. Margaritis, . . . K. Vekrellis (2010). "Cell-produced alpha-synuclein is secreted in a calcium-dependent manner by exosomes and impacts neuronal survival." J Neurosci **30**(20): 6838-6851.
Esposito, G., F. Ana Clara and P. Verstreken (2012). "Synaptic vesicle trafficking and Parkinson's disease." Dev Neurobiol **72**(1): 134-144.
Feng, Y., D. He, Z. Yao and D. J. Klionsky (2014). "The machinery of macroautophagy." Cell Res **24**(1): 24-41.
Fraldi, A., F. Annunziata, A. Lombardi, H. J. Kaiser, D. L. Medina, C. Spampanato, . . . A. Ballabio (2010). "Lysosomal fusion and SNARE function are impaired by cholesterol accumulation in lysosomal storage disorders." EMBO J **29**(21): 3607-3620.
Fraser, K. B., A. B. Rawlins, R. G. Clark, R. N. Alcalay, D. G. Standaert, N. Liu and A. B. West (2016). "Ser(P)-1292 LRRK2 in urinary exosomes is elevated in idiopathic Parkinson's disease." Mov Disord **31**(10): 1543-1550.
Frost, L. S., A. Dhingra, J. Reyes-Reveles and K. Boesze-Battaglia (2017). "The Use of DQ-BSA to Monitor the Turnover of Autophagy-Associated Cargo." Methods Enzymol **587**: 43-54.
Fuchs, J., C. Nilsson, J. Kachergus, M. Munz, E. M. Larsson, B. Schule, . . . M. J. Farrer (2007). "Phenotypic variation in a large Swedish pedigree due to SNCA duplication and triplication." Neurology **68**(12): 916-922.
Fuji, R. N., M. Flagella, M. Baca, M. A. Baptista, J. Brodbeck, B. K. Chan, . . . R. J. Watts (2015). "Effect of selective LRRK2 kinase inhibition on nonhuman primate lung." Sci Transl Med **7**(273): 273ra215.
Giros, B., M. Jaber, S. R. Jones, R. M. Wightman and M. G. Caron (1996). "Hyperlocomotion and indifference to cocaine and amphetamine in mice lacking the dopamine transporter." Nature **379**(6566): 606-612.
Glessner, J. T., M. P. Reilly, C. E. Kim, N. Takahashi, A. Albano, C. Hou, . . . H. Hakonarson (2010). "Strong synaptic transmission impact by copy number variations in schizophrenia." Proc Natl Acad Sci U S A **107**(23): 10584-10589.

Gloeckner, C. J., N. Kinkl, A. Schumacher, R. J. Braun, E. O'Neill, T. Meitinger, . . . M. Ueffing (2006). "The Parkinson disease causing LRRK2 mutation I2020T is associated with increased kinase activity." Hum Mol Genet **15**(2): 223-232.
Goedert, M., M. G. Spillantini, K. Del Tredici and H. Braak (2013). "100 years of Lewy pathology." Nat Rev Neurol **9**(1): 13-24.
Greggio, E., S. Jain, A. Kingsbury, R. Bandopadhyay, P. Lewis, A. Kaganovich, . . . M. R. Cookson (2006). "Kinase activity is required for the toxic effects of mutant LRRK2/dardarin." Neurobiol Dis **23**(2): 329-341.
Greggio, E., I. Zambrano, A. Kaganovich, A. Beilina, J. M. Taymans, V. Daniëls, . . . M. R. Cookson (2008). "The Parkinson disease-associated leucine-rich repeat kinase 2 (LRRK2) is a dimer that undergoes intramolecular autophosphorylation." J Biol Chem **283**(24): 16906-16914.
Gutierrez, M. G., D. B. Munafo, W. Beron and M. I. Colombo (2004). "Rab7 is required for the normal progression of the autophagic pathway in mammalian cells." J Cell Sci **117**(Pt 13): 2687-2697.
Haberman, A., W. R. Williamson, D. Epstein, D. Wang, S. Rina, I. A. Meinertzhagen and P. R. Hiesinger (2012). "The synaptic vesicle SNARE neuronal Synaptobrevin promotes endolysosomal degradation and prevents neurodegeneration." J Cell Biol **196**(2): 261-276.
Halliday, G. M., Y. W. Li, P. C. Blumbergs, T. H. Joh, R. G. Cotton, P. R. Howe, . . . L. B. Geffen (1990). "Neuropathology of immunohistochemically identified brainstem neurons in Parkinson's disease." Ann Neurol **27**(4): 373-385.
Hamedani, S. Y., J. Gharesouran, R. Noroozi, A. Sayad, M. D. Omrani, A. Mir, . . . M. Taheri (2017). "Ras-like without CAAX 2 (RIT2): a susceptibility gene for autism spectrum disorder." Metab Brain Dis **32**(3): 751-755.
Hara, T., K. Nakamura, M. Matsui, A. Yamamoto, Y. Nakahara, R. Suzuki-Migishima, . . . N. Mizushima (2006). "Suppression of basal autophagy in neural cells causes neurodegenerative disease in mice." Nature **441**(7095): 885-889.
Hasegawa, T., M. Matsuzaki, A. Takeda, A. Kikuchi, H. Akita, G. Perry, . . . Y. Itoyama (2004). "Accelerated alpha-synuclein aggregation after differentiation of SH-SY5Y neuroblastoma cells." Brain Res **1013**(1): 51-59.
Hatano, Y., Y. Li, K. Sato, S. Asakawa, Y. Yamamura, H. Tomiyama, . . . N. Hattori (2004). "Novel PINK1 mutations in early-onset parkinsonism." Ann Neurol **56**(3): 424-427.
He, C. and D. J. Klionsky (2009). "Regulation mechanisms and signaling pathways of autophagy." Annu Rev Genet **43**: 67-93.
Henchcliffe, C. and M. Parmar (2018). "Repairing the Brain: Cell Replacement Using Stem Cell-Based Technologies." J Parkinsons Dis **8**(s1): S131-S137.
Henry, A. G., S. Aghamohammadzadeh, H. Samaroo, Y. Chen, K. Mou, E. Needle and W. D. Hirst (2015). "Pathogenic LRRK2 mutations, through increased kinase activity, produce enlarged lysosomes with reduced degradative capacity and increase ATP13A2 expression." Hum Mol Genet **24**(21): 6013-6028.
Hernandez, D., C. A. Torres, W. Setlik, C. Cebrian, E. V. Mosharov, G. Tang, . . . D. Sulzer (2012). "Regulation of presynaptic neurotransmission by macroautophagy." Neuron **74**(2): 277-284.
Herzig, M. C., C. Kolly, E. Persohn, D. Theil, T. Schweizer, T. Hafner, . . . D. R. Shimshek (2011). "LRRK2 protein levels are determined by kinase function and are crucial for kidney and lung homeostasis in mice." Hum Mol Genet **20**(21): 4209-4223.
Hetz, C. and L. H. Glimcher (2011). "Protein homeostasis networks in physiology and disease." Curr Opin Cell Biol **23**(2): 123-125.
Ho, D. H., H. Kim, D. Nam, H. Sim, J. Kim, H. G. Kim, . . . W. Seol (2018). "LRRK2 impairs autophagy by mediating phosphorylation of leucyl-tRNA synthetase." Cell Biochem Funct **36**(8): 431-442.
Ho, P. W., C. T. Leung, H. Liu, S. Y. Pang, C. S. Lam, J. Xian, . . . S. L. Ho (2019). "Age-dependent accumulation of oligomeric SNCA/alpha-synuclein from impaired degradation in mutant LRRK2 knockin mouse model of Parkinson disease: role for therapeutic activation of chaperone-mediated autophagy (CMA)." Autophagy: 1-24.

Hockey, L. N., B. S. Kilpatrick, E. R. Eden, Y. Lin-Moshier, G. C. Brailoiu, E. Brailoiu, . . . S. Patel (2015). "Dysregulation of lysosomal morphology by pathogenic LRRK2 is corrected by TPC2 inhibition." J Cell Sci **128**(2): 232-238.
Ibanez, P., A. M. Bonnet, B. Debarges, E. Lohmann, F. Tison, P. Pollak, . . . A. Brice (2004). "Causal relation between alpha-synuclein gene duplication and familial Parkinson's disease." Lancet **364**(9440): 1169-1171.
Inoshita, T., T. Arano, Y. Hosaka, H. Meng, Y. Umezaki, S. Kosugi, . . . N. Hattori (2017). "Vps35 in cooperation with LRRK2 regulates synaptic vesicle endocytosis through the endosomal pathway in Drosophila." Hum Mol Genet **26**(15): 2933-2948.
Ip, C. W., L. C. Klaus, A. A. Karikari, N. P. Visanji, J. M. Brotchie, A. E. Lang, . . . J. B. Koprich (2017). "AAV1/2-induced overexpression of A53T-alpha-synuclein in the substantia nigra results in degeneration of the nigrostriatal system with Lewy-like pathology and motor impairment: a new mouse model for Parkinson's disease." Acta Neuropathol Commun **5**(1): 11.
Islam, M. S. and D. J. Moore (2017). "Mechanisms of LRRK2-dependent neurodegeneration: role of enzymatic activity and protein aggregation." Biochem Soc Trans **45**(1): 163-172.
Itakura, E., C. Kishi-Itakura and N. Mizushima (2012). "The hairpin-type tail-anchored SNARE syntaxin 17 targets to autophagosomes for fusion with endosomes/lysosomes." Cell **151**(6): 1256-1269.
Itakura, E. and N. Mizushima (2010). "Characterization of autophagosome formation site by a hierarchical analysis of mammalian Atg proteins." Autophagy **6**(6): 764-776.
Jahreiss, L., F. M. Menzies and D. C. Rubinsztein (2008). "The itinerary of autophagosomes: from peripheral formation to kiss-and-run fusion with lysosomes." Traffic **9**(4): 574-587.
Kalia, L. V. and A. E. Lang (2016). "Parkinson disease in 2015: Evolving basic, pathological and clinical concepts in PD." Nat Rev Neurol **12**(2): 65-66.
Kalia, L. V., A. E. Lang, L. N. Hazrati, S. Fujioka, Z. K. Wszolek, D. W. Dickson, . . . C. Marras (2015). "Clinical correlations with Lewy body pathology in LRRK2-related Parkinson disease." JAMA Neurol **72**(1): 100-105.
Kalinderi, K., S. Bostantjopoulou and L. Fidani (2016). "The genetic background of Parkinson's disease: current progress and future prospects." Acta Neurol Scand.
Kamentsky, L., T. R. Jones, A. Fraser, M. A. Bray, D. J. Logan, K. L. Madden, . . . A. E. Carpenter (2011). "Improved structure, function and compatibility for CellProfiler: modular high-throughput image analysis software." Bioinformatics **27**(8): 1179-1180.
Kaushik, S., A. C. Massey, N. Mizushima and A. M. Cuervo (2008). "Constitutive activation of chaperone-mediated autophagy in cells with impaired macroautophagy." Mol Biol Cell **19**(5): 2179-2192.
Khan, N. L., E. Graham, P. Critchley, A. E. Schrag, N. W. Wood, A. J. Lees, . . . N. Quinn (2003). "Parkin disease: a phenotypic study of a large case series." Brain **126**(Pt 6): 1279-1292.
Kim, I., S. Rodriguez-Enriquez and J. J. Lemasters (2007). "Selective degradation of mitochondria by mitophagy." Arch Biochem Biophys **462**(2): 245-253.
Kimura, S., T. Noda and T. Yoshimori (2008). "Dynein-dependent movement of autophagosomes mediates efficient encounters with lysosomes." Cell Struct Funct **33**(1): 109-122.
Kish, S. J., K. Shannak and O. Hornykiewicz (1988). "Uneven pattern of dopamine loss in the striatum of patients with idiopathic Parkinson's disease. Pathophysiologic and clinical implications." N Engl J Med **318**(14): 876-880.
Kitada, T., S. Asakawa, N. Hattori, H. Matsumine, Y. Yamamura, S. Minoshima, . . . N. Shimizu (1998). "Mutations in the parkin gene cause autosomal recessive juvenile parkinsonism." Nature **392**(6676): 605-608.
Klionsky, D. J., K. Abdelmohsen, A. Abe, M. J. Abedin, H. Abeliovich, A. Acevedo Arozena, . . . S. M. Zughaier (2016). "Guidelines for the use and interpretation of assays for monitoring autophagy (3rd edition)." Autophagy **12**(1): 1-222.
Klionsky, D. J., J. M. Cregg, W. A. Dunn, Jr., S. D. Emr, Y. Sakai, I. V. Sandoval, . . . Y. Ohsumi (2003). "A unified nomenclature for yeast autophagy-related genes." Dev Cell **5**(4): 539-545.

Klucken, J., A. M. Poehler, D. Ebrahimi-Fakhari, J. Schneider, S. Nuber, E. Rockenstein, . . . J. Winkler (2012). "Alpha-synuclein aggregation involves a bafilomycin A 1-sensitive autophagy pathway." Autophagy **8**(5): 754-766.
Kluss, J. H., M. M. Conti, A. Kaganovich, A. Beilina, H. L. Melrose, M. R. Cookson and A. Mamais (2018). "Detection of endogenous S1292 LRRK2 autophosphorylation in mouse tissue as a readout for kinase activity." NPJ Parkinsons Dis **4**: 13.
Komatsu, M., S. Waguri, T. Chiba, S. Murata, J. Iwata, I. Tanida, . . . K. Tanaka (2006). "Loss of autophagy in the central nervous system causes neurodegeneration in mice." Nature **441**(7095): 880-884.
Kon, M. and A. M. Cuervo (2010). "Chaperone-mediated autophagy in health and disease." FEBS Lett **584**(7): 1399-1404.
Kordower, J. H., Y. Chu, R. A. Hauser, T. B. Freeman and C. W. Olanow (2008). "Lewy body-like pathology in long-term embryonic nigral transplants in Parkinson's disease." Nat Med **14**(5): 504-506.
Kordower, J. H., Y. Chu, R. A. Hauser, C. W. Olanow and T. B. Freeman (2008). "Transplanted dopaminergic neurons develop PD pathologic changes: a second case report." Mov Disord **23**(16): 2303-2306.
Krebs, C. E., S. Karkheiran, J. C. Powell, M. Cao, V. Makarov, H. Darvish, . . . C. Paisan-Ruiz (2013). "The Sac1 domain of SYNJ1 identified mutated in a family with early-onset progressive Parkinsonism with generalized seizures." Hum Mutat **34**(9): 1200-1207.
Kremer, H. P. and G. T. Bots (1993). "Lewy bodies in the lateral hypothalamus: do they imply neuronal loss?" Mov Disord **8**(3): 315-320.
Kruger, R., W. Kuhn, T. Muller, D. Woitalla, M. Graeber, S. Kosel, . . . O. Riess (1998). "Ala30Pro mutation in the gene encoding alpha-synuclein in Parkinson's disease." Nat Genet **18**(2): 106-108.
Krüger, R., W. Kuhn, T. Müller, D. Woitalla, M. Graeber, S. Kösel, . . . O. Riess (1998). "Ala30Pro mutation in the gene encoding alpha-synuclein in Parkinson's disease." Nat Genet **18**(2): 106-108.
Lang, A. E. and A. M. Lozano (1998). "Parkinson's disease. First of two parts." N Engl J Med **339**(15): 1044-1053.
Langston, J. W., P. Ballard, J. W. Tetrud and I. Irwin (1983). "Chronic Parkinsonism in humans due to a product of meperidine-analog synthesis." Science **219**(4587): 979-980.
Latourelle, J. C., A. Dumitriu, T. C. Hadzi, T. G. Beach and R. H. Myers (2012). "Evaluation of Parkinson disease risk variants as expression-QTLs." PLoS One **7**(10): e46199.
Lee, H. J., E. D. Cho, K. W. Lee, J. H. Kim, S. G. Cho and S. J. Lee (2013). "Autophagic failure promotes the exocytosis and intercellular transfer of alpha-synuclein." Exp Mol Med **45**: e22.
Lees, A. J., J. Hardy and T. Revesz (2009). "Parkinson's disease." Lancet **373**(9680): 2055-2066.
Leo, D., I. Sukhanov, F. Zoratto, P. Illiano, L. Caffino, F. Sanna, . . . R. R. Gainetdinov (2018). "Pronounced Hyperactivity, Cognitive Dysfunctions, and BDNF Dysregulation in Dopamine Transporter Knock-out Rats." J Neurosci **38**(8): 1959-1972.
Lesage, S., V. Drouet, E. Majounie, V. Deramecourt, M. Jacoupy, A. Nicolas, . . . A. Brice (2016). "Loss of VPS13C Function in Autosomal-Recessive Parkinsonism Causes Mitochondrial Dysfunction and Increases PINK1/Parkin-Dependent Mitophagy." Am J Hum Genet **98**(3): 500-513.
Lesage, S., A. Dürr, M. Tazir, E. Lohmann, A. L. Leutenegger, S. Janin, . . . F. P. s. D. G. S. Group (2006). "LRRK2 G2019S as a cause of Parkinson's disease in North African Arabs." N Engl J Med **354**(4): 422-423.
Lewis, P. A., E. Greggio, A. Beilina, S. Jain, A. Baker and M. R. Cookson (2007). "The R1441C mutation of LRRK2 disrupts GTP hydrolysis." Biochem Biophys Res Commun **357**(3): 668-671.
Li, W. W., J. Li and J. K. Bao (2012). "Microautophagy: lesser-known self-eating." Cell Mol Life Sci **69**(7): 1125-1136.
Lin, M. K. and M. J. Farrer (2014). "Genetics and genomics of Parkinson's disease." Genome Med **6**(6): 48.
Lipinski, M. M., B. Zheng, T. Lu, Z. Yan, B. F. Py, A. Ng, . . . J. Yuan (2010). "Genome-wide analysis reveals mechanisms modulating autophagy in normal brain aging and in Alzheimer's disease." Proc Natl Acad Sci U S A **107**(32): 14164-14169.

Lis, P., S. Burel, M. Steger, M. Mann, F. Brown, F. Diez, . . . D. R. Alessi (2018). "Development of phospho-specific Rab protein antibodies to monitor in vivo activity of the LRRK2 Parkinson's disease kinase." Biochem J **475**(1): 1-22.
Liu, Z. H., J. F. Guo, Y. Q. Wang, K. Li, Q. Y. Sun, Q. Xu, . . . B. S. Tang (2015). "Assessment of RIT2 rs12456492 association with Parkinson's disease in Mainland China." Neurobiol Aging **36**(3): 1600 e1609-1611.
Livak, K. J. and T. D. Schmittgen (2001). "Analysis of relative gene expression data using real-time quantitative PCR and the 2(-Delta Delta C(T)) Method." Methods **25**(4): 402-408.
Lobbestael, E., L. Civiero, T. De Wit, J. M. Taymans, E. Greggio and V. Baekelandt (2016). "Pharmacological LRRK2 kinase inhibition induces LRRK2 protein destabilization and proteasomal degradation." Sci Rep **6**: 33897.
Lotharius, J. and P. Brundin (2002). "Pathogenesis of Parkinson's disease: dopamine, vesicles and alpha-synuclein." Nat Rev Neurosci **3**(12): 932-942.
Luk, K. C., V. Kehm, J. Carroll, B. Zhang, P. O'Brien, J. Q. Trojanowski and V. M. Lee (2012). "Pathological alpha-synuclein transmission initiates Parkinson-like neurodegeneration in nontransgenic mice." Science **338**(6109): 949-953.
Luk, K. C., V. M. Kehm, B. Zhang, P. O'Brien, J. Q. Trojanowski and V. M. Lee (2012). "Intracerebral inoculation of pathological alpha-synuclein initiates a rapidly progressive neurodegenerative alpha-synucleinopathy in mice." J Exp Med **209**(5): 975-986.
Lynch-Day, M. A., K. Mao, K. Wang, M. Zhao and D. J. Klionsky (2012). "The role of autophagy in Parkinson's disease." Cold Spring Harb Perspect Med **2**(4): a009357.
MacLeod, D., J. Dowman, R. Hammond, T. Leete, K. Inoue and A. Abeliovich (2006). "The familial Parkinsonism gene LRRK2 regulates neurite process morphology." Neuron **52**(4): 587-593.
MacLeod, D. A., H. Rhinn, T. Kuwahara, A. Zolin, G. Di Paolo, B. D. McCabe, . . . A. Abeliovich (2013). "RAB7L1 interacts with LRRK2 to modify intraneuronal protein sorting and Parkinson's disease risk." Neuron **77**(3): 425-439.
Maday, S. and E. L. Holzbaur (2016). "Compartment-Specific Regulation of Autophagy in Primary Neurons." J Neurosci **36**(22): 5933-5945.
Manzoni, C. and P. A. Lewis (2017). "LRRK2 and Autophagy." Adv Neurobiol **14**: 89-105.
Manzoni, C., A. Mamais, S. Dihanich, P. McGoldrick, M. J. Devine, J. Zerle, . . . P. A. Lewis (2013). "Pathogenic Parkinson's disease mutations across the functional domains of LRRK2 alter the autophagic/lysosomal response to starvation." Biochem Biophys Res Commun **441**(4): 862-866.
Marín, I. (2006). "The Parkinson disease gene LRRK2: evolutionary and structural insights." Mol Biol Evol **23**(12): 2423-2433.
Martinez-Vicente, M. and A. M. Cuervo (2007). "Autophagy and neurodegeneration: when the cleaning crew goes on strike." Lancet Neurol **6**(4): 352-361.
Matta, S., K. Van Kolen, R. da Cunha, G. van den Bogaart, W. Mandemakers, K. Miskiewicz, . . . P. Verstreken (2012). "LRRK2 controls an EndoA phosphorylation cycle in synaptic endocytosis." Neuron **75**(6): 1008-1021.
Mauthe, M., I. Orhon, C. Rocchi, X. Zhou, M. Luhr, K. J. Hijlkema, . . . F. Reggiori (2018). "Chloroquine inhibits autophagic flux by decreasing autophagosome-lysosome fusion." Autophagy **14**(8): 1435-1455.
McGlinchey, R. P. and J. C. Lee (2015). "Cysteine cathepsins are essential in lysosomal degradation of alpha-synuclein." Proc Natl Acad Sci U S A **112**(30): 9322-9327.
Menzies, F. M., A. Fleming, A. Caricasole, C. F. Bento, S. P. Andrews, A. Ashkenazi, . . . D. C. Rubinsztein (2017). "Autophagy and Neurodegeneration: Pathogenic Mechanisms and Therapeutic Opportunities." Neuron **93**(5): 1015-1034.
Mercatelli, D., P. Bolognesi, M. Frassineti, C. A. Pisano, F. Longo, D. R. Shimshek and M. Morari (2019). "Leucine-rich repeat kinase 2 (LRRK2) inhibitors differentially modulate glutamate release and Serine935 LRRK2 phosphorylation in striatal and cerebrocortical synaptosomes." Pharmacol Res Perspect **7**(3): e00484.

Mizushima, N., T. Yoshimori and Y. Ohsumi (2011). "The role of Atg proteins in autophagosome formation." Annu Rev Cell Dev Biol **27**: 107-132.
Moghal, S., A. H. Rajput, C. D'Arcy and R. Rajput (1994). "Prevalence of movement disorders in elderly community residents." Neuroepidemiology **13**(4): 175-178.
Monastyrska, I., E. Rieter, D. J. Klionsky and F. Reggiori (2009). "Multiple roles of the cytoskeleton in autophagy." Biol Rev Camb Philos Soc **84**(3): 431-448.
Nakamura, S. and T. Yoshimori (2017). "New insights into autophagosome-lysosome fusion." J Cell Sci **130**(7): 1209-1216.
Nalls, M. A., C. Blauwendraat, C. L. Vallerga, K. Heilbron, S. Bandres-Ciga, D. Chang, . . . A. B. Singleton (2019). "Expanding Parkinson's disease genetics: novel risk loci, genomic context, causal insights and heritable risk." bioRxiv: 388165.
Nalls, M. A., N. Pankratz, C. M. Lill, C. B. Do, D. G. Hernandez, M. Saad, . . . A. G. A. Group (2014). "Large-scale meta-analysis of genome-wide association data identifies six new risk loci for Parkinson's disease." Nat Genet **46**(9): 989-993.
Nalls, M. A., N. Pankratz, C. M. Lill, C. B. Do, D. G. Hernandez, M. Saad, . . . A. B. Singleton (2014). "Large-scale meta-analysis of genome-wide association data identifies six new risk loci for Parkinson's disease." Nat Genet **46**(9): 989-993.
Navaroli, D. M., Z. H. Stevens, Z. Uzelac, L. Gabriel, M. J. King, L. M. Lifshitz, . . . H. E. Melikian (2011). "The plasma membrane-associated GTPase Rin interacts with the dopamine transporter and is required for protein kinase C-regulated dopamine transporter trafficking." J Neurosci **31**(39): 13758-13770.
Nie, K., S. J. Feng, H. M. Tang, G. X. Ma, R. Gan, X. Zhao, . . . L. J. Wang (2015). "RIT2 polymorphism is associated with Parkinson's disease in a Han Chinese population." Neurobiol Aging **36**(3): 1603 e1615-1607.
Nishioka, K., O. A. Ross, K. Ishii, J. M. Kachergus, K. Ishiwata, M. Kitagawa, . . . N. Hattori (2009). "Expanding the clinical phenotype of SNCA duplication carriers." Mov Disord **24**(12): 1811-1819.
Nixon, R. A. (2013). "The role of autophagy in neurodegenerative disease." Nat Med **19**(8): 983-997.
O'Hara, D. M., S. K. Kalia and L. V. Kalia (2018). "Emerging disease-modifying strategies targeting alpha-synuclein for the treatment of Parkinson's disease." Br J Pharmacol **175**(15): 3080-3089.
Obergasteiger, J., G. Frapporti, P. P. Pramstaller, A. A. Hicks and M. Volta (2018). "A new hypothesis for Parkinson's disease pathogenesis: GTPase-p38 MAPK signaling and autophagy as convergence points of etiology and genomics." Mol Neurodegener **13**(1): 40.
Okun, M. S., H. H. Fernandez, R. L. Rodriguez and K. D. Foote (2007). "Identifying candidates for deep brain stimulation in Parkinson's disease: the role of the primary care physician." Geriatrics **62**(5): 18-24.
Olanow, C. W. and P. Brundin (2013). "Parkinson's disease and alpha synuclein: is Parkinson's disease a prion-like disorder?" Mov Disord **28**(1): 31-40.
Oliveras-Salva, M., A. Van der Perren, N. Casadei, S. Stroobants, S. Nuber, R. D'Hooge, . . . V. Baekelandt (2013). "rAAV2/7 vector-mediated overexpression of alpha-synuclein in mouse substantia nigra induces protein aggregation and progressive dose-dependent neurodegeneration." Mol Neurodegener **8**: 44.
Orenstein, S. J., S. H. Kuo, I. Tasset, E. Arias, H. Koga, I. Fernandez-Carasa, . . . A. M. Cuervo (2013). "Interplay of LRRK2 with chaperone-mediated autophagy." Nat Neurosci **16**(4): 394-406.
Ozelius, L. J., G. Senthil, R. Saunders-Pullman, E. Ohmann, A. Deligtisch, M. Tagliati, . . . S. B. Bressman (2006). "LRRK2 G2019S as a cause of Parkinson's disease in Ashkenazi Jews." N Engl J Med **354**(4): 424-425.
Paisan-Ruiz, C., S. Jain, E. W. Evans, W. P. Gilks, J. Simon, M. van der Brug, . . . A. B. Singleton (2004). "Cloning of the gene containing mutations that cause PARK8-linked Parkinson's disease." Neuron **44**(4): 595-600.
Paisan-Ruiz, C., P. A. Lewis and A. B. Singleton (2013). "LRRK2: cause, risk, and mechanism." J Parkinsons Dis **3**(2): 85-103.

Palmieri, M., S. Impey, H. Kang, A. di Ronza, C. Pelz, M. Sardiello and A. Ballabio (2011). "Characterization of the CLEAR network reveals an integrated control of cellular clearance pathways." Hum Mol Genet **20**(19): 3852-3866.
Pankiv, S., E. A. Alemu, A. Brech, J. A. Bruun, T. Lamark, A. Overvatn, . . . T. Johansen (2010). "FYCO1 is a Rab7 effector that binds to LC3 and PI3P to mediate microtubule plus end-directed vesicle transport." J Cell Biol **188**(2): 253-269.
Pankratz, N., G. W. Beecham, A. L. DeStefano, T. M. Dawson, K. F. Doheny, S. A. Factor, . . . P. G. Consortium (2012). "Meta-analysis of Parkinson's disease: identification of a novel locus, RIT2." Ann Neurol **71**(3): 370-384.
Patel, B. and A. M. Cuervo (2015). "Methods to study chaperone-mediated autophagy." Methods **75**: 133-140.
Pattaro, C., F. Marroni, A. Riegler, D. Mascalzoni, I. Pichler, C. B. Volpato, . . . P. P. Pramstaller (2007). "The genetic study of three population microisolates in South Tyrol (MICROS): study design and epidemiological perspectives." BMC Med Genet **8**: 29.
Pfeffer, S. R. (2017). "Rab GTPases: master regulators that establish the secretory and endocytic pathways." Mol Biol Cell **28**(6): 712-715.
Pfeifer, U. (1978). "Inhibition by insulin of the formation of autophagic vacuoles in rat liver. A morphometric approach to the kinetics of intracellular degradation by autophagy." J Cell Biol **78**(1): 152-167.
Piccoli, G., S. B. Condliffe, M. Bauer, F. Giesert, K. Boldt, S. De Astis, . . . M. Ueffing (2011). "LRRK2 controls synaptic vesicle storage and mobilization within the recycling pool." J Neurosci **31**(6): 2225-2237.
Piras, A., L. Collin, F. Gruninger, C. Graff and A. Ronnback (2016). "Autophagic and lysosomal defects in human tauopathies: analysis of post-mortem brain from patients with familial Alzheimer disease, corticobasal degeneration and progressive supranuclear palsy." Acta Neuropathol Commun **4**: 22.
Plowey, E. D., J. W. Johnson, E. Steer, W. Zhu, D. A. Eisenberg, N. M. Valentino, . . . C. T. Chu (2014). "Mutant LRRK2 enhances glutamatergic synapse activity and evokes excitotoxic dendrite degeneration." Biochim Biophys Acta **1842**(9): 1596-1603.
Poewe, W., K. Seppi, C. M. Tanner, G. M. Halliday, P. Brundin, J. Volkmann, . . . A. E. Lang (2017). "Parkinson disease." Nat Rev Dis Primers **3**: 17013.
Polymeropoulos, M. H., J. J. Higgins, L. I. Golbe, W. G. Johnson, S. E. Ide, G. Di Iorio, . . . R. C. Duvoisin (1996). "Mapping of a gene for Parkinson's disease to chromosome 4q21-q23." Science **274**(5290): 1197-1199.
Polymeropoulos, M. H., C. Lavedan, E. Leroy, S. E. Ide, A. Dehejia, A. Dutra, . . . R. L. Nussbaum (1997). "Mutation in the alpha-synuclein gene identified in families with Parkinson's disease." Science **276**(5321): 2045-2047.
Pu, J., C. M. Guardia, T. Keren-Kaplan and J. S. Bonifacino (2016). "Mechanisms and functions of lysosome positioning." J Cell Sci **129**(23): 4329-4339.
Purlyte, E., H. S. Dhekne, A. R. Sarhan, R. Gomez, P. Lis, M. Wightman, . . . D. R. Alessi (2018). "Rab29 activation of the Parkinson's disease-associated LRRK2 kinase." EMBO J **37**(1): 1-18.
Ramirez, A., A. Heimbach, J. Grundemann, B. Stiller, D. Hampshire, L. P. Cid, . . . C. Kubisch (2006). "Hereditary parkinsonism with dementia is caused by mutations in ATP13A2, encoding a lysosomal type 5 P-type ATPase." Nat Genet **38**(10): 1184-1191.
Rao, S. S., L. A. Hofmann and A. Shakil (2006). "Parkinson's disease: diagnosis and treatment." Am Fam Physician **74**(12): 2046-2054.
Ravikumar, B., A. Acevedo-Arozena, S. Imarisio, Z. Berger, C. Vacher, C. J. O'Kane, . . . D. C. Rubinsztein (2005). "Dynein mutations impair autophagic clearance of aggregate-prone proteins." Nat Genet **37**(7): 771-776.
Ravikumar, B., R. Duden and D. C. Rubinsztein (2002). "Aggregate-prone proteins with polyglutamine and polyalanine expansions are degraded by autophagy." Hum Mol Genet **11**(9): 1107-1117.

Ravikumar, B., S. Sarkar, J. E. Davies, M. Futter, M. Garcia-Arencibia, Z. W. Green-Thompson, . . . D. C. Rubinsztein (2010). "Regulation of mammalian autophagy in physiology and pathophysiology." Physiol Rev **90**(4): 1383-1435.
Reinhardt, P., B. Schmid, L. F. Burbulla, D. C. Schöndorf, L. Wagner, M. Glatza, . . . J. Sterneckert (2013). "Genetic correction of a LRRK2 mutation in human iPSCs links parkinsonian neurodegeneration to ERK-dependent changes in gene expression." Cell Stem Cell **12**(3): 354-367.
Rubinsztein, D. C., G. Marino and G. Kroemer (2011). "Autophagy and aging." Cell **146**(5): 682-695.
Saez-Atienzar, S., L. Bonet-Ponce, J. R. Blesa, F. J. Romero, M. P. Murphy, J. Jordan and M. F. Galindo (2014). "The LRRK2 inhibitor GSK2578215A induces protective autophagy in SH-SY5Y cells: involvement of Drp-1-mediated mitochondrial fission and mitochondrial-derived ROS signaling." Cell Death Dis **5**: e1368.
Samaranch, L., O. Lorenzo-Betancor, J. M. Arbelo, I. Ferrer, E. Lorenzo, J. Irigoyen, . . . P. Pastor (2010). "PINK1-linked parkinsonism is associated with Lewy body pathology." Brain **133**(Pt 4): 1128-1142.
Sanchez-Danes, A., Y. Richaud-Patin, I. Carballo-Carbajal, S. Jimenez-Delgado, C. Caig, S. Mora, . . . A. Raya (2012). "Disease-specific phenotypes in dopamine neurons from human iPS-based models of genetic and sporadic Parkinson's disease." EMBO Mol Med **4**(5): 380-395.
Sasaki, S. (2011). "Autophagy in Spinal Cord Motor Neurons in Sporadic Amyotrophic Lateral Sclerosis." Journal of Neuropathology & Experimental Neurology **70**(5): 349-359.
Sato, S., T. Uchihara, T. Fukuda, S. Noda, H. Kondo, S. Saiki, . . . N. Hattori (2018). "Loss of autophagy in dopaminergic neurons causes Lewy pathology and motor dysfunction in aged mice." Sci Rep **8**(1): 2813.
Schapansky, J., S. Khasnavis, M. P. DeAndrade, J. D. Nardozzi, S. R. Falkson, J. D. Boyd, . . . M. J. LaVoie (2018). "Familial knockin mutation of LRRK2 causes lysosomal dysfunction and accumulation of endogenous insoluble alpha-synuclein in neurons." Neurobiol Dis **111**: 26-35.
Scrivo, A., M. Bourdenx, O. Pampliega and A. M. Cuervo (2018). "Selective autophagy as a potential therapeutic target for neurodegenerative disorders." Lancet Neurol **17**(9): 802-815.
Semchuk, K. M., E. J. Love and R. G. Lee (1993). "Parkinson's disease: a test of the multifactorial etiologic hypothesis." Neurology **43**(6): 1173-1180.
Settembre, C. and A. Ballabio (2011). "TFEB regulates autophagy: an integrated coordination of cellular degradation and recycling processes." Autophagy **7**(11): 1379-1381.
Settembre, C., C. Di Malta, V. A. Polito, M. Garcia Arencibia, F. Vetrini, S. Erdin, . . . A. Ballabio (2011). "TFEB links autophagy to lysosomal biogenesis." Science **332**(6036): 1429-1433.
Shi, G. X. and D. A. Andres (2005). "Rit contributes to nerve growth factor-induced neuronal differentiation via activation of B-Raf-extracellular signal-regulated kinase and p38 mitogen-activated protein kinase cascades." Mol Cell Biol **25**(2): 830-846.
Shi, G. X., W. Cai and D. A. Andres (2013). "Rit subfamily small GTPases: regulators in neuronal differentiation and survival." Cell Signal **25**(10): 2060-2068.
Shi, G. X., J. Han and D. A. Andres (2005). "Rin GTPase couples nerve growth factor signaling to p38 and b-Raf/ERK pathways to promote neuronal differentiation." J Biol Chem **280**(45): 37599-37609.
Shin, N., H. Jeong, J. Kwon, H. Y. Heo, J. J. Kwon, H. J. Yun, . . . W. Seol (2008). "LRRK2 regulates synaptic vesicle endocytosis." Exp Cell Res **314**(10): 2055-2065.
Shojaei, S., N. Koleini, E. Samiei, M. Aghaei, L. K. Cole, J. Alizadeh, . . . S. Ghavami (2019). "Simvastatin increases temozolomide-induced cell death by targeting the fusion of autophagosomes and lysosomes." FEBS J.
Shu, Y., J. Ming, P. Zhang, Q. Wang, F. Jiao and B. Tian (2016). "Parkinson-Related LRRK2 Mutation R1628P Enables Cdk5 Phosphorylation of LRRK2 and Upregulates Its Kinase Activity." PLoS One **11**(3): e0149739.
Sidransky, E., T. Samaddar and N. Tayebi (2009). "Mutations in GBA are associated with familial Parkinson disease susceptibility and age at onset." Neurology **73**(17): 1424-1425, author reply 1425-1426.

Simanshu, D. K., D. V. Nissley and F. McCormick (2017). "RAS Proteins and Their Regulators in Human Disease." Cell **170**(1): 17-33.
Singleton, A. B., M. Farrer, J. Johnson, A. Singleton, S. Hague, J. Kachergus, . . . K. Gwinn-Hardy (2003). "alpha-Synuclein locus triplication causes Parkinson's disease." Science **302**(5646): 841.
Singleton, A. B., M. J. Farrer and V. Bonifati (2013). "The genetics of Parkinson's disease: progress and therapeutic implications." Mov Disord **28**(1): 14-23.
Smith, W. W., Z. Pei, H. Jiang, V. L. Dawson, T. M. Dawson and C. A. Ross (2006). "Kinase activity of mutant LRRK2 mediates neuronal toxicity." Nat Neurosci **9**(10): 1231-1233.
Soukup, S. F. and P. Verstreken (2017). "EndoA/Endophilin-A creates docking stations for autophagic proteins at synapses." Autophagy **13**(5): 971-972.
Spencer, M. L., H. Shao, H. M. Tucker and D. A. Andres (2002). "Nerve growth factor-dependent activation of the small GTPase Rin." J Biol Chem **277**(20): 17605-17615.
Spillantini, M. G., M. L. Schmidt, V. M. Lee, J. Q. Trojanowski, R. Jakes and M. Goedert (1997). "Alpha-synuclein in Lewy bodies." Nature **388**(6645): 839-840.
Steger, M., F. Tonelli, G. Ito, P. Davies, M. Trost, M. Vetter, . . . M. Mann (2016). "Phosphoproteomics reveals that Parkinson's disease kinase LRRK2 regulates a subset of Rab GTPases." Elife **5**.
Steinlechner, S., J. Stahlberg, B. Volkel, A. Djarmati, J. Hagenah, A. Hiller, . . . R. Lencer (2007). "Co-occurrence of affective and schizophrenia spectrum disorders with PINK1 mutations." J Neurol Neurosurg Psychiatry **78**(5): 532-535.
Stenmark, H. (2009). "Rab GTPases as coordinators of vesicle traffic." Nat Rev Mol Cell Biol **10**(8): 513-525.
Stern, M. B., A. Lang and W. Poewe (2012). "Toward a redefinition of Parkinson's disease." Mov Disord **27**(1): 54-60.
Surmeier, D. J., J. A. Obeso and G. M. Halliday (2017). "Parkinson's Disease Is Not Simply a Prion Disorder." J Neurosci **37**(41): 9799-9807.
Surmeier, D. J., J. A. Obeso and G. M. Halliday (2017). "Selective neuronal vulnerability in Parkinson disease." Nat Rev Neurosci **18**(2): 101-113.
Sweeney, C. G., P. J. Kearney, R. R. Fagan, L. A. Smith, N. C. Bolden, R. Zhao-Shea, . . . H. E. Melikian (2019). "Conditional, inducible gene silencing in dopamine neurons reveals a sex-specific role for Rit2 GTPase in acute cocaine response and striatal function." Neuropsychopharmacology.
Taipa, R., C. Pereira, I. Reis, I. Alonso, A. Bastos-Lima, M. Melo-Pires and M. Magalhaes (2016). "DJ-1 linked parkinsonism (PARK7) is associated with Lewy body pathology." Brain **139**(Pt 6): 1680-1687.
Tanik, S. A., C. E. Schultheiss, L. A. Volpicelli-Daley, K. R. Brunden and V. M. Lee (2013). "Lewy body-like alpha-synuclein aggregates resist degradation and impair macroautophagy." J Biol Chem **288**(21): 15194-15210.
Thomas, B. and M. F. Beal (2007). "Parkinson's disease." Human Molecular Genetics **16**(R2): R183-R194.
Till, A., R. Lakhani, S. F. Burnett and S. Subramani (2012). "Pexophagy: the selective degradation of peroxisomes." Int J Cell Biol **2012**: 512721.
Tofaris, G. K. (2017). "A Critical Assessment of Exosomes in the Pathogenesis and Stratification of Parkinson's Disease." J Parkinsons Dis **7**(4): 569-576.
Trinh, J. and M. Farrer (2013). "Advances in the genetics of Parkinson disease." Nat Rev Neurol **9**(8): 445-454.
Tsika, E. and D. J. Moore (2013). "Contribution of GTPase activity to LRRK2-associated Parkinson disease." Small GTPases **4**(3): 164-170.
Tsukada, M. and Y. Ohsumi (1993). "Isolation and characterization of autophagy-defective mutants of Saccharomyces cerevisiae." FEBS Lett **333**(1-2): 169-174.
Tsuyuki, S., M. Takabayashi, M. Kawazu, K. Kudo, A. Watanabe, Y. Nagata, . . . K. Yoshida (2014). "Detection of WIPI1 mRNA as an indicator of autophagosome formation." Autophagy **10**(3): 497-513.
Tysnes, O.-B. and A. Storstein (2017). "Epidemiology of Parkinson's disease." Journal of Neural Transmission **124**(8): 901-905.

Uenaka, T., W. Satake, P. C. Cha, H. Hayakawa, K. Baba, S. Jiang, . . . T. Toda (2018). "In silico drug screening by using genome-wide association study data repurposed dabrafenib, an anti-melanoma drug, for Parkinson's disease." Hum Mol Genet **27**(22): 3974-3985.
Vadlamudi, R. K., I. Joung, J. L. Strominger and J. Shin (1996). "p62, a phosphotyrosine-independent ligand of the SH2 domain of p56lck, belongs to a new class of ubiquitin-binding proteins." J Biol Chem **271**(34): 20235-20237.
Vancraenenbroeck, R., J. De Raeymaecker, E. Lobbestael, F. Gao, M. De Maeyer, A. Voet, . . . J. M. Taymans (2014). "In silico, in vitro and cellular analysis with a kinome-wide inhibitor panel correlates cellular LRRK2 dephosphorylation to inhibitor activity on LRRK2." Front Mol Neurosci **7**: 51.
Vijayan, V. and P. Verstreken (2017). "Autophagy in the presynaptic compartment in health and disease." J Cell Biol **216**(7): 1895-1906.
Vilarino-Guell, C., C. Wider, O. A. Ross, J. C. Dachsel, J. M. Kachergus, S. J. Lincoln, . . . M. J. Farrer (2011). "VPS35 mutations in Parkinson disease." Am J Hum Genet **89**(1): 162-167.
Volpicelli-Daley, L. A., H. Abdelmotilib, Z. Liu, L. Stoyka, J. P. Daher, A. J. Milnerwood, . . . A. B. West (2016). "G2019S-LRRK2 Expression Augments alpha-Synuclein Sequestration into Inclusions in Neurons." J Neurosci **36**(28): 7415-7427.
Volpicelli-Daley, L. A., K. C. Luk, T. P. Patel, S. A. Tanik, D. M. Riddle, A. Stieber, . . . V. M. Lee (2011). "Exogenous alpha-synuclein fibrils induce Lewy body pathology leading to synaptic dysfunction and neuron death." Neuron **72**(1): 57-71.
Volta, M. and H. Melrose (2017). "LRRK2 mouse models: dissecting the behavior, striatal neurochemistry and neurophysiology of PD pathogenesis." Biochem Soc Trans **45**(1): 113-122.
Volta, M., A. J. Milnerwood and M. J. Farrer (2015). "Insights from late-onset familial parkinsonism on the pathogenesis of idiopathic Parkinson's disease." Lancet Neurol **14**(10): 1054-1064.
Wallings, R., N. Connor-Robson and R. Wade-Martins (2019). "LRRK2 interacts with the vacuolar-type H+-ATPase pump a1 subunit to regulate lysosomal function." Hum Mol Genet **28**(16): 2696-2710.
Wallings, R., C. Manzoni and R. Bandopadhyay (2015). "Cellular processes associated with LRRK2 function and dysfunction." FEBS J **282**(15): 2806-2826.
Weber, J. J., P. Pereira Sena, E. Singer and H. P. Nguyen (2019). "Killing Two Angry Birds with One Stone: Autophagy Activation by Inhibiting Calpains in Neurodegenerative Diseases and Beyond." Biomed Res Int **2019**: 4741252.
Weidberg, H., E. Shvets and Z. Elazar (2011). "Biogenesis and cargo selectivity of autophagosomes." Annu Rev Biochem **80**: 125-156.
Wersinger, C., M. Banta and A. Sidhu (2004). "Comparative analyses of alpha-synuclein expression levels in rat brain tissues and transfected cells." Neurosci Lett **358**(2): 95-98.
West, A. B. (2015). "Ten years and counting: moving leucine-rich repeat kinase 2 inhibitors to the clinic." Mov Disord **30**(2): 180-189.
West, A. B., D. J. Moore, S. Biskup, A. Bugayenko, W. W. Smith, C. A. Ross, . . . T. M. Dawson (2005). "Parkinson's disease-associated mutations in leucine-rich repeat kinase 2 augment kinase activity." Proc Natl Acad Sci U S A **102**(46): 16842-16847.
West, A. B., D. J. Moore, C. Choi, S. A. Andrabi, X. Li, D. Dikeman, . . . T. M. Dawson (2007). "Parkinson's disease-associated mutations in LRRK2 link enhanced GTP-binding and kinase activities to neuronal toxicity." Hum Mol Genet **16**(2): 223-232.
Williams, G. P., A. M. Schonhoff, A. Jurkuvenaite, A. D. Thome, D. G. Standaert and A. S. Harms (2018). "Targeting of the class II transactivator attenuates inflammation and neurodegeneration in an alpha-synuclein model of Parkinson's disease." J Neuroinflammation **15**(1): 244.
Wong, Y. C. and E. L. Holzbaur (2014). "The regulation of autophagosome dynamics by huntingtin and HAP1 is disrupted by expression of mutant huntingtin, leading to defective cargo degradation." J Neurosci **34**(4): 1293-1305.
Xiao, F. H., X. Q. Chen, Q. Yu, Y. Ye, Y. W. Liu, D. Yan, . . . Q. P. Kong (2018). "Transcriptome evidence reveals enhanced autophagy-lysosomal function in centenarians." Genome Res **28**(11): 1601-1610.

Yakhine-Diop, S. M., J. M. Bravo-San Pedro, R. Gomez-Sanchez, E. Pizarro-Estrella, M. Rodriguez-Arribas, V. Climent, . . . R. A. Gonzalez-Polo (2014). "G2019S LRRK2 mutant fibroblasts from Parkinson's disease patients show increased sensitivity to neurotoxin 1-methyl-4-phenylpyridinium dependent of autophagy." Toxicology **324**: 1-9.
Yorimitsu, T. and D. J. Klionsky (2005). "Autophagy: molecular machinery for self-eating." Cell Death Differ **12 Suppl 2**: 1542-1552.
Zarranz, J. J., J. Alegre, J. C. Gómez-Esteban, E. Lezcano, R. Ros, I. Ampuero, . . . J. G. de Yebenes (2004). "The new mutation, E46K, of alpha-synuclein causes Parkinson and Lewy body dementia." Ann Neurol **55**(2): 164-173.
Zhang, L., K. Wahlin, Y. Li, T. Masuda, Z. Yang, D. J. Zack and N. Esumi (2013). "RIT2, a neuron-specific small guanosine triphosphatase, is expressed in retinal neuronal cells and its promoter is modulated by the POU4 transcription factors." Mol Vis **19**: 1371-1386.
Zhang, X. D., L. Qi, J. C. Wu and Z. H. Qin (2013). "DRAM1 regulates autophagy flux through lysosomes." PLoS One **8**(5): e63245.
Zhao, H. T., N. John, V. Delic, K. Ikeda-Lee, A. Kim, A. Weihofen, . . . L. A. Volpicelli-Daley (2017). "LRRK2 Antisense Oligonucleotides Ameliorate alpha-Synuclein Inclusion Formation in a Parkinson's Disease Mouse Model." Mol Ther Nucleic Acids **8**: 508-519.
Zhen, Y. and H. Stenmark (2015). "Cellular functions of Rab GTPases at a glance." J Cell Sci **128**(17): 3171-3176.
Zhou, Q., J. Li, H. Wang, Y. Yin and J. Zhou (2011). "Identification of nigral dopaminergic neuron-enriched genes in adult rats." Neurobiol Aging **32**(2): 313-326.
Zhu, Z., C. Yang, A. Iyaswamy, S. Krishnamoorthi, S. G. Sreenivasmurthy, J. Liu, . . . M. Li (2019). "Balancing mTOR Signaling and Autophagy in the Treatment of Parkinson's Disease." Int J Mol Sci **20**(3).
Zimprich, A., A. Benet-Pages, W. Struhal, E. Graf, S. H. Eck, M. N. Offman, . . . T. M. Strom (2011). "A mutation in VPS35, encoding a subunit of the retromer complex, causes late-onset Parkinson disease." Am J Hum Genet **89**(1): 168-175.
Zimprich, A., S. Biskup, P. Leitner, P. Lichtner, M. Farrer, S. Lincoln, . . . T. Gasser (2004). "Mutations in LRRK2 cause autosomal-dominant parkinsonism with pleomorphic pathology." Neuron **44**(4): 601-607.

Acknowledgements

First, I want to thank my supervisors Prof. Morari Michele and Mattia Volta. I would like to express my gratitude to Prof. Morari for the support of my Ph.D study, despite the distance. It was a great experience to spend some time in the laboratory and I felt welcome from the first moment. Thank you Salvatore, Clarissa, Daniela.

I want to thank Mattia for his guidance, inspiration and huge support during the last years. I could benefit from his huge amount of knowledge and he always helped me in research- or writing-related questions. I am grateful that I had the possibility to work under his supervision and hope that we will keep working together in the future.

I also want to thank Corrado for being my supervisor and first contact during my master thesis. I was able to learn many things from him and profit from his experience. I want to thank Christa for being the best lab partner I´ve ever had and now for still being my friend. We met at Eurac and from the beginning, we had a great connection in the lab and outside. I also would like to thank Giulia for her hard work and commitment to our work. I could count on her and it was great working with you. A big thank goes to the best PhD colleagues: Ale and Paulina. On one side for the intense scientific discussion, but even more important for the moral support in the dark times and the many hours of fun and laughter. Colleagues like them make you love go to work every day. Recently, Giada joined the PhD club and lights our days with her singing skills.

I want to sincerely thank Sara and Giulia for the work they did during my period abroad and more importantly, for the work in the lab they did, so I could concentrate on writing.

I would also like to thank Prof. Martin Levesque for giving me the possibility to spend time in his group and expand my skills. It was a great experience to be part of the group and I want to thank especially Marina for helping me and being such a great colleague and friend. I also want to thank Vero, Axelle and all the other people of the group for supporting me during the internship. Charles deserves a special thank you. He was the person I could ask for help in the beginning. He was always willing to help me and he still is. You made my time in Quebec an experience I will never forget, because I met you. It took some time for me to realize what a wonderful person you are, but since the moment, I realized I cannot imagine my life without you anymore.

I want to thank all my friends for, at least, pretending to listen to my work stories and being my moral support. Especially, Eli, Melly, Karin, Babs, Steffi and Anita. Finally yet importantly, I would like to thank my parents for supporting me throughout my scientific career.